Verification of two numerical implementations of small-strain stiffness within the HSsmall model

Assessing their impact on overshooting behaviour to improve the accuracy of deformation predictions in geotechnical analyses

Msc Thesis

E.R. (Evira) Eman

TU Delft

SEEQUENT

Verification of two numerical implementations of small-strain stiffness within the HSsmall model

Assessing their impact on overshooting behaviour to improve the accuracy of deformation predictions in geotechnical analyses

by

E.R. (Evira) Eman

Thesis Committee:	Dr.ir. R.B.J. Brinkgreve	TU Delft (Chair)
	Dr.ir. E. Kementzetzidis	TU Delft
	Dr.ir. C. Zwanenburg	Deltares
	Dr. R Azeiteiro	PLAXIS, part of Seequent the Bentley Subsurface company
	Dr. I. del Brocco	PLAXIS, part of Seequent the Bentley Subsurface company

In partial fulfillment of the requirements for the degree of Master of Science in Civil Engineering specializing in Geotechnical Engineering at the Delft University of Technology

November 2025

Preface

The study you are about to read is my master's thesis at the Technical University of Delft and is titled: *"Verification of two numerical implementations of small-strain stiffness within the HSsmall model"*. The thesis was conducted in collaboration with PLAXIS.

I would like to express my sincere gratitude to my supervisors from PLAXIS, Ricardo Azeiteiro and Ilaria del Brocco, for their valuable insights and the many interesting discussions we had. Their guidance helped me bring this thesis to a higher level, and I learned a great deal during my time at PLAXIS. In particular, I would like to thank Ricardo. It is not something to be taken for granted when a supervisor treats you as an equal, is always willing to make time for you, and has the patience to explain complex matters clearly.

I would also like to thank my supervisors at the TU Delft, Ronald Brinkgreve, Vagelis Kementzetzidis, and Cor Zwanenburg (TU Delft / Deltares), for their guidance and feedback.

I am especially grateful to my main supervisor, Ronald Brinkgreve. I greatly appreciated his supervision throughout the process and the enthusiasm he brought to every discussion. There was always time for questions and room to discuss any difficulties. I learned a great deal from him. To me, this is what good and helpful supervision truly looks like.

This thesis brings my time as a student at this university to an end. I have truly enjoyed my years at the TU Delft and look back on them with cherished memories.

E.R. (Evira) Eman
Delft, November 2025

Summary

The current Hardening Soil small-strain (HSsmall) model, developed by Benz (2007), is capable of capturing the behaviour of a wide range of soil types, including their small-strain response. However, under specific conditions, the model exhibits *overshooting*, which is the overestimation of the material's elastic stiffness upon the closure of a small unloading–reloading (UL–RL) cycle interrupting monotonic loading, rather than recovering the stiffness corresponding to the onset of the cycle, as observed in real soil behaviour. *Overshooting* leads to underestimated deformations and consequently non-conservative results.

To address this issue, PLAXIS (part of Seequent, the Bentley Subsurface company) proposed two formulations: the Continuous Brick (CB) formulation, which replaces the small-strain component of the HSsmall model, and a Memory-Surface-Based (MSB) formulation, which extends it. Both have been implemented in the source code of the existing HSsmall constitutive model. However, their implementations had not yet been verified in the literature, nor had an assessment of overshooting, the motivation behind their development, been conducted.

This research aims to close that gap and to determine which of the two formulations provides the most suitable approach. Implementing the best-performing formulation into the HSsmall model results in a new more robust state-of-the-art model.

Accordingly, the following research question is posed:

'To what extent do the Continuous Brick formulation, as a new formulation for small-strain stiffness, and the Memory-Surface-based formulation, as an extension to the existing small-strain stiffness formulation within the Hardening Soil small-strain model, reduce the overshooting observed in the current formulation?'

This question is addressed through a structured test plan consisting of two main components: (i) single stress point simulations to verify whether the formulations behave as expected at the most fundamental level, and (ii) a boundary value problem to evaluate their performance under more numerically demanding conditions representative of practical applications in the pre-failure range, where small strain stiffness strongly influences the magnitude of deformations.

It was found that both formulations reduce overshooting to a negligible level. However, their effectiveness decreases in simulations involving nested cycles, as both formulations exhibit the limitation of retaining the memory of only a single UL–RL cycle. Although both formulations perform well, the MSB formulation proves to be the most suitable approach: it is easier to interpret, appears more robust, retains the small-strain component of the original HSsmall model, and yields a response consistent with the HSsmall model under monotonic loading.

One of the main challenges of this study was identifying the cause of the unloading-reloading cycles in the boundary value problem, as the initial assumption was found to be incorrect. This challenge was tackled by systematically reducing the complexity of the problem, which led to the discovery that redistributions of stresses were the cause.

Extending the HSsmall model with the MSB formulation leads to more accurate deformation estimations in geotechnical problems especially within the pre-failure range, as deformations will no longer be underestimated, without introducing additional model parameters. Moreover, adopting this formulation will not have major consequences for the end user, since its behaviour is consistent with that of the HSsmall model, except that overshooting no longer occurs.

Contents

List of Figures

List of Tables

Nomenclature

Abbreviations

Abbreviation	Definition
2D	two-dimensional
3D	three-dimensional
BVP	Boundary Value Problem
C	*Consolidation*
CB	Continuous Brick
CD	Consolidated Drained
DSS	Direct Simple Shear
FCFD	*Fully coupled flow–deformation*
GWL	groundwater level
HS	Hardening Soil
HSS	Hardening Soil small-strain
HSsmall	Hardening Soil small-strain
LSST	Lotung Large-Scale Test
MSB	Memory-Surface-Based
OED	Oedometer
PU	*Plastic* undrained
SSO	Small Strain Overlay
SR	Strain Reversal
UL–RL	Unloading–Reloading

Symbols

Symbol	Definition	Unit
a	control parameter	[-]
de	current deviatoric strain increment	[-]
F	Memory Surface value	[-]
G_0	maximum initial elastic shear modulus at small strains	[kPa]
G_{act}	actual elastic shear modulus	[kPa]
$G_{BrickNext}$	elastic shear modulus corresponding to the brick to be activated next	[kPa]
G_s	Secant elastic shear modulus	[kPa]
G_{UR}	Unloading-Reloading elastic shear modulus	[kPa]
H	deviatoric strain history tensor	[-]
$\mathbf{H_{SR,UL}}$	deviatoric strain history tensor at last strain reversal triggering unloading	[-]
h	hydraulic head	[m]
$i_{BrickNext}$	number of the brick to be activated next	[-]
m	scalar state variable that represents the radius of the Memory Surface	[kPa]
q	deviatoric stress	[kPa]
q	groundwater flow velocity	$[md^{-1}]$

Symbol	Definition	Unit
s	tensorial quantity that represents the current deviatoric stress state	[kPa]
$\mathbf{s_0}$	deviatoric stress at the start of the calculation step	[kPa]
$s_{BrickNextProj}$	shear strain measure corresponding to the projection of the string length of the brick to be activated next along the current deviatoric strain loading direction	
u	pore water pressure	[kPa]
u_{excess}	excess pore water pressure	[kPa]
$u_{steady-state}$	steady-state pore water pressure	[kPa]
α	tensorial state variable that represents the centre of the Memory Surface in the deviatoric stress space	[Pa]
β	dimensionless coefficient satisfying $\eta + \beta = 1$	[-]
γ	shear strain measure	[-]
$\gamma_{0.7}$	threshold shear strain at which $G_s = 0.722G_0$	[-]
$\gamma BrickLast$	shear strain measure corresponding to lastly activated brick	[-]
$\gamma_{BrickNext}$	shear strain measure corresponding to brick to be activated next	[-]
$\gamma_{cut-off}$	cut-off shear strain measure	[-]
γ_{HIST}	shear strain measure that represents the projection of the deviatoric strain history tensor **H** onto the direction of the current deviatoric strain increment	[-]
$\Delta\gamma$	shear strain measure accumulation since the onset of loading (either initial loading or reloading), brick activation or a Strain Reversal	[-]
$\Delta\gamma_{actv}$	shear strain measure accumulation required to activate the next brick	[-]
$\Delta\gamma_{SR,UL}$	shear strain measure accumulation since the activation of the last brick until a strain reversal triggering unloading has occurred	[-]
$\Delta\gamma_{tot}$	total shear strain measure accumulation since the last strain reversal	[-]
$\Delta\gamma_{tot,SR,UL-SR,RL}$	the total shear strain measure accumulation from the last strain reversal triggering reloading to the last strain reversal triggering reloading	[-]
Δq	change in deviatoric stress	[kPa]
$\Delta\sigma$	total stress change	[kPa]
η	dimensionless coefficient satisfying $\eta + \beta = 1$	[-]
σ	total stress vector	[kPa]
σ'	effective stress vector	[kPa]

1
Introduction

1.1. Research Context

The incorporation of small-strain stiffness in the constitutive models of soils has been widely recognized and supported in the literature (Cudny & Truty, 2020). Accurately predicting displacements requires incorporating small-strain stiffness and its non-linear dependency on strain amplitude (Benz, 2007). However, existing constitutive models often fall short, either because incorporating a proper formulation of small-strain stiffness makes them overly complex and less user-friendly for practical applications, or because of their limitations in accurately capturing behaviour in the small-strain range. Therefore, there was a need to develop a model that effectively describes small-strain stiffness while remaining simple for practical engineering applications (Benz, 2007).

1.2. Research Problem

The Hardening Soil (HS) model, initially introduced by Schanz et al. (1999), is widely used because its parameters can be easily identified through standard laboratory tests and/or field tests and/or empirical correlations. However, it lacks the capability to accurately describe small-strain behaviour, as it does not account for strain-dependency of stiffness. To address this shortcoming, Benz (2007) proposed an extension to the model by incorporating a small-strain stiffness formulation, resulting in the Hardening Soil small-strain (HSsmall) model.

Over time, a significant drawback of the HSsmall model became evident referred to as *overshooting* in the literature, which is the over prediction of the material's elastic stiffness upon closure of a small unloading–reloading (UL–RL) cycle interrupting a monotonic loading path, rather than recovering the stiffness corresponding to the onset of the cycle, as is observed in real soil behaviour (Niemunis & Cudny, 2018). When a soil undergoes a strain reversal (SR), the elastic shear modulus, representing the elastic stiffness of the material under shear stress, is reset to its high initial value. Less stiffness reduction occurs during reloading compared to that occurring during initial loading, leading to a higher stiffness upon closure of the cycle. These UL–RL cycles can be either caused by small numerical inconsistencies or physically induced, which, given their small magnitude, would likely have no effect on the soil's response (Cudny & Truty, 2020).

Overshooting results in underestimated deformations, consequently, non-conservative results. This highlights a critical limitation in the model's ability to accurately predict small-strain behaviour, and due to its popularity, it is even more important that overshooting is addressed (Niemunis & Cudny, 2018).

To solve this problem, two formulations, aiming to improve robustness of the small-strain stiffness component of the HSsmall model, have been implemented in the source code of the existing HSsmall constitutive model of PLAXIS (part of Seequent, the Bentley Subsurface company) and are discussed in more detail in chapter 2:

1. Memory-Surface-Based (MSB) formulation

2. Continuous Brick (CB) formulation

1.3. Research Objectives

The main objective of this study was to assess whether the MSB formulation and the CB formulation effectively reduce overshooting. Both formulations are theoretically capable of describing the evolution of small-strain stiffness. However, it was determined whether their numerical implementations also effectively mitigate overshooting. To this end, it was essential to verify that they have been implemented in such a way that they correctly reproduce their underlying analytical formulations. This verification included assessing whether the numerical tolerances have been properly defined and identifying potential errors in the source code.

Furthermore, the study identified possible modifications that could improve or refine the two proposed formulations, thereby improving their ability to reduce overshooting and enhance their robustness.

An additional objective was to evaluate whether the results obtained with the two proposed formulations under monotonic loading are consistent with that of the original HSsmall model. If the results deviated significantly, this could influence which of the two formulations is preferred, as larger deviations have greater consequences for end users.

Finally, this study determined which of the two formulations provides the most suitable approach, not only in terms of minimising overshooting but also in terms of robustness of the formulations. If both formulations were found to be ineffective in reducing overshooting, the literature was consulted to find alternative solutions.

1.4. Research Questions

Based on the research problem and objectives, the following research question was formulated and addressed throughout this study:

"To what extent do the Continuous Brick formulation, as a new formulation for small-strain stiffness, and the Memory-Surface-based formulation, as an extension to the existing small-strain stiffness formulation within the Hardening Soil small-strain model, reduce the overshooting observed in the current formulation?"

The research question was addressed by answering the following sub-questions:

1. What factors influence the extent of overshooting, and how?
2. To what extent do the numerical implementations of the two proposed formulations correctly reproduce their underlying analytical formulation?
3. What potential changes can be identified to improve or refine the two proposed formulations?
4. How do the results obtained with the two proposed formulations differ from those obtained with the original Hardening Soil small-strain model?
5. To what extent do the two proposed formulations effectively reduce overshooting at a single stress point level?
6. How effective are the two proposed formulations in reducing overshooting when applied to a boundary value problem?

1.5. Research theory and methods

The verification and assessment of overshooting were performed by conducting a structured test plan. This test plan consisted of two components, in which stress path analysis was frequently adopted:

1. Single stress point simulations to assess whether the formulations behave as expected at the most fundamental level
2. Two-dimensional (2D) boundary value problem (BVP) to assess overshooting not only at the level of single stress point simulations, but also within numerical simulations of practical 2D problems

2

Literature Review

The HS model, initially introduced by Schanz et al. (1999), is considered one of the leading constitutive models in geotechnical engineering, primarily because its parameters can be easily identified through standard laboratory tests and/or field tests and/or empirical correlations. The model is capable of simulating the behaviour of a wide range of soil types, including granular soils, fine grained-soils, and, to some extent, soft organic soils, as well as capturing numerous essential features of soil behaviour, such as stress-dependency, dilatancy and shear strength. Despite its broad adoption, the HS model lacks the capability of describing small-strain behaviour, including strain-induced elastic stiffness reduction during monotonic loading, the recovery of the high initial elastic stiffness after the occurrence of a SR and hysteretic behaviour under cyclic loading.

To address this shortcoming, (Benz, 2007) proposed the HSsmall model, which extends the original HS model by introducing strain-dependent stiffness behaviour. However, a shortcoming of the HSsmall model was identified by Niemunis and Cudny (2018), commonly referred to as *overshooting*, which is the overestimation of the material's elastic stiffness upon closure of a small UL–RL cycle interrupting a monotonic loading path.

To address this shortcoming, Cudny and Truty (2020) proposed the Hardening Soil Brick model, which reproduces the stiffness reduction relationship of the HSsmall model (in a discrete, stepwise manner).

The first section of this literature review discusses the historical development of small-strain stiffness in the HS model, beginning with a brief explanation of the HS model itself. The second section presents two formulations currently under development, proposed by PLAXIS (part of Seequent, the Bentley Subsurface company) to address overshooting, which form the main focus of this research.

2.1. Historical development of small-strain stiffness in the Hardening Soil model

This section first provides a brief description of the HS model, followed by an explanation of the small-strain component proposed by Benz (2007). The overshooting issue is then discussed, after which the Hardening Soil Brick model proposed by Cudny and Truty (2020) is explained.

2.1.1. Hardening Soil model

The HS model is a double hardening elasto-plastic constitutive model that includes a stress-dependent stiffness formulation for primary loading and for UL–RL conditions based on a power law formulation (Schanz et al., 1999). Within the elastic domain, i.e., UL–RL conditions, the model assumes isotropic elasticity, governed by a power law function including a stress-dependent unloading-reloading Young's modulus and a constant Poisson's ratio.

The model incorporates two hardening mechanisms: shear hardening, which is associated with the generation of plastic strains along deviatoric loading paths, and cap hardening, which occurs due to the development of plastic strains during isotropic compression. Together, these mechanisms capture the non-linear stress–strain behaviour of soils. Both yield surfaces are always active from the onset of loading, unless pre-loading is applied, meaning that the initial response is always elasto-plastic. Shear hardening can continue until the stress state reaches the Mohr-Coulomb failure envelope, which defines the onset of failure. As the material undergoes hardening, both its elastic domain and shear strength increase. The conceptual behaviour of the HS model is illustrated in Figure 2.1. For further information on the HS model, the reader is referred to Schanz et al. (1999).

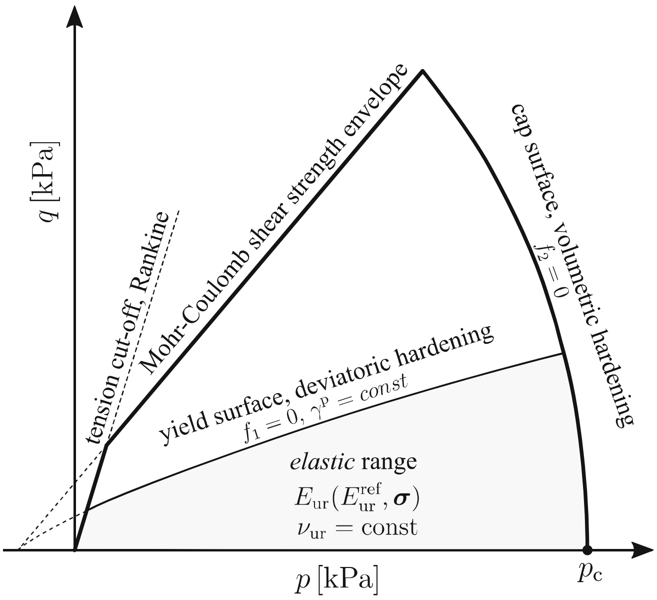

Figure 2.1: Conceptual behaviour of the HS model including the elastic range, cap hardening yield surface, shear hardening yield surface and the Mohr-Coulomb shear strength envelope (Cudny & Truty, 2020).

2.1.2. Hardening Soil small-strain model

The small-strain component of the HSsmall model, developed by Benz (2007) and referred to as the Small Strain Overlay (SSO) model, extends the original HS model by introducing strain-dependent stiffness behaviour at small strains. The SSO model is a non-linear elastic model in which the non-linearity is represented by an elastic modulus reduction curve. This curve describes the reduction of the elastic shear modulus with an increasing shear strain measure and follows Formula 2.1.

$$G_s = \frac{G_0}{1 + \frac{a}{N} \frac{\gamma}{\gamma_{ref}}} \tag{2.1}$$

where:

G_0	initial elastic shear modulus [kPa]
a	curve-shaping parameter $[-]$
γ	shear strain measure $[-]$
N	scaling factor $[-]$
γ_{ref}	reference shear strain measure $[-]$

The elastic modulus reduction curve is derived from a so-called modified hyperbolic backbone curve, which relates shear stress to shear strain at small strain levels and is described by Formula 2.2 (Hardin & Drnevich, 1972).

$$\tau = G_0 \frac{1}{1 + \frac{a}{N} \frac{\gamma}{\gamma_{ref}}} \gamma \tag{2.2}$$

The elastic modulus reduction curve is defined by three material parameters: the initial maximum elastic shear modulus at small strains G_0, the curve-shaping parameter a, and a reference shear strain level γ_{ref}. The parameters a and γ_{ref} control the shape of the reduction curve. In the HSsmall model within PLAXIS, a constant value of 0.385 is adopted for a, which implies that γ_{ref} represents the shear strain level at which the secant elastic shear modulus G_s is reduced to approximately 70% of G_0. Therefore, γ_{ref} is denoted as $\gamma_{0.7}$ (Santos & Correia, 2001). Furthermore, γ is replaced with γ_{Hist} in the HSsmall model, which represents the projection of the strain history tensor **H** onto the direction of the current deviatoric strain increment (Benz, 2007).

Soils exhibit hysteretic behaviour (Seed & Idriss, 1970), meaning that under cyclic loading, the stress-strain response forms closed loops. Masing (1926) described this behaviour through two rules. According to the second Masing rule, the UL–RL curves follow the same shape as the initial loading curve, but their scale is doubled. In the SSO model, this second Masing rule is implemented by scaling the parameter $\gamma_{0.7}$ by a factor of 2 (Benz, 2007) (see the scaling factor N in Formulas 2.1 and 2.2). As noted by Benz (2007) "in combination with the HS model, the threshold shear strain $\gamma_{0.7}$ in the Small-Strain Overlay model is always doubled for reloading. If a primary loading conditions exists, this will be accounted for by plastic hardening of the yield locus" (p. 85). Consequently, in the PLAXIS implementation of the SSO model, it is assumed that $N = 2$ for both primary loading and UL–RL conditions (Plaxis, 2025c).

Once the shear strain measure exceeds a certain threshold, i.e., $\gamma_{cut-off}$, the tangent shear modulus reaches its lower bound, defined as the UL–RL shear modulus G_{ur} (Benz, 2007). In most soil constitutive models, the stiffness under elastic (i.e., UL–RL) conditions is considered constant and equal to G_{ur}. However, when taking into account small-strain behaviour, the maximum (initial) elastic stiffness at small strains is even higher and gradually reduces with increasing shear strain, as discussed, until it reaches G_{ur}, where it remains constant until a SR occurs (Benz, 2007). This strain dependency of stiffness was recognised early in dynamic soil analyses (see for example Seed and Idriss (1970)), but was long disregarded in static analyses. However, over time it became clear that small-strain stiffness is also highly important for static analyses, because the majority of strains in the serviceability limit state of geotechnical problems are very small (Burland, 1989).

Accurate determination of the elastic shear modulus requires tracking of the deviatoric strain history. In the HSsmall model, this is achieved by using the second-order deviatoric strain history tensor **H** (Benz, 2007). Unlike most elasto-plastic models, where evolution is based on plastic strain increments, **H** evolves based on total strain increments (Niemunis & Cudny, 2018). Consequently, even infinitesimally small elastic strain increments can influence the tensor. Each time a SR occurs, **H** is erased and, as a result, the elastic shear modulus returns to its high initial value.

For further information on the HSsmall model, the reader is referred to Benz (2007).

2.1.3. Overshooting

A shortcoming of the HSsmall model was identified by Niemunis and Cudny (2018), commonly referred to as *overshooting* in literature, which is the overestimation of the material's elastic stiffness upon the closure of a small UL–RL cycle interrupting monotonic loading. When a soil undergoes a SR, the elastic shear modulus, representing the elastic stiffness of the material under shear stress, is reset to its high initial value. Less stiffness reduction occurs during reloading of an UL-RL cycle compared to that occurring during initial loading, leading to a higher stiffness upon the closure of the cycle. This phenomenon is clearly illustrated with Figure 2.2 retrieved from Kan and Taiebat (2014). Overshooting is not only inherent to the HSsmall model, but also occurs in other constitutive models (Kan & Taiebat, 2014) (Tafili et al., 2024).

In real soil behaviour, the stiffness corresponding to the onset of an UL–RL cycle is recovered upon its closure, implying that the response during continuation of the initial loading remains identical to that without the interruption. In other words, the soil does not "feel" the small UL–RL cycle. This overestimation is triggered by small numerical inconsistencies and by physically induced UL–RL cycles, that, given their small magnitude, would likely have no effect on the soil's response (Cudny & Truty, 2020).

Overshooting results in underestimated deformations, consequently, non-conservative results. This highlights a critical limitation in the model's ability to accurately predict small-strain behaviour.

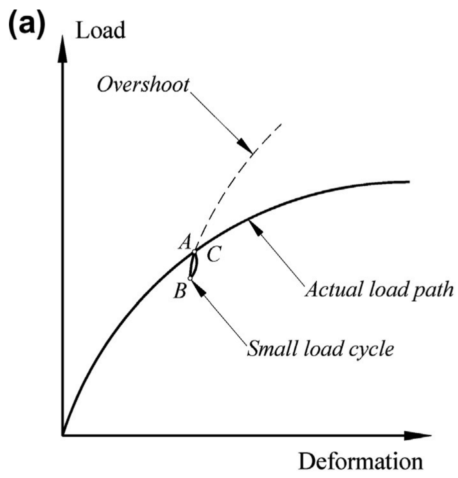

Figure 2.2: The overshooting issue (Kan & Taiebat, 2014).

As discussed in Section 2.1.2, the elastic shear modulus has a lower bound (cut-off value) equal to G_{ur} (see Figure 2.3), and corresponds to a user defined cut-off shear strain measure. When shear strains exceed this cut-off value, the small-strain stiffness formulation becomes inactive, i.e., the elastic shear modulus no longer reduces, but still keeps track of the strain loading history. Consequently, an accumulated shear strain measure larger than the cut-off value can be considered large.

Overshooting only occurs if during reloading in a UL–RL cycle less reduction takes place than what already occurred during the initial monotonic loading phase. Typically, the lower bound of the elastic shear modulus is reached quickly during monotonic loading. In other words, it is assumed that overshooting only occurs when this lower bound is not reached during reloading. If the UL–RL cycle is sufficiently large to reach the lower bound during reloading, the cycle can be considered large, and overshooting does not occur.

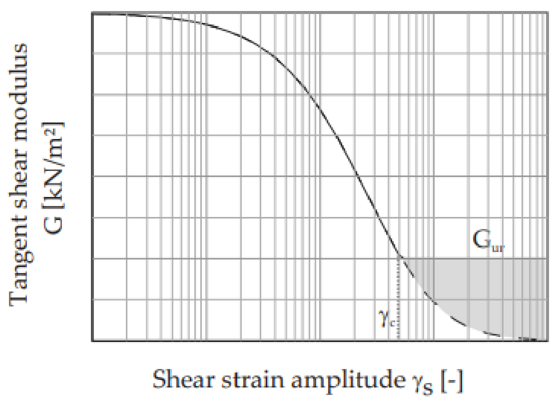

Figure 2.3: Elastic modulus reduction curve including the lower limit of the elastic shear modulus, G_{UR}, and the corresponding shear strain measure γ_c (Benz, 2007).

2.1.4. Hardening Soil Brick model

The Hardening Soil Brick model proposed by Cudny and Truty (2020) is derived from the Simpson's brick model (Simpson, 1992). The model adopts an analogy in which a soil element is represented by a person connected to several bricks via strings of various lengths. The movement of the person represents deviatoric strain, while the lengths of the strings represent radii of circular yield surfaces in the deviatoric strain space. Initially, all the strings are slack. As the person begins to move, the strings become taut one by one. Once a string becomes taut, the corresponding brick is being pulled, resulting in a reduction of the stiffness in a discrete, stepwise manner. A simple representation of the described analogy is shown in Figure 2.4.

Upon a SR, all strings become slack and the initial high elastic shear modulus, G_0, is recovered. A small amount of unloading results in a slight loosening of the strings, allowing for a quick reactivation of the bricks upon reloading. Each activation corresponds to a drop in the elastic shear modulus. Since the same bricks become active as were active prior to the UL-RL cycle, the same elastic shear modulus is obtained. Thus, the locations of the bricks in the deviatoric strain space implicitly represent the deviatoric strain history. As a result, the elastic shear modulus corresponding to the strain level just before the SR is restored more quickly, without having to traverse the entire elastic region (Cudny & Truty, 2020).

This formulation reproduces the elastic modulus reduction relationship of the HSsmall model (in a discrete, stepwise manner), while effectively addressing the overshooting issue.

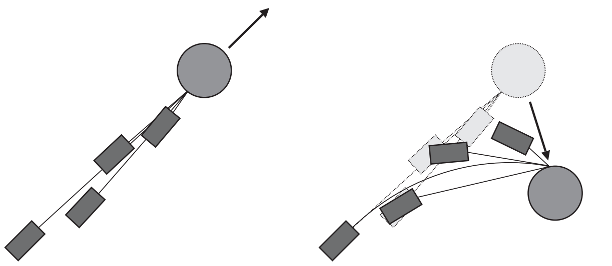

Figure 2.4: Visual representation of the brick analogy. Left: all the strings are taut.
Right: change of loading direction resulting in slack strings and recovery of the high initial stiffness (Benz, 2007).

2.2. Formulations proposed by Plaxis

To address the issue of overshooting, PLAXIS (part of Seequent, the Bentley Subsurface company) proposed two formulations that are currently under development: a formulation incorporating a Memory Surface (Plaxis, 2025a) and the CB formulation (Plaxis, 2025b). This research focuses on these two formulations, whose concepts are described in this section.

2.2.1. Memory-Surface-Based formulation

The MSB formulation extends the current small-strain stiffness formulation of the HSsmall model while employing the same elastic modulus reduction curve. In conventional soil mechanics, a Memory Surface is typically associated with the plastic component of a constitutive model, particularly within the Bounding Surface plasticity framework (Li & Liu, 2020), although with a different objective[1]. In the present context, however, the Memory Surface is applied to the elastic component. It encloses the recently experienced deviatoric stress states, and reaching the Memory Surface implies reaching a deviatoric stress state not recently experienced by the material (Plaxis, 2025a). The formulation does not require additional model parameters but introduces new elastic state variables. This section explains the principles of the MSB formulation and how it tackles overshooting.

The Memory Surface is defined by Formula 2.3:

$$F = |\mathbf{s} - \boldsymbol{\alpha}| - m, \tag{2.3}$$

where:

F	Memory Surface value [kPa]
$\mathbf{s}$	current deviatoric stress (tensor) [kPa]
$\boldsymbol{\alpha}$	centre of the Memory Surface (tensor) [kPa]

[1] To simulate ratcheting behaviour

m radius of the Memory Surface (scalar) [kPa]

The following situations can occur and are illustrated in Figure 2.5:

1. $F < 0$: this condition implies that the norm of the difference between s and $\boldsymbol{\alpha}$ is smaller than the radius of the Memory Surface, indicating that the current deviatoric stress point lies inside the Memory Surface.
2. $F = 0$: this condition implies that the norm of the difference between s and $\boldsymbol{\alpha}$ is equal to the radius of the Memory Surface, indicating that the current deviatoric stress point lies on the Memory Surface, within a given tolerance.
3. $F > 0$: this condition implies that the norm of the difference between s and $\boldsymbol{\alpha}$ is larger than the radius of the Memory Surface, indicating that the current deviatoric stress point lies outside the Memory Surface. However, when this situation occurs, the Memory Surface should expand. Recall that the Memory Surface encloses the recently experienced deviatoric stress states. Having a stress point outside of the Memory Surface would contradict this. This behaviour is analogous to that of a yield surface.

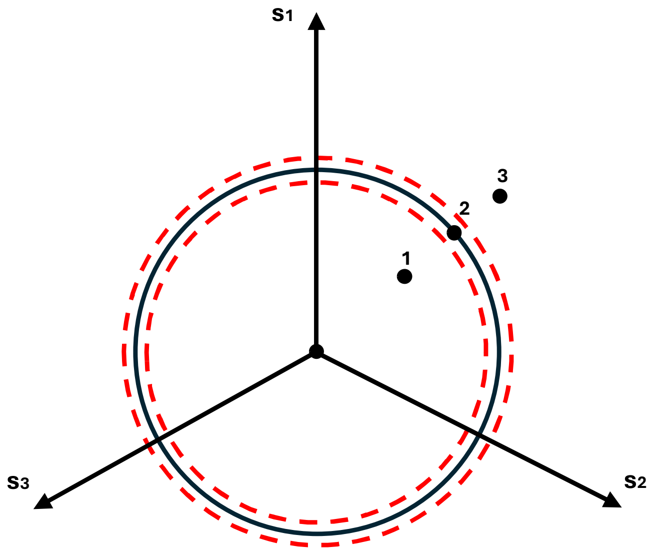

Figure 2.5: Possible scenarios of the Memory Surface value F in the deviatoric stress space. Point 1 is located inside the Memory Surface ($F < 0$). Point 2 is located on the Memory Surface within a given tolerance ($F = 0$). Point 3 is located outside the Memory Surface ($F > 0$).

The evolution of the Memory Surface is as follows:

a) During initial loading, the Memory Surface expands. The deviatoric strain history tensor **H** remains equal to the current deviatoric strain tensor. At the onset of loading **H** is equal to zero (Figure 2.6a).

b) Upon a SR triggering unloading, the expansion halts and the deviatoric stress point moves into the small-strain domain. When a SR triggering unloading occurs, the corresponding **H** is stored in the elastic state variable $\mathbf{H}_{SR,UL}$ (deviatoric strain history tensor at the last SR triggering unloading). Subsequently, **H** is reset such that the maximum elastic small-strain stiffness, G_0, is restored and starts accumulating the deviatoric strain history until a new SR is detected. Note that G_0 is also restored upon a SR triggering reloading (Figure 2.6b).

c) The Memory Surface resumes its evolution when a SR triggering reloading occurs. Its centre relocates to the point where the reversal took place (point 3 in Figure 2.6c), a process referred to as *kinematic evolution*, and its radius is defined by the distance between the two reversal points (points 2 and 3 in Figure 2.6c), i.e., the norm of the difference between the deviatoric stress states corresponding to the SRs triggering unloading and reloading, effectively representing the amount of unloading (Figure 2.6c). It should be noted, to avoid confusion, that in Figure 2.6c the updated Memory Surface appears to coincide with point 1, however, this is not the case.

d) The expansion is halted once more until the deviatoric stress point reaches the updated Memory Surface. Upon reaching the Memory Surface, **H** is reset to the value stored at the most recent SR triggering unloading (point 2), i.e., the value stored in the elastic state variable $\mathbf{H}_{SR,UL}$. This recovers the elastic shear modulus corresponding to the onset of the UL–RL cycle and thereby reducing overshooting. (Figure 2.6d) (Plaxis, 2025a)

The procedure for detecting a SR is in accordance with that of the HSsmall model (Benz, 2007). However, unlike in the HSsmall model, the MSB formulation must distinguish whether the detected SR triggers unloading or reloading. To this end, the inner product between the deviatoric stress at the beginning of a calculation step,$\mathbf{s_0}$, and the deviatoric stress increment, $\mathbf{ds}$, is computed. A negative value indicates a SR triggering unloading, whereas a positive value indicates a SR triggering reloading (Plaxis, 2025a).

Overshooting
In conclusion, overshooting is mitigated by restoring elastic state variable **H**, the deviatoric strain history tensor, corresponding to the onset of an UL–RL cycle upon its closure. As explained in Section 2.1.2, this elastic state variable is used to determine the elastic shear modulus.

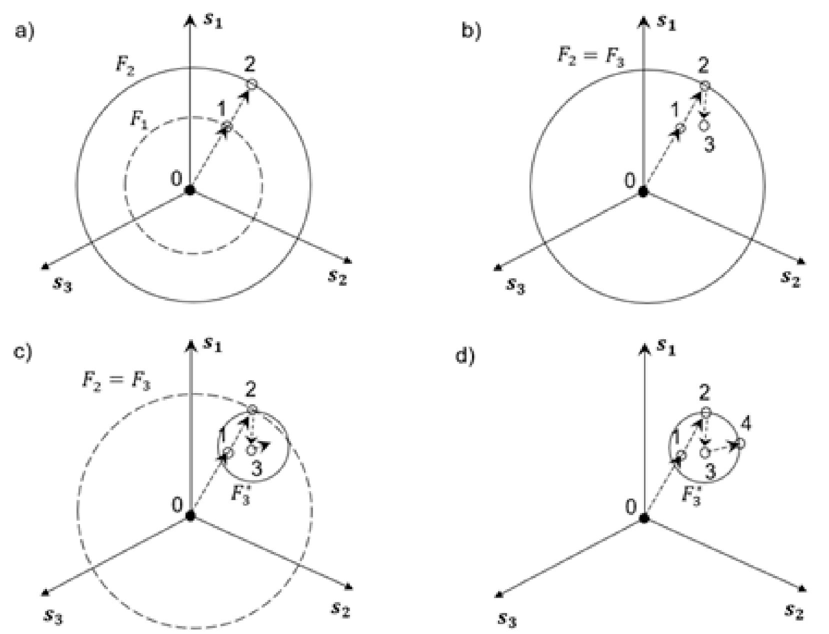

Figure 2.6: Memory Surface evolution. a) Isotropic expansion of the Memory Surface during monotonic, initial loading b) Expansion halts upon a reversal triggering unloading and the stress points moves into the small-strain domain c) Relocation of the Memory Surface to the reversal triggering reloading point and adjustment of the radius of the Memory Surface to the distance between the deviatoric stresses at which the SRs triggering unloading and reloading occurred d) Expansion is halted until the stress point reaches the updated Memory Surface (Plaxis, 2025a).

2.2.2. Continuous Brick formulation

A continuous representation of stiffness reduction provides a more realistic description of soil behaviour than a stepwise approach. If the Hardening Soil Brick model (see Section 2.1.4) were to be used for this purpose, an infinite number of bricks would be required to represent the reduction curve. Each brick consists of a second-order symmetric deviatoric strain tensor, referred to as *deviatoric strain points*, introducing six elastic state variables. These deviatoric strain points store information about the previous deviatoric strain loading history. An excessive number of state variables would be needed for a continuous representation, leading to substantial computer memory consumption (Plaxis, 2025b).

The CB formulation provides a continuous representation of stiffness reduction while reducing computer memory consumption. It uses the Hardening Soil Brick model developed by Cudny and Truty (2020) as a starting point, which itself is based on the concepts of Simpson's Brick model (Simpson, 1992). Like the Hardening Soil Brick model, the CB formulation retrieves the elastic stiffness corresponding to the onset of an UL–RL cycle upon its closure, indicating its ability to track the deviatoric strain loading history and detection of SRs. However, two important modifications have been introduced. First, elastic stiffness reduction occurs continuously by incorporating additional parameters in the form of scalar state descriptors of the strain loading history. Second, the formulation requires fewer bricks, which is made possible by the additional parameters, and significantly reduces computer memory consumption (Plaxis, 2025b).

The last brick to be activated, referred to as the *cut-off brick*, is placed at the lower bound, serving as a reference point. Beyond this cut-off point (lower bound), no further reduction occurs, and the stiffness remains constant and equal to the UL–RL elastic shear modulus. Together with other bricks (at least one brick in addition to the *cut-off brick*) and the scalar descriptors required by the continuous part, the formulation can determine the elastic shear modulus corresponding to the current shear strain measure (Plaxis, 2025b).

As each brick is defined by six state variables, the use of only two bricks results in twelve state variables, excluding those required for the continuous small-strain formulation (Plaxis, 2025b) and those inherited from the original HSsmall model (Benz, 2007). The formulation entirely replaces the second-order deviatoric strain history tensor H, which is used in the HSsmall model, and does not introduce new model parameters (Plaxis, 2025b).

The functioning of the model is explained with reference to Figure 2.7, considering only two bricks: the cut-off brick and one additional brick.

a) At the start of the simulation, each brick, including the cut-off brick, and the current deviatoric strain point are located at the origin of the deviatoric strain space. The actual (current) elastic shear modulus, G_{act}, is equal to the initial elastic shear modulus G_0. Upon deviatoric loading, the elastic state variable $\Delta\gamma$, which is the accumulated shear strain measure from the onset of loading (either initial loading or reloading), brick activation, or a SR, begins to accumulate. The total shear strain measure accumulation required to activate the next brick is defined by the elastic state variable $\Delta\gamma_{actv}$, which is updated at each step.

b) The first brick is activated when $\Delta\gamma = \Delta\gamma_{actv}$. Under initial loading, brick activation corresponds to reaching a specific value of the elastic shear modulus on the elastic modulus reduction curve (see Figure 2.8). Between the activation of bricks, the value of the elastic shear modulus is determined with γ_{Hist}, which is the current shear strain measure. γ_{Hist} is determined by Formula 2.4, and consequently, G_{act} is determined by Formula 2.5:

$$\gamma_{Hist} = \gamma_{BrickLast} + \frac{\Delta\gamma}{\Delta\gamma_{actv}} \left(\gamma_{BrickNext} - \gamma_{BrickLast}\right) \tag{2.4}$$

$$G_{act} = G_0 * \left(\frac{1}{1 + \frac{0.385}{N}\frac{\gamma_{Hist}}{\gamma_{0.7}}}\right)^2 \tag{2.5}$$

The value of the scaling factor N adopted in the CB formulation is different from that adopted in the HSsmall model and is discussed later in this section.

c) A SR triggering unloading is detected. The formulation makes use of two conditions to detect SRs:

   a. A check whether a brick becomes inactive given the current deviatoric strain increment
   b. If no brick is active, a check whether the deviatoric strain point is moving away from the cut-off brick while it was initially moving towards it, and vice versa

   At each SR, the initial elastic shear modulus, G_0, is recovered. Additionally, it is determined whether the SR triggers unloading or reloading. This is evaluated by computing the inner product of the deviatoric stress at the start of the calculation step, s_0, and the deviatoric strain increment, de. If the inner product is negative, a SR triggering unloading is detected, otherwise, a SR triggering reloading.

d) A SR triggering reloading is detected. Recall that the previous SR triggered unloading. Therefore, the deviatoric strain point is now moving towards the point where that SR occurred, i.e., the UL–RL cycle is in reloading conditions.

e) Brick one is activated during reloading and, subsequently, $\Delta\gamma$ is set equal to $\Delta\gamma_{SR,UL}$. Thereby, restoring the shear strain measure accumulated prior to the UL-RL cycle and resuming the elastic shear stiffness reduction from the point where it was interrupted, and thus, retrieving the elastic shear modulus at the start of the UL-RL cycle. If a brick becomes active during unloading, $\Delta\gamma$ won't be set equal to $\Delta\gamma_{SR,UL}$, but equal to zero

f) The cut-off brick is activated, meaning that the lower bound of the elastic shear modulus, G_{UR}, is reached and remains constant until the brick is deactivated (Plaxis, 2025b)

In the CB formulation, a scaling factor of 1 is applied to the elastic modulus reduction curve for both primary loading and UL–RL conditions (Formula 2.5), whereas a value of 2 is used in the HSsmall model (Section 2.1.2). Consequently, the CB formulation yields a softer response, but only under elasto-plastic conditions. Under elastic (UL–RL) conditions, the CB formulation inherently behaves stiffer, because the current deviatoric strain point must move more than one brick's string length to activate it, having already moved to some extent in the opposite direction (assuming a linear strain path). This results in a larger $\Delta\gamma_{actv}$ (Formula 2.4) and consequently a larger G_{act} (Formula 2.5). For example, in Figure 2.7f, the cut-off brick is being activated. If a SR were to occur subsequently, the current deviatoric strain point would first have to move to the position of the cut-off brick and then the same distance further to activate brick 1.

The softer response in primary loading can be partially counteracted by multiplying the user-defined $\gamma_{0.7}$ by a factor of 2. In an indirect manner, the response in primary loading is thus scaled by a factor of 2 and becomes closer to that of the HSsmall model, while the scaling factor itself remains 1. Recall that the HSsmall model applies a scaling factor of 2 for primary loading.

However, this solution is not ideal, as it will not always produce exactly the same results as the HSsmall model. Both the HSsmall model and the CB formulation use a scaling factor of 1 for a different operation that involves the yield functions. When $\gamma_{0.7}$ is scaled by a factor of 2, this factor is indirectly scaled as well, which causes a deviation from the HSsmall model.

Overshooting
In conclusion, overshooting is mitigated by restoring the elastic state variable $\Delta\gamma$, the accumulated shear strain measure, corresponding to the onset of an UL-RL cycle, upon its closure. As discussed in this section, this elastic state variable is used for the determination of the elastic shear modulus.

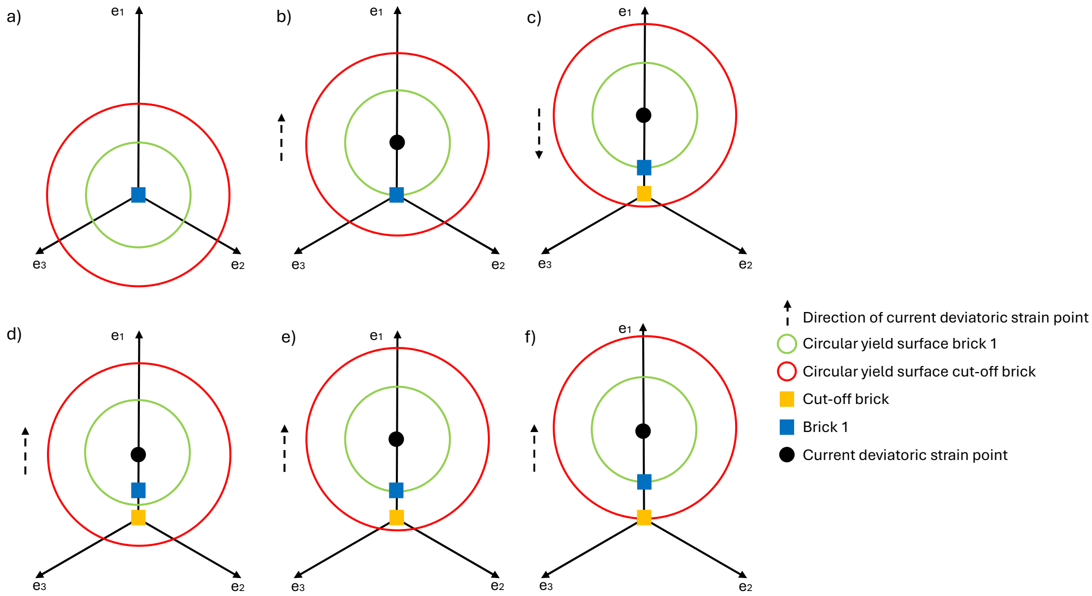

Figure 2.7: Functioning of the CB Formulation: a) Initial configuration, b) Start of deviatoric loading, c) Activation of brick one, d) Unloading, e) Reloading up to reactivation of brick one, f) Activation of the cut-off brick.

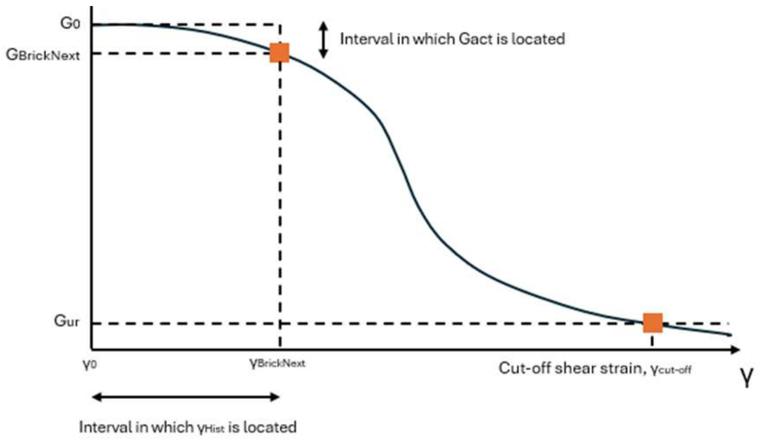

Figure 2.8: Elastic modulus reduction curve with the cut-off brick corresponding to the unloading-reloading elastic shear modulus and one additional brick, corresponding to a specific value of the elastic shear modulus.

2.3. Research gap

The CB formulation and the MSB formulation have been proposed to address overshooting. However, these formulations have not yet been verified in literature, nor has an assessment of overshooting, the motivation behind their implementation, been carried out. If the study demonstrates that overshooting is effectively reduced, implementing the best-performing formulation into the HSsmall model will result in a new, more robust, state-of-the-art model. Conversely, if overshooting is not effectively reduced, this study rules out these alternatives.

3
Methodology

This chapter outlines the methodology adopted to answer the main research question and the corresponding sub-questions. It consists of three phases, each of which is described in more detail in the sections below:

1. In-depth study of the HSsmall model, the MSB formulation, and the CB formulation.
2. Analysis of factors influencing the extent of overshooting
3. Verification and assessment of overshooting through a structured test plan

The first two phases mainly provide the background information required to interpret the results obtained in the third part. The third phase forms the basis on which the conclusions of this study are drawn.

This study requires the use of PLAXIS software. Given that the thesis is conducted at PLAXIS, access to the required software is available.

3.1. In-depth study of the Hardening Soil small-strain model, the Memory-Surface-Based formulation, and the Continuous Brick formulation

The small-strain stiffness component of the HSsmall model is studied in detail to gain a thorough understanding of how small-strain behaviour is currently formulated, which is required to interpret results obtained with the HSsmall model, particularly with respect to the model's response upon closing an UL–RL cycle.

PLAXIS internal documentation (see Plaxis (2025a) and Plaxis (2025b)) is consulted to gain understanding of the MSB formulation and the CB formulation. Additionally, test results in terms of deviatoric stresses and deviatoric strains, as well as the evolution of the elastic state variables, from a stress-controlled consolidated drained (CD) triaxial compression test simulation conducted with SoilTest, are analysed to examine the formulations in detail. A thorough understanding enables the correct verification of the formulations, the identification of potential improvements, the assessment of overshooting, and the analysis of differences in results when compared with the HSsmall model.

Explanations of the HSsmall model and the two proposed formulations are provided in Chapter 2.

Although laboratory tests are typically strain-controlled, all laboratory test simulations presented in this study are stress-controlled, since overshooting, which results from UL–RL cycles, is being assessed. Stress-controlled simulations allow for the specification of clear UL–RL cycles, making them easier to visualise.

SoilTest is a tool developed by PLAXIS that enables numerical simulations of various laboratory tests, such as the triaxial test, the direct simple shear (DSS) test, the oedometer (OED) test and a general test. All laboratory test simulations presented in this study are conducted using SoilTest.

SoilTest does not require the creation of a finite element model, as it uses a single-point algorithm, which means that the numerical calculations are restricted to a single stress point. This enables the analysis of the constitutive behaviour of the simulated material according to the applied constitutive model. The simplified way in which soil laboratory tests are simulated in SoilTest involves applying stress and strain boundary conditions representative of real laboratory testing on small soil specimens. The self-weight of the specimen is neglected, as the applied stresses are much higher than its own weight. Single stress point simulations ensure that the results reflect only the constitutive response of the material, independent of local variations in loading conditions or displacements, making them ideal for verification purposes.

3.2. Analysis of factors influencing the extent of overshooting

To visualise overshooting in the HSsmall model and to demonstrate its impact on the deviatoric stress-deviatoric strain response, two CD triaxial compression tests are simulated and compared: (i) monotonic loading up to a deviatoric stress of $150\,\mathrm{kPa}$, and (ii) loading up to a deviatoric stress of $150\,\mathrm{kPa}$, interrupted by UL–RL cycles with a deviatoric stress amplitude, Δq, of $0.5\,\mathrm{kPa}$, applied at intervals of $25\,\mathrm{kPa}$. The loading sequences are provided in Table 3.1.

Case	Description	Loading sequence (deviatoric stress q in kPa)
1	Monotonic loading	$0 \rightarrow 150$
2	Loading with UL–RL cycles	$0 \rightarrow 25 \rightarrow 24.5 \rightarrow 25 \rightarrow 50 \rightarrow 49.5 \rightarrow 50$ $\rightarrow 75 \rightarrow 74.5 \rightarrow 75 \rightarrow 100 \rightarrow 99.5 \rightarrow 100$ $\rightarrow 125 \rightarrow 124.5 \rightarrow 125 \rightarrow 150$

Table 3.1: Loading sequences corresponding to the simulations.

Unless stated otherwise, the pre-loading listed in Table 3.2 is applied in each simulation to ensure purely elastic behaviour during the shearing phase, since overshooting is associated with the elastic component of the HSsmall model. The pre-loading is simulated with CD triaxial compression test conditions. The stress state at the start of the shearing phase is an isotropic stress of $-100\,\mathrm{kPa}$.

Pre-loading	Value	Unit
Isotropic	-300	kPa
Deviatoric	195	kPa

Table 3.2: Pre-loading conditions for purely elastic conditions

Subsequently, different factors potentially influencing the extent of overshooting are analysed to gain further insight into overshooting. The factors considered include:

1. **Amplitude of UL–RL cycles**
   UL–RL cycles are applied at intervals of $25\,\mathrm{kPa}$, with deviatoric stress amplitudes of $0.5\,\mathrm{kPa}$ and $5\,\mathrm{kPa}$. The corresponding loading sequences are provided in Table 3.3
2. **Timing of UL–RL cycles along the deviatoric stress-deviatoric strain response**
   UL–RL cycles with a deviatoric stress amplitude of $0.5\,\mathrm{kPa}$ are introduced either at the beginning of the simulation (i.e., the first UL–RL cycle is applied at a deviatoric stress of $5\,\mathrm{kPa}$) or at the end of the simulation (i.e., the first UL–RL cycle is applied at a deviatoric stress of $125\,\mathrm{kPa}$). The cycles are applied at intervals of $5\,\mathrm{kPa}$. The corresponding loading sequences are provided in Table 3.4
3. **Elasto-plasticity**
   The sample is not subjected to isotropic and deviatoric pre-loading, meaning that the shearing is applied to the sample from the start, resulting in an elasto-plastic response. Note that, in the HSsmall model, the shear hardening yield surface is always active from the onset of loading,

leading to an elasto-plastic response until the first unloading takes place (Schanz et al., 1999). The same loading sequences as listed in Table 3.4 are used.

It should be noted that the factors analysed do not exclusively influence the extent of overshooting. Other factors may also play a role, but lie outside the scope of this study.

Case	Description	Loading sequence (deviatoric stress q in kPa)
1	Monotonic loading	$0 \rightarrow 150$
2	UL–RL cycles with $\Delta q = 0.5\,\mathrm{kPa}$	$0 \rightarrow 25 \rightarrow 24.5 \rightarrow 25 \rightarrow 50 \rightarrow 49.5 \rightarrow 50$ $\rightarrow 75 \rightarrow 74.5 \rightarrow 75 \rightarrow 100 \rightarrow 99.5 \rightarrow 100$ $\rightarrow 125 \rightarrow 124.5 \rightarrow 125 \rightarrow 150$
3	UL–RL cycles with $\Delta q = 5\,\mathrm{kPa}$	$0 \rightarrow 25 \rightarrow 20 \rightarrow 25 \rightarrow 50 \rightarrow 45 \rightarrow 50$ $\rightarrow 75 \rightarrow 70 \rightarrow 75 \rightarrow 100 \rightarrow 95 \rightarrow 100$ $\rightarrow 125 \rightarrow 120 \rightarrow 125 \rightarrow 150$

Table 3.3: Loading sequences for the analysis of the amplitude of UL–RL cycles

Case	Description	Loading sequence (deviatoric stress q in kPa)
1	Monotonic loading	$0 \rightarrow 150$
2	UL–RL cycles applied at beginning	$0 \rightarrow 5 \rightarrow 4.5 \rightarrow 5 \rightarrow 10 \rightarrow 9.5 \rightarrow 10$ $\rightarrow 15 \rightarrow 14.5 \rightarrow 15 \rightarrow 20 \rightarrow 19.5 \rightarrow 20$ $\rightarrow 25 \rightarrow 24.5 \rightarrow 25 \rightarrow 150$
3	UL–RL cycles applied at end	$0 \rightarrow 125 \rightarrow 124.5 \rightarrow 125 \rightarrow 130 \rightarrow 129.5 \rightarrow 130$ $\rightarrow 135 \rightarrow 134.5 \rightarrow 135 \rightarrow 140 \rightarrow 139.5 \rightarrow 140$ $\rightarrow 145 \rightarrow 144.5 \rightarrow 145 \rightarrow 150$

Table 3.4: Loading sequences for the analysis of the timing of UL–RL cycles along the deviatoric stress–deviatoric strain response

3.3. Verification and assessment of overshooting through a structured test plan

This section presents the test plan adopted to verify the MSB formulation and the CB formulation and to evaluate the extent of overshooting within these formulations.

The test plan consists of two phases:

1. Single stress point simulations
2. Boundary value problem (BVP)

These phases are described in more detail in the following sections.

3.3.1. Single stress point simulations

Several single stress point simulations are performed to verify whether the formulations behave as expected at the most fundamental level. Recall that PLAXIS's tool SoilTest is used for this purpose. The simulations are designed to enable analysis of small-strain behaviour, such as elastic shear stiffness reduction. To this end, deviatoric strains must develop during the simulations, since the elastic shear modulus decreases with increasing shear strain measure.

According to Cudny and Truty (2020), overshooting is generally independent of the material parameter set (i.e., model parameter set). Therefore, a standard set can be used for all tests. The material parameter set of the silty sand layer reported by Amorosi et al. (2016) is adopted. The silty sand layer is the top layer of the soil profile at the Lotung Large-Scale Test site (LSST) in Lotung, Taiwan. The material parameter set is provided in Table 3.5:

Parameter	Symbol	Unit	Value
(Effective) cohesion	c'	kPa	0
(Effective) angle of internal friction	φ'	°	30
K_0-value$^{(1)}$ for normal consolidation	K_0^{nc}	–	0.5
Reference shear modulus at very small strains	G_0^{ref}	MPa	90
Threshold shear strain at which $G_s{}^{(2)} = 0.722 G_0$	$\gamma_{0.7}$	%	0.011
Power for stress-level dependency of stiffness	m	–	0.54
Poisson's ratio for unloading-reloading	ν_{ur}	–	0.3
Unloading/Reloading modulus from drained triaxial test	E_{ur}^{ref}	MPa	60
Secant stiffness in standard drained triaxial test	E_{50}^{ref}	MPa	20
Tangent stiffness for primary oedometer loading	E_{oed}^{ref}	MPa	20

Table 3.5: Material parameter set single stress point simulations

Five laboratory test simulations are performed. The first three are specifically designed to evaluate overshooting and represent fundamental laboratory tests: (i) the CD triaxial compression test, (ii) the undrained DSS test, and (iii) the OED test. They are performed under both stress-independent, purely elastic conditions to isolate small-strain behaviour, and stress-dependent, elasto-plastic conditions to simulate more realistic soil behaviour:

1. **Stress-independent, purely elastic conditions**
   The verification process should primarily focus on the small-strain formulation rather than the entire constitutive model, as the main objective is to ensure the correct implementation of this formulation. When testing the full model, both elastic and plastic strains are generated and cannot be easily isolated. This complicates the verification process, as the small-strain stiffness formulation is based on elasticity rather than plasticity, making plastic strains undesirable in this context. Therefore, deviatoric and isotropic pre-loading, as listed in Table 3.2, are applied to the sample prior to the shearing phase to ensure that the soil's constitutive response remains purely elastic. Otherwise, hardening could occur and plastic strains may develop. Similar to the procedure described in Section 3.2, pre-loading is simulated under CD triaxial compression test conditions. The stress state at the start of the shearing phase is an isotropic stress of $-100\,\mathrm{kPa}$.

   Stress-dependency is deactivated by setting the model parameter m equal to zero. This model parameter governs the amount of stress-dependency. A value of zero means no stress-dependency. Stress-dependency is deactivated to isolate strain-dependent behaviour.
2. **stress-dependent, elasto-plastic conditions**
   No pre-loading is applied to the sample prior to the shearing phase, ensuring that the soil's response is elasto-plastic. The model parameter m is set equal to 0.54, consistent with the value used for the silty sand layer in Amorosi et al. (2016), thereby introducing stress-dependency of stiffness.

The final two laboratory test simulations are CD triaxial tests, designed to investigate specific aspects of the formulations: (i) CD triaxial compression test simulation with nested UL–RL cycles to assess the formulations' ability to retain memory and, (ii) CD triaxial test to investigate the detection of SRs in triaxial extension and compression. Recall from Sections 2.2.1 and 2.2.2 that the correct classification

[1] Coefficient of lateral earth pressure at rest.
[2] Secant elastic shear modulus.

of a SR as triggering either unloading or reloading strongly depends on the sign of the stress state, which reverses when changing between triaxial compression and extension. Only stress-independent, purely elastic conditions are considered in these simulations.

A brief description of the test specifications is provided below. Note that only the shearing phase is described, since under stress-independent, purely elastic conditions, the pre-loading conditions have already been detailed in Section 3.2. The first three tests include two cases: one with monotonic loading, serving as a reference, and one with small UL–RL cycles.

1. **CD triaxial compression test simulation**
   Case 1: monotonic loading up to a deviatoric stress of $150\,\mathrm{kPa}$.
   Case 2: loading up to a deviatoric stress of $150\,\mathrm{kPa}$, interrupted by UL–RL cycles with a deviatoric stress amplitude of $0.5\,\mathrm{kPa}$, applied at intervals of $25\,\mathrm{kPa}$.
   For this test, the loading sequences are identical as those listed in Table 3.1 in Section 3.2.
2. **Undrained DSS test simulation**
   Case 1: monotonic loading up to a shear stress of $35\,\mathrm{kPa}$.
   Case 2: loading up to a shear stress of $35\,\mathrm{kPa}$, interrupted by UL–RL cycles with a shear stress amplitude of $0.5\,\mathrm{kPa}$, applied at intervals of $5\,\mathrm{kPa}$.
   The loading sequences are listed in Table 3.6.

Case	Description	Loading sequence (shear stress τ_{xy} in kPa)
1	Monotonic loading	$0 \rightarrow 35$
2	Loading with UL–RL cycles	$0 \rightarrow 5 \rightarrow 4.5 \rightarrow 5 \rightarrow 10 \rightarrow 9.5 \rightarrow 10$ $\rightarrow 15 \rightarrow 14.5 \rightarrow 15 \rightarrow 20 \rightarrow 19.5 \rightarrow 20$ $\rightarrow 25 \rightarrow 24.5 \rightarrow 25 \rightarrow 30 \rightarrow 29.5 \rightarrow 30 \rightarrow 35$

Table 3.6: Loading sequences of the undrained DSS test simulations.

3. **Drained OED test simulation**
   Case 1: monotonic loading up to an axial stress of $-135\,\mathrm{kPa}$ (i.e., a deviatoric axial stress of $35\,\mathrm{kPa}$).
   Case 2: loading up to an axial stress of $-135\,\mathrm{kPa}$ (i.e., a deviatoric axial stress of $35\,\mathrm{kPa}$), interrupted by UL–RL cycles with a deviatoric stress amplitude of $0.5\,\mathrm{kPa}$, applied at intervals of $5\,\mathrm{kPa}$.
   The loading sequences are listed in Table 3.7

Case	Description	Loading sequence (axial stress σ_{yy} in kPa)
1	Monotonic loading	$0 \rightarrow -135$
2	Loading with UL–RL cycles	$-100 \rightarrow -105 \rightarrow -104.5 \rightarrow -105 \rightarrow -110$ $\rightarrow -109.5 \rightarrow -110 \rightarrow -115 \rightarrow -114.5 \rightarrow -115$ $\rightarrow -120 \rightarrow -119.5 \rightarrow -120 \rightarrow -125 \rightarrow -124.5$ $\rightarrow -125 \rightarrow -130 \rightarrow -129.5 \rightarrow -130 \rightarrow -135$

Table 3.7: Loading sequences of the OED test simulations.

4. **Tailored CD triaxial compression test simulation with nested UL–RL cycles to assess the formulations' ability to retain memory**
   Loading sequence in terms of deviatoric stress level: $0 \rightarrow 20 \rightarrow 5 \rightarrow 10 \rightarrow 9.5 \rightarrow 10 \rightarrow 20 \rightarrow 25 \rightarrow 24.5 \rightarrow 25 \rightarrow 35\,\mathrm{kPa}$
5. **Tailored CD triaxial test simulation to investigate the detection of SRs in triaxial extension and compression**
   Loading sequence in terms of deviatoric stress level: $0 \rightarrow -20 \rightarrow -10 \rightarrow -10.5 \rightarrow -10 \rightarrow 20 \rightarrow 10 \rightarrow 10.5 \rightarrow 10 \rightarrow -20\,\mathrm{kPa}$

Deviatoric stress is an invariant that, in principle, can only take positive values. However, in this context its absolute value is not taken and, therefore, positive values represent triaxial extension and negative values triaxial compression.

Appendix A can be consulted for further details on the test conditions (e.g., boundary conditions, number of phases, etc.).

Three main aspects of the laboratory test simulations are considered:

1. **Unexpected results**
   Unexpected results are identified and analysed mainly by examining the evolution of the elastic shear modulus throughout the simulations. They are classified as either consistent with the ingredients of the formulation, indicating that the observed behaviour is in accordance with the formulation but there is potentially room for improvement, or inconsistent with the ingredients of the formulation, and therefore relevant to the verification process.
2. **Comparison between monotonic loading and loading with small UL–RL cycles**
   This comparison evaluates whether the CB formulation and the MSB formulation effectively reduce overshooting. This conclusion is supported if, upon the closure of an UL–RL cycle, the deviatoric stress-deviatoric strain response, continues in accordance with the monotonic loading case.
3. **Comparison between the HSsmall model, CB Formulation and MSB Formulation**
   This comparison examines the implications of the newly implemented formulations on the deviatoric stress-deviatoric strain response relative to that obtained with the original HSsmall model. The comparison is carried out only under stress-independent, purely elastic conditions.

Note that only the first aspect is considered in the analyses of the two tailored CD triaxial tests.

3.3.2. Boundary Value Problem

According to Cudny and Truty (2020), it is important to assess overshooting not only at the level of single stress point simulations but also within numerical analyses of practical 2D geotechnical problems. This is because, in practical applications concerning the pre-failure range (serviceability limit states), the small-strain stiffness strongly influences the magnitude of deformations.

Overshooting is not observed in every numerical analysis of practical 2D geotechnical problems. It occurs only under specific conditions. Cudny and Truty (2020) present three cases that were specifically designed to assess overshooting: (i) a loading case involving a shallow foundation, (ii) an unloading case involving an excavation, and (iii) a dynamic case. Therefore, one of these cases is adopted for the BVP analysed in this study

The unloading case involving an excavation is repeated in this study, as the HSsmall model was originally proposed for excavation-type of problems (Benz, 2007). Moreover, the small UL–RL cycles observed in the simulation are assumed to result from short breaks in the excavation that allow for consolidation. It is therefore considered that the overshooting observed in the BVP arises from the modelling sequence, but it represents a realistic sequence. The model parameter set reported by Cudny and Truty (2020) is used for this BVP. It should be noted that the dilatancy angle, ψ, and the coefficient of lateral earth pressure at rest for normal consolidation, K_0^{nc}, were chosen to have different values. The dilatancy angle was set to zero to avoid the generation of excess pore water pressures due to dilatancy, which would complicate the interpretation of the BVP, whereas K_0^{nc} was assigned a value of 0.63, as this was the closest possible value to that reported in Cudny and Truty (2020) within the constraints of the PLAXIS 2D software. The parameter set is provided in Table 3.8.

Parameter	Symbol	Unit	Value
(Effective) cohesion	c'	kPa	6
(Effective) angle of internal friction	φ'	°	28
Dilatancy angle	ψ'	°	0
K_0-value for normal consolidation	K_0^{nc}	–	0.63
Reference shear modulus at very small strains	G_0^{ref}	MPa	60
Threshold shear strain at which $G_s = 0.722G_0$	$\gamma_{0.7}$	%	0.0003
Power for stress-level dependency of stiffness	m	–	0.7
Poisson's ratio for unloading-reloading	ν_{ur}	–	0.29
Unloading/Reloading modulus from drained triaxial test	E_{ur}^{ref}	MPa	25.75
Secant stiffness in standard drained triaxial test	E_{50}^{ref}	MPa	8.5
Tangent stiffness for primary oedometer loading	E_{oed}^{ref}	MPa	6.15
Horizontal permeability	k_x	ms^{-1}	1.16×10^{-10}
Vertical permeability	k_y	ms^{-1}	1.16×10^{-10}

Table 3.8: Material parameter set BVP

The case involves a four-metre-deep excavation, executed in four phases of one metre each. Two modelling sequences are considered:

1. Monotonic excavation with simultaneous consolidation in four phases, followed by a final consolidation phase
2. Excavation in four phases with simultaneous consolidation, each phase separated by a short intermediate consolidation phase, followed by a final consolidation phase

The results under monotonic loading (excavation without intermediate consolidation phases) serves as a reference, as no overshooting is expected in the absence of intermediate consolidation phases. The reference case is compared to the case including UL–RL cycles (excavation with intermediate consolidation phases), to assess whether overshooting is effectively reduced when using the proposed formulations. The UL–RL cycles are unlikely to affect the soil's primary loading response, as their magnitude is expected to be small due to the very short duration of the intermediate consolidation phases.

A numerical simulation of an excavation with simultaneous consolidation can be performed using a *fully coupled flow-deformation* (FCFD) analysis in PLAXIS 2D. An FCFD analysis is characterised by the coupling of flow and deformation, which yields more realistic behaviour but makes interpretation more challenging. In such analyses, the correct specification of hydraulic boundary conditions is crucial, as the pore water pressure distribution is computed on the basis of these conditions. For a more detailed explanation of this type of analysis, the reader is referred to Bentley Systems (2024).

The hydraulic boundary conditions specified for this BVP are as follows:

1. Neumann boundary condition at the axis of symmetry (see $y = 0\,\mathrm{m}$ in Figure 3.1) and at the bottom of the model (see $x = 0\,\mathrm{m}$ in Figure 3.1), where the groundwater flow q is set to $0\,\mathrm{m\,d^{-1}}$.
2. Dirichlet boundary condition at the ground surface (see $y = 20\,\mathrm{m}$ in Figure 3.1), where the hydraulic head h is determined from the GWL. However, since the top layer is modelled as dry, $h = 0\,\mathrm{m}$.
3. Dirichlet boundary condition at the right outer boundary of the model (see $x = 35\,\mathrm{m}$ in Figure

3.1), where the hydraulic head h along the height is determined from the GWL. Above the GWL, $h = 0\,\mathrm{m}$, as the top layer is modelled as dry.

The groundwater level (GWL) is located one metre below the ground surface (see $y = 19\,\mathrm{m}$ in Figure 3.1). As each excavation phase removes one metre of soil, the first phase involves a dry excavation, and the hydraulic boundary conditions therefore remain unchanged. During the second, third and fourth excavation phases, the excavation is dewatered by lowering the water level by one metre in each phase. This is achieved by adjusting the hydraulic boundary condition at the bottom of the current excavation. This boundary condition is defined as a Dirichlet boundary condition, where the groundwater head h is set equal to the height of the bottom of the current excavation with respect to the reference system of the model. Consequently, the pore water pressure at the bottom of the current excavation equals $0\,\mathrm{kPa}$.

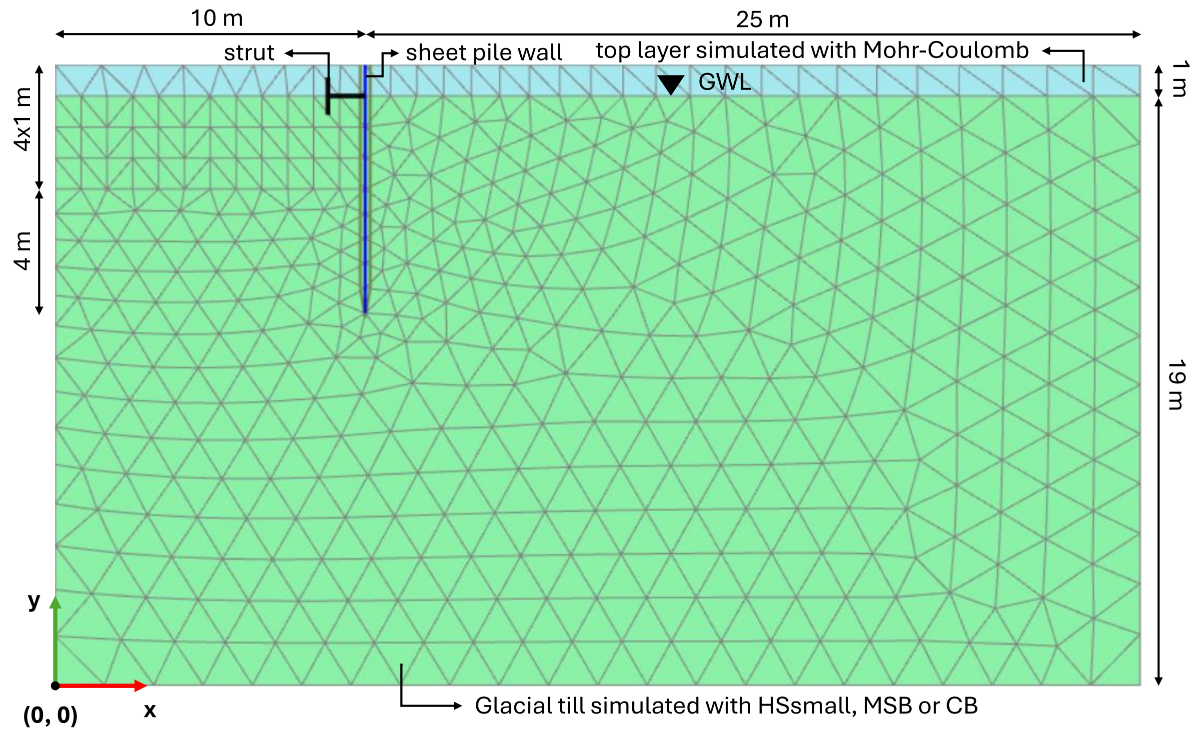

Figure 3.1: Overview of the model and generated mesh.

A detailed description of the two modelling sequences is provided in Tables 3.9 and 3.10. An overview of the BVP and the adopted mesh is presented in Figure 3.1. The mesh consists of 15-noded triangular elements and is refined along the sheet pile wall, within the excavation area, and beneath its base.

Phase	Duration [days]
Initial	0
Installation of the sheet pile wall	1.5
First excavation and installation of struts	0.5
Second excavation with simultaneous dewatering	0.5
Third excavation with simultaneous dewatering	0.5
Fourth excavation with simultaneous dewatering	0.5
Final consolidation	50,000

Table 3.9: Modelling sequence of the monotonic excavation.

Phase	Duration [days]
Initial	0
Installation of the sheet pile wall	1.5
First excavation and installation of struts	0.5
First intermediate consolidation phase	0.1
Second excavation with simultaneous dewatering	0.5
Second intermediate consolidation phase	0.1
Third excavation with simultaneous dewatering	0.5
Third intermediate consolidation phase	0.1
Fourth excavation with simultaneous dewatering	0.5
Final consolidation	50,000

Table 3.10: Modelling sequence of the excavation including short intermediate consolidation phases.

It should be noted that the end of the final consolidation phase does not exactly coincide with the end of consolidation. For the assessment of overshooting, the exact moment is not important. What matters is that the change in excess pore pressure, and consequently for instance in vertical displacement, is negligible. Therefore, a very long duration is adopted for the final consolidation phase. The actual time required to reach the end of consolidation is shorter.

The analysis of the BVP consists of the following three main components:

1. **Cause of the UL–RL cycles**
   Results obtained with the original HSsmall model are examined to verify whether the assumption that the UL–RL cycles responsible for overshooting are caused by short intermediate consolidation phases is valid. Understanding where the UL-RL cycles originate in this specific practical case provides valuable insights into the types of geotechnical problems for which settlement predictions can be improved by employing a small-strain stiffness formulation that does not exhibit overshooting. It should be noted that these insights do not imply that the identified cause is solely responsible for the UL-RL cycles observed in the presented case, nor that overshooting will not occur in other types of geotechnical problems. The extent of overshooting in the simulations is evaluated by analysing the time-dependent vertical displacement of node 225, i.e., the node located at the centre of the final excavation bottom, indicated in Figure 3.2. In addition, stress point

10083, also shown in Figure 3.2, is used in this investigation.

2. **Analysis of the results obtained with the MSB formulation**
Results obtained with the MSB formulation are analysed with the aim of verifying the formulation, assessing whether the extent of overshooting is reduced, identifying potential improvements, and comparing the results both with the original HSsmall model and with the formulation proposed by Cudny and Truty (2020).
3. **Analysis of the results obtained with the CB formulation**
Results obtained with the CB formulation are analysed with the same objectives as those defined for the MSB formulation.
4. **Bending moments in the sheet pile wall**
The influence of overshooting on the sheet pile wall is evaluated by analysing the bending moments. In the loading case with UL–RL cycles, the soil response becomes stiffer due to overshooting. The stiffer a material, the larger the share of the load it carries. Therefore, the bending moments in the wall are expected to be smaller than in the monotonic reference case, as a larger portion of the load is taken by the soil. The results obtained with the MSB formulation and the CB formulation are also presented to assess whether the reduction in bending moments is no longer observed.

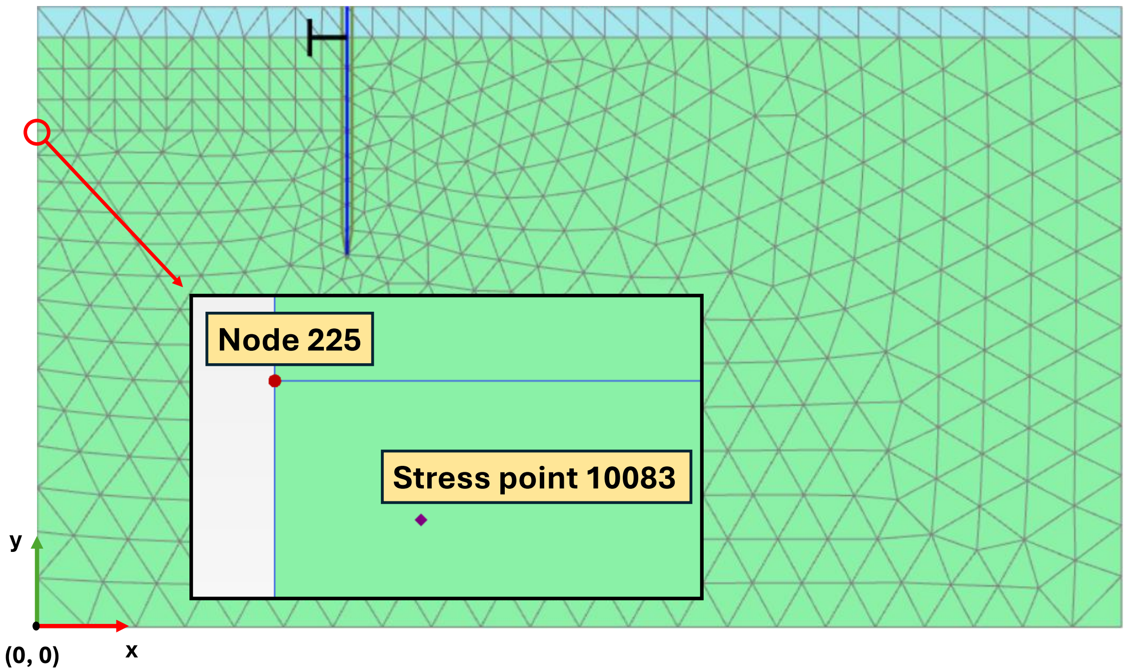

Figure 3.2: Selected node and stress point in the model used for investigating the cause of the UL-RL cycle.

The second and third parts each consist of the following four steps:

1. **Analysis of the vertical displacement of the node located at the centre of the final excavation bottom**
The first step addresses the vertical displacement of node 225 (Figure 3.2). Although overshooting is the most straightforward to assess from the deviatoric stress-deviatoric strain response, analysing the vertical displacement at the final excavation bottom provides a more practical perspective. Moreover, since Cudny and Truty (2020) presented their results in terms of vertical displacements, this approach allows for a comparison with the model proposed in their study. The results obtained with the HSsmall model are presented in the same figures in order to evaluate differences between the formulations.

Although the final consolidation phase has a total duration of $50\,000\,\mathrm{d}$, the results are presented up to $100\,\mathrm{d}$ to enable a comparison with the results reported by Cudny and Truty (2020), which were also limited to $100\,\mathrm{d}$.

2. **Examination of the deviatoric stress-deviatoric strain response at three stress points selected in the model**
The deviatoric stress-deviatoric strain response at three stress points selected in the model is examined to assess overshooting: (i) a point on the final excavation bottom between the axis of symmetry and the sheet pile wall, where overshooting is expected to be most pronounced (stress point 9757 indicated in Figure 3.3), (ii) a point near the ground surface on the right side of the sheet pile wall where a building could potentially exist (stress point 9188 indicated in Figure 3.3), and (iii) a point on the right side of the sheet pile wall where deformation of the wall is approximately largest (stress point 10181 indicated in Figure 3.3). The results obtained with the HSsmall model are presented in the same figures in order to evaluate differences between the formulations.

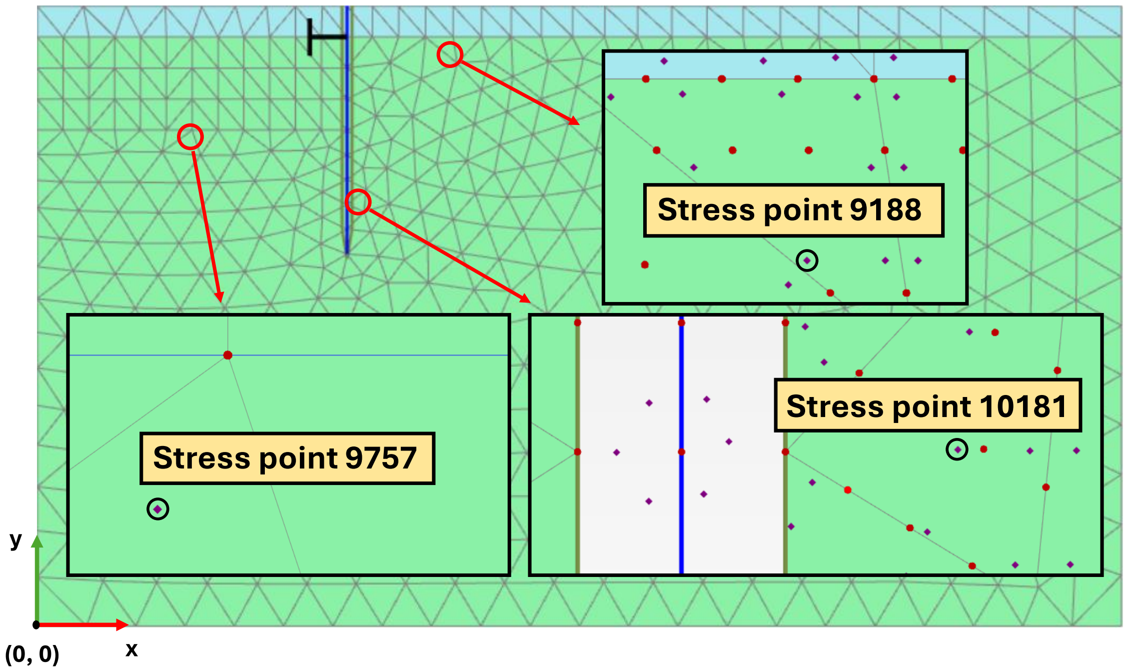

Figure 3.3: Selected stress points in the model for the analysis of deviatoric stress-deviatoric strain responses.

In contrast to the previous step, these results include the entire final consolidation phase of $50\,000\,\mathrm{d}$, allowing for the evaluation of the ultimate difference in the extent of overshooting between the monotonic (reference) case and the case with UL–RL cycles. Nevertheless, presenting the results up to $100\,\mathrm{d}$ already provides a sufficient assessment of overshooting, as overshooting is generated during the excavation period, assuming that the UL–RL cycles originate from the intermediate consolidation phases.

3. **Detailed analysis of the soil response at the first selected stress point**
A detailed analysis of the soil response at the first selected stress point (stress point 9757 indicated in Figure 3.3) is provided, with two objectives: (i) verification of the formulations and (ii) identification of potential improvements.

4. **Comparison with the results reported by Cudny and Truty (2020)**
The results obtained with the CB and MSB formulations are compared with those reported by Cudny and Truty (2020) to evaluate whether they show improvement or are at least of comparable quality. If not, consideration should be given to whether these formulations are the most effective approach to mitigate overshooting. The same scale is applied in the figures showing the results

of the MSB and CB formulations as in the figure showing the results of the model proposed by Cudny and Truty (2020), enabling a comparison.

Once an unexpected result is encountered in the analyses, the evolution of the elastic state variables and debug files will be consulted to determine whether the behaviour is consistent or inconsistent with the ingredients of the formulation, as in the single stress point simulations. If the behaviour is inconsistent, it will be explained how it should have behaved, whereas if the behaviour is consistent but nevertheless unexpected, possible improvements will be discussed.

4 Overshooting analyses

The first part of this chapter presents and discusses the results of simulations conducted to visualise overshooting in the HSsmall model, whereas the second part examines the influence of different factors on the extent of overshooting.

For each simulation, three plots are presented: (i) the deviatoric stress-deviatoric strain response, (ii) the elastic shear modulus versus loading step, and (iii) the applied deviatoric stress versus loading step. Note that the loading steps represent the modelling sequence. To improve readability of the figures, a baseline correction was applied to both the loading step and the deviatoric strain by subtracting their values at the onset of the shearing phase. The pre-loading phase is not included in the results. Recall that each simulation includes a pre-loading phase, except for those investigating the influence of elasto-plasticity on overshooting.

4.1. Overshooting in the Hardening Soil small-strain model

In Figure 4.1a, a clear difference is observed between the deviatoric stress-deviatoric strain response under monotonic loading and that under loading with UL–RL cycles. The attained deviatoric strain level, and consequently the resulting deformation, under loading with UL–RL cycles is much smaller than that under monotonic loading, as expected (see 2.1.3).

The elastic shear modulus at the beginning of an UL–RL cycle is not recovered upon its closure. For instance, the elastic shear modulus at loading step 4 is not recovered at loading step 6 in Figure 4.1b. Because the elastic shear modulus is not recovered and, since stiffness reduction is strain-dependent, less stiffness reduction occurs during reloading than during initial loading, the deviatoric stress-deviatoric strain response becomes stiffer from the moment the cycle closes compared to that under monotonic loading.

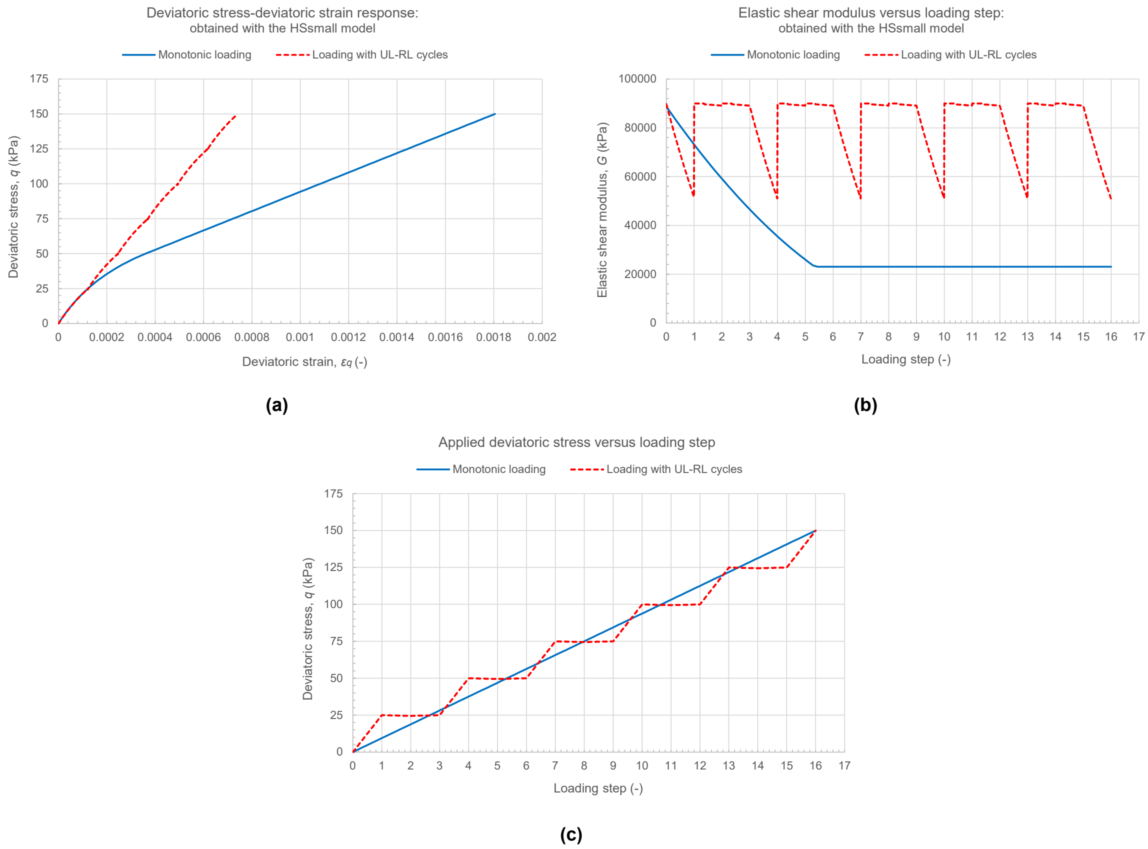

Figure 4.1: Overshooting in the HSsmall model

4.2. Factors influencing the extent of overshooting

Amplitude of UL–RL cycles

The amplitude of the UL–RL cycles has a strong influence on the extent of overshooting, as clearly shown in Figure 4.2a. The extent of overshooting in the red dashed case, which has a smaller UL–RL cycle amplitude than the black dotted case, is greater. The larger the amplitude of the cycle, the greater the stiffness reduction during reloading, resulting in smaller difference between the value of the elastic shear modulus at the onset and at the closure of an UL–RL cycle. This trend is also observed in Figure 4.1b: at loading step 1, an UL–RL cycle starts, while at loading step 3, it closes. The elastic shear modulus at loading step 3 of the black dotted case is clearly closer to its value at the beginning of the cycle than that of the red dashed case.

Note that, in the particular case where the amplitude of the UL–RL cycle would be equal to that of the initial loading, there would be no overshooting, meaning that the deviatoric stress-deviatoric strain response of the initial loading and that of reloading would be identical (a case not shown in the figure for brevity of the presentation). Note that this is only true when the response of the soil is purely elastic (i.e., when pre-loading has been previously applied).

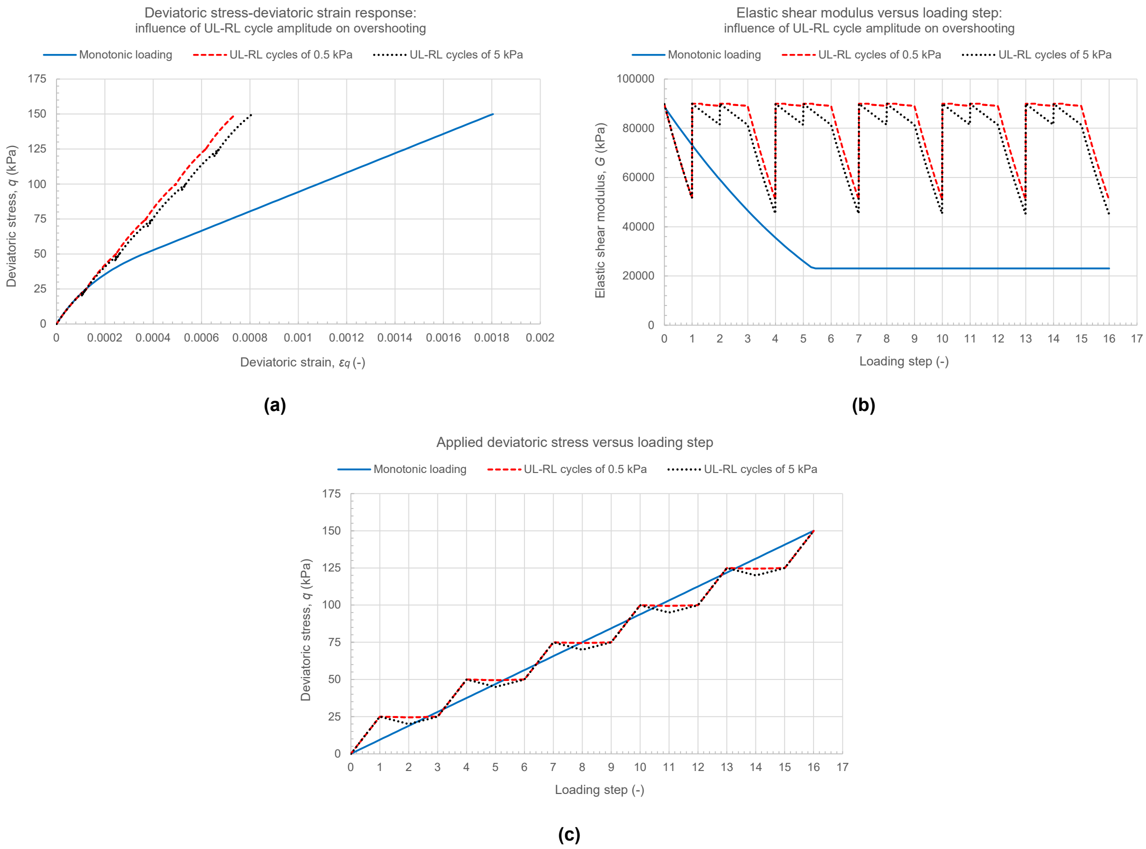

Figure 4.2: Influence of the amplitude of an UL–RL cycle on the extent of overshooting

Timing of UL–RL cycles along the deviatoric stress-deviatoric strain response
Figure 4.3 shows that the timing of the UL–RL cycles along the deviatoric stress-deviatoric response does not influence the extent of overshooting when the response is fully elastic. Both the case in which the UL–RL cycles occur at the beginning of the response and in which they occur at the end show approximately the same extent of overshooting. As detailed later, a different conclusion is obtained when the modelled response is elasto-plastic (i.e., with no pre-loading). Figure 4.3b demonstrates that the evolution of the elastic shear modulus is very similar in both cases.

Elasto-plasticity
Figure 4.4 shows the influence of elasto-plasticity on the extent of overshooting. Further along the deviatoric stress-deviatoric strain response, i.e., towards the end of the simulation, the plastic component becomes more dominant than the elastic component. Consequently, overshooting of the elastic component becomes less pronounced when the cycles are applied at the end. At the beginning of the simulation, the elastic component has a greater contribution, resulting in more evident overshooting of the elastic component. Figure B.2 indeed demonstrates that the elastic shear modulus remains much higher in the red dashed case.

4.3. Sub-conclusion

It was found that both the amplitude of an UL–RL cycle and the degree of elasto-plastic behaviour influence the extent of overshooting. Specifically, a larger amplitude results in a smaller extent of overshooting, and the more dominant the plastic component of the HSsmall model becomes, the smaller the extent of overshooting. When the response is fully elastic, the timing of the UL–RL cycles along the deviatoric stress-deviatoric strain path did not influence the extent of overshooting.

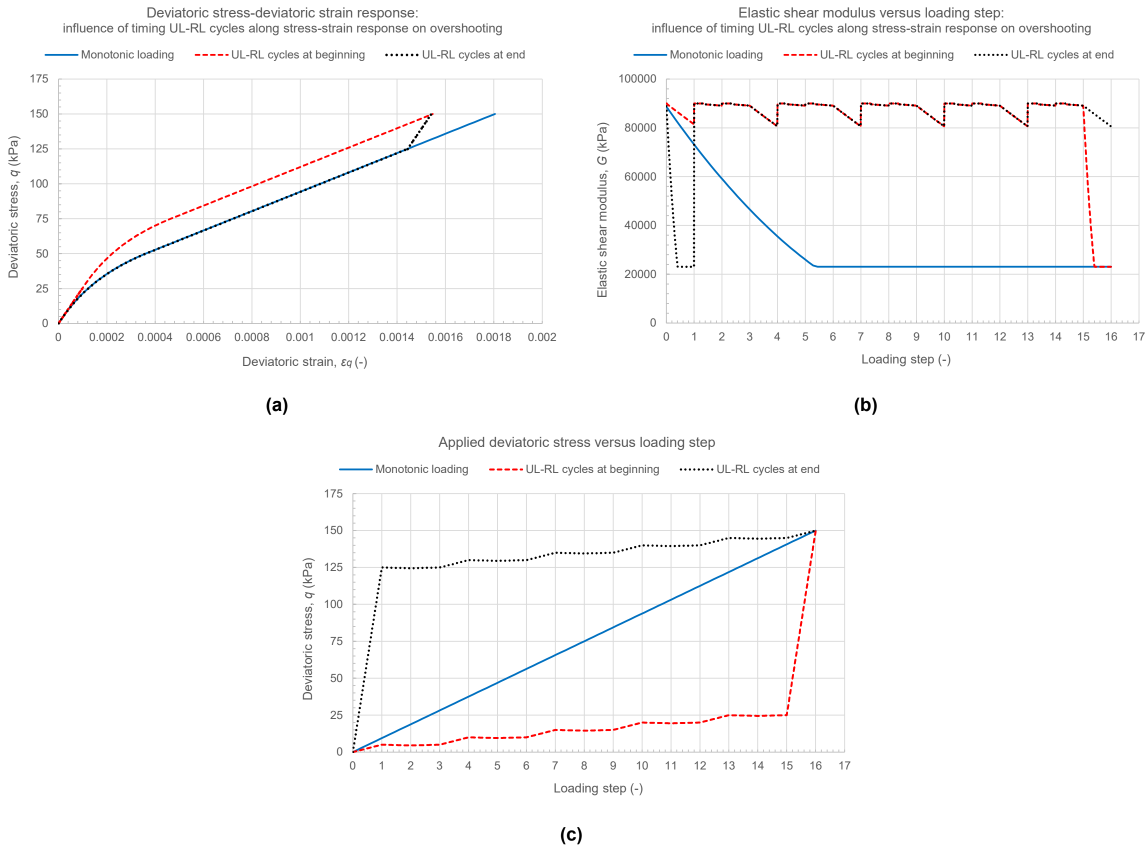

Figure 4.3: Influence of the timing of UL–RL cycles along the deviatoric stress-deviatoric strain response on the extent of overshooting.

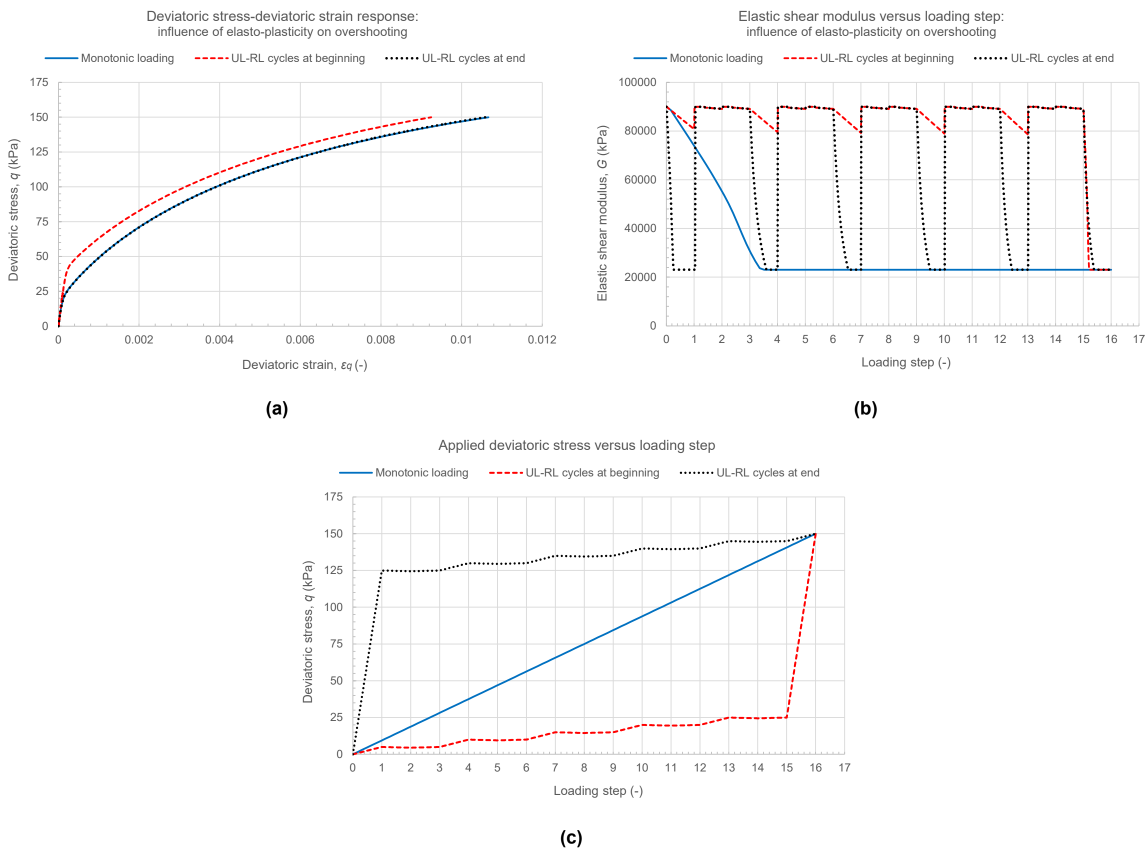

Figure 4.4: Influence of elasto-plasticity on the extent of overshooting.

5 Single stress point simulations

This chapter presents and discusses the results of the single stress point simulations. The first three sections focus on three fundamental soil laboratory tests: (i) the CD triaxial compression test, (ii) the undrained DSS test, and (iii) the drained OED test. The final two sections each focus on a specific aspect of the formulations: (i) a CD triaxial compression test simulation with nested UL–RL cycles to assess the formulations' ability to retain memory, and (ii) a CD triaxial test simulations to investigate the detection of SRs in triaxial extension and compression.

For brevity of the presentation, only the results under stress-independent, purely elastic (i.e., including pre-loading) conditions are presented. The figures of the CD triaxial compression test simulation obtained with the MSB formulation are discussed in detail to clarify their interpretation. These figures are repeated for each test, unless they do not give any new information. The graphical results under stress-dependent, elasto-plastic conditions are provided in Appendix B for conciseness, while the relevant findings are discussed in Section 5.4 to demonstrate whether the formulations also perform reliably under such conditions.

5.1. Consolidated drained triaxial compression test simulation

5.1.1. Results obtained with the Memory-Surface-Based formulation

Figure 5.1 presents the stress-independent, purely elastic results of the CD triaxial compression test simulation using the MSB formulation. Both the results under monotonic loading conditions (blue solid line) and under loading with small UL–RL cycles (red dashed line) are included. Specifically, the following figures are presented:

1. Figure 5.1a shows the stress-strain response, consisting of the deviatoric pre-loading and unloading phases, followed by the purely elastic shearing phase. UL–RL cycles are introduced during the shearing phase.
2. Figure 5.1b provides a zoomed-in view of the shearing phase in the stress-strain figure to better visualise the section where overshooting is assessed.
3. Figure 5.1c shows the applied loading throughout the simulation, including the isotropic decompression phase zero, the deviatoric pre-loading and unloading phases, and the subsequent shearing phase. The type of stress on the vertical axis depends on the simulated test.
4. Figure 5.1d provides a detailed view of an UL–RL cycle from 5.1c, clearly illustrating how such cycles are simulated.
5. Figure 5.1e shows the effective stress path in terms of deviatoric stress versus mean effective stress, including both isotropic and deviatoric pre-loading and unloading, as well as the subsequent shearing phase. In this test, the stress path of the shearing phase coincides with that of the deviatoric pre-loading.
6. Figure 5.1f presents the elastic shear modulus as a function of the loading step. Note that the

loading steps represent the modelling sequence. From loading step 0 to 1, isotropic decompression is simulated. Between loading step 1 and 2, deviatoric pre-loading takes place. Deviatoric unloading occurs from loading step 2 to 3, after which the shearing phase begins. Each time the elastic shear modulus becomes constant, it means that its lower bound (i.e., the UL–RL elastic shear modulus) has been reached. Generally, a jump to (approximately) its initial value (i.e., its maximum value) indicates the occurrence of a SR, whereas a sudden and sharp drop to a lower value indicates the closure of an UL–RL cycle. Any deviation from this general pattern is explicitly explained.

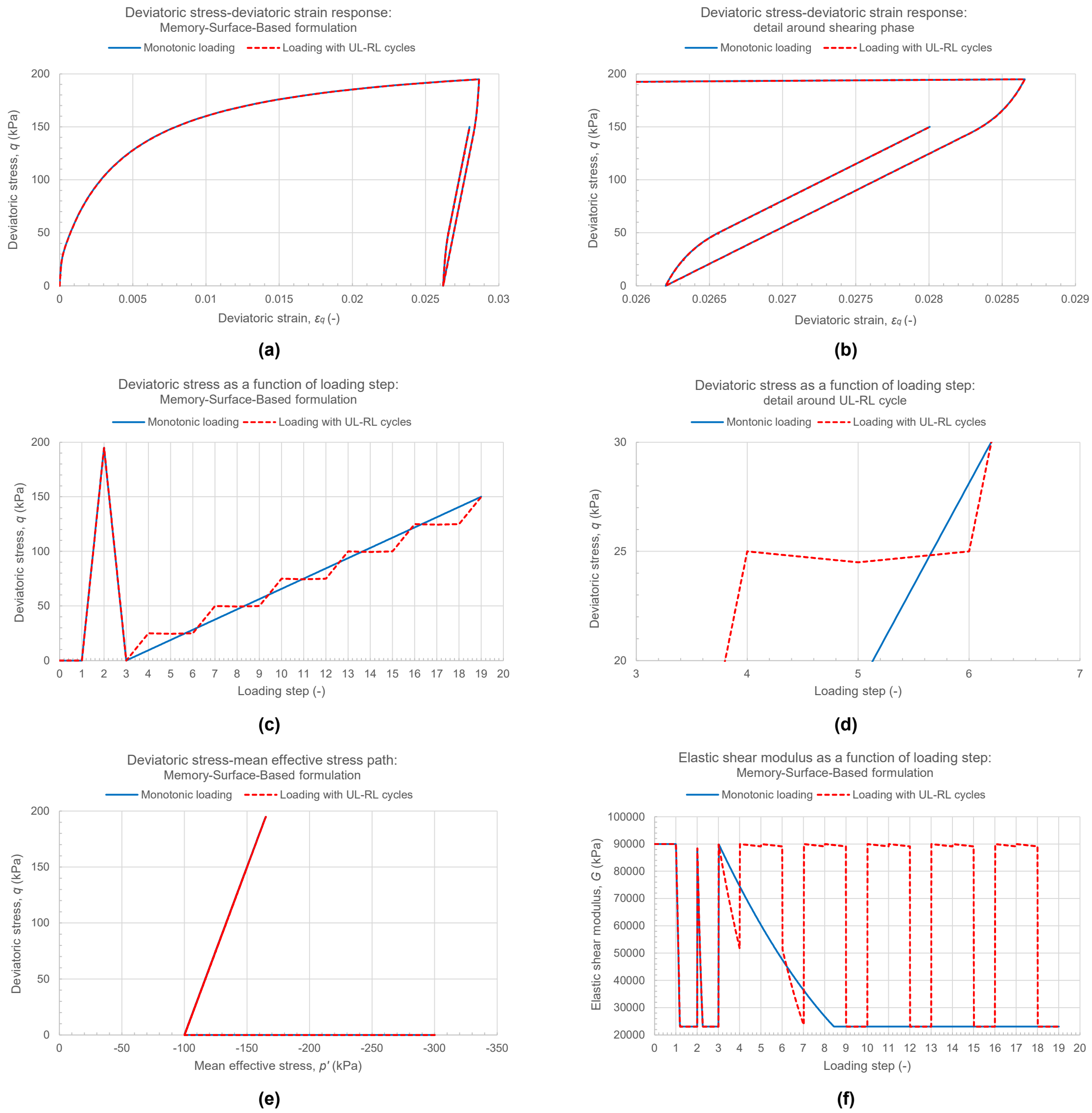

Figure 5.1: Results of the CD triaxial compression test simulation under stress-independent, purely elastic conditions obtained with the MSB formulation.

Figure 5.1f clearly demonstrates that the results are consistent with the ingredients of the formulation. At each SR, the high initial elastic shear modulus is restored (at loading steps 2, 3, 4, 5, 7, etc.). Additionally, upon the closing of each UL–RL cycle, the stiffness at the start of that cycle is recovered. For instance, the stiffness at loading step 4 and 6 is identical, as intended. Moreover, the deviatoric stress-deviatoric strain response obtained in the monotonic simulation coincides with that of the simulation with UL–RL cycles, indicating that overshooting does not occur.

5.1.2. Results obtained with the Continuous Brick formulation

The results obtained with the CB formulation are presented in Figure 5.2, with the figures having the same meaning as those presented for the MSB formulation in the previous section. Unexpected behaviour was identified, as detailed below. The improvements implemented by PLAXIS are subsequently explained.

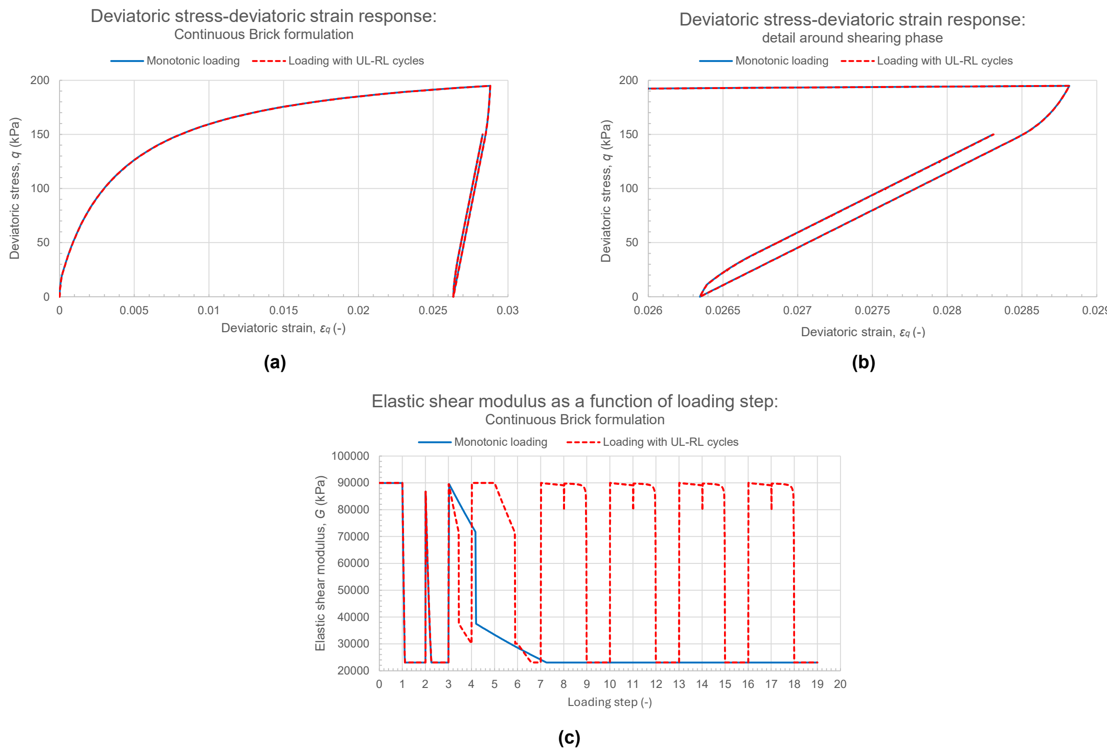

Figure 5.2: Results of the CD triaxial compression test simulation under stress-independent, purely elastic conditions obtained with the CB formulation.

Unexpected results

False detection of a SR triggering unloading at loading step 3

By examining the evolution of the elastic state variables, an inaccuracy in the results became apparent, which cannot be inferred from Figure 5.2. Figure 5.3 shows that, at loading step 3, the elastic state variable $\Delta\gamma_{SR,UL}$ is updated, which only happens when a SR triggering unloading is detected. This means that the formulation failed to detect a SR triggering reloading (note that, at loading step 3, the deviatoric stress starts increasing once again).

To find the root cause of this inaccuracy, the criterion for detecting a SR triggering unloading is analysed, which is explained in Section 2.2.2: a SR triggering unloading is detected whenever the inner product of the deviatoric stress at the start of the step, $\mathbf{s_0}$, and the deviatoric strain increment, $d\mathbf{e}$, is negative ($\mathbf{s_0} : d\mathbf{e} < 0$). After debugging, it became apparent that the result of the inner product at loading step 3 was not exactly zero, but a small negative number (-0.209E-014), resulting in the detection of a SR triggering unloading. To conclude: the unexpected behaviour is consistent with the ingredients of the formulation, but there is room for improvement. This type of corner cases mostly arise from numerical inaccuracies. The implemented strategy will be presented later.

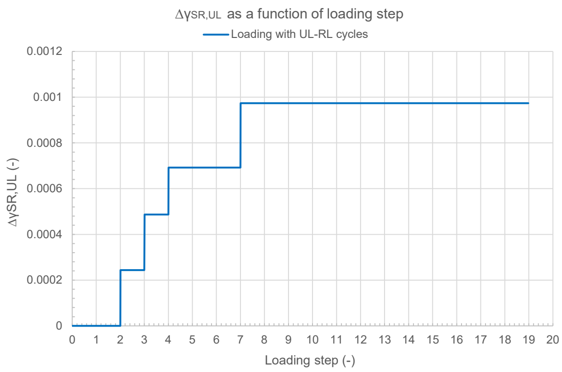

Figure 5.3: Shear strain measure accumulation since the activation of the last brick until a SR triggering unloading has occurred as a function of loading step.

Drop of the elastic shear modulus during reloading when the first brick is being activated
Figure 5.2c shows a sudden drop in the elastic shear modulus between loading steps 3 and 4. The elastic state variable $i_{BrickNext}$ indicates which brick is to be activated next. Figure 5.4 shows that the drop in the elastic shear modulus coincides with the activation of the first brick (note that the sign of $i_{BrickNext}$ is not important in this context).

According to the formulation, when a brick is activated during reloading, the accumulated shear strain measure accumulated prior to the UL–RL cycle is restored, resulting in a drop of the elastic shear modulus, as its value is dependent on this measure. Thus, the behaviour observed in Figure 5.4 is consistent with the ingredients of the formulation. However, it would be logical that a drop in the elastic shear stiffness would only happen if a brick were activated upon the closure of an UL–RL, which is not the case. In fact, the UL–RL cycle associated with the restored shear strain measure corresponds to the start of deviatoric unloading following the deviatoric pre-loading. This means that, between loading step 3 and 4, the reloading has not yet reached the deviatoric stress level at the start of unloading and, consequently, the cycle is not yet closed. Thus, there is room for improving the formulation, as detailed later.

Drops in the elastic shear modulus after the detection of a SR while no brick is active
Figure 5.2c shows sudden drops in the elastic shear modulus at loading steps 8, 11, 14 and 17. These drops are the result of a bug in the code. A variable involved in the check for SRs when no brick is active was being incorrectly initialised prior to this check. This behaviour is naturally inconsistent with the ingredients of the formulation, as no drops in the elastic shear modulus should occur after the detection of a SR.

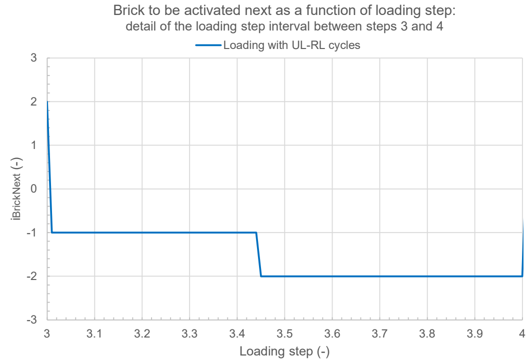

(a)

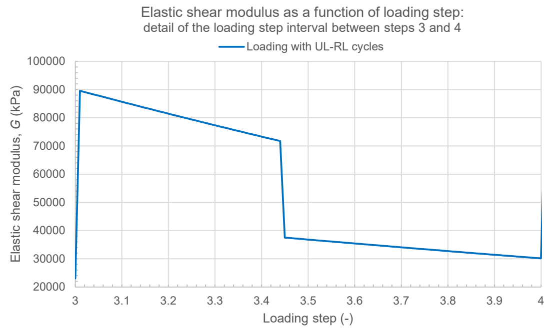

(b)

Figure 5.4: Drop of the elastic shear modulus during reloading when the first brick is being activated in between loading steps 3 and 4.

Improvements

False detection of a SR triggering unloading at loading step 3

To prevent the detection of false SRs triggering unloading, the criterion for its detection is changed to determining whether the inner product of the current deviatoric stress, $\mathbf{s}$, and the deviatoric strain increment, $d\mathbf{e}$, is negative ($\mathbf{s} : d\mathbf{e} < 0$), rather than $\mathbf{s_0} : d\mathbf{e} < 0$. After implementing this new criterion, $\Delta\gamma_{SR,UL}$ is no longer updated at loading step 3, as can be seen in Figure 5.5, meaning that a SR triggering reloading is detected, rather than a SR triggering unloading.

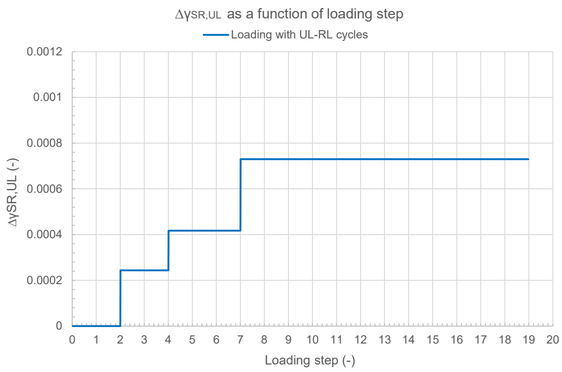

Figure 5.5: Shear strain measure accumulation since the activation of the last brick until a SR triggering unloading has occurred as a function of loading step after implementing the discussed improvement.

Jump of the elastic shear modulus during reloading when the first brick is being activated

To ensure that the shear strain measure accumulated prior to an UL–RL cycle is only restored when a cycle is closed, two new elastic state variables are added to the formulation:

1. $\Delta\gamma_{tot}$: the total shear strain accumulation since the last SR
2. $\Delta\gamma_{tot,SR,UL-SR,RL}$: the total shear strain measure accumulation from the last SR triggering unloading to the last SR triggering reloading

Upon activation of a brick during reloading, the accumulated shear strain measure since the start of reloading is compared to $\Delta\gamma_{tot,SR,UL-SR,RL}$. If the difference is smaller than a certain tolerance, the cycle is considered closed and the accumulated shear strain measure accumulated prior to the corresponding cycle is restored. Otherwise, the cycle is considered not to be closed and the elastic shear modulus reduction proceeds continuously. In other words, the "distances" in the deviatoric strain space (i.e., measures of the shear strain accumulation) are compared.

Drops in the elastic shear modulus after the detection of a SR while no brick is active
As previously mentioned, an error in the code was identified involving a variable used to check for a SR when no brick is active. This issue was resolved by correctly initializing that variable.

Figure 5.6 shows the results obtained after implementing all the discussed improvements. From Figure 5.6c, it is evident that the sudden drop in the elastic shear modulus between loading step 3 and 4, as well as the drops at loading steps 8, 11, 14 and 17, no longer occur.

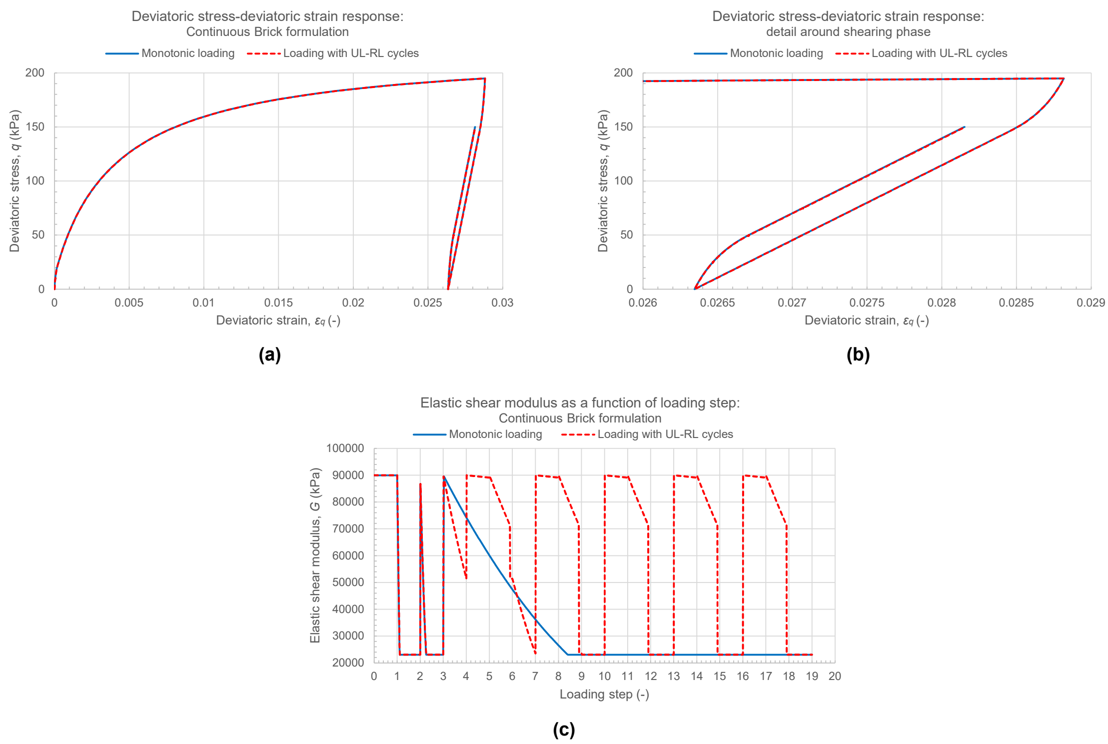

Figure 5.6: Results of the CD triaxial compression test simulation under stress-independent, purely elastic conditions obtained with the CB formulation after implementing the discussed improvements.

Comparison between monotonic loading and loading with unloading–reloading cycles

No overshooting is observed in the deviatoric stress-deviatoric strain response obtained with the version of the CB formulation that does not yet include the discussed improvements (see Figure 5.2b). However, as discussed, the loading case with UL–RL cycles exhibits a sudden drop in the elastic shear modulus during the first reloading phase following pre-loading (i.e., between loading steps 3 and 4). This drop occurs not only in the loading case with UL–Rl cycles but also in the monotonic loading case. As a result, the response in both cases is softer compared to that obtained with the version in which the discussed improvements are implemented.

For the improved version, it is evident that the deviatoric stress-deviatoric strain response obtained under loading with UL–RL cycles also coincides with that under monotonic loading (see Figure 5.6b).

5.1.3. Comparison between the results obtained with the HSsmall model, the Continuous Brick formulation and the Memory-Surface-Based formulation

Figures 5.7a and 5.7b compare the original HSsmall model, the MSB formulation, and the CB formulation. Figure 5.7c shows the applied deviatoric stress throughout the simulations, which is independent of the model or formulation used. Note that in Figures 5.7a and 5.7b, the blue solid, black dotted, and yellow dotted/dashed lines coincide.

The loading case with UL–RL cycles of the HS small model deviates from its monotonic loading case, as expected due to the overshooting inherent to this model. In contrast, Figures 5.7a and 5.7b clearly show that both the MSB formulation and the CB formulation reproduce the monotonic response of the HSsmall model. It should be noted that these responses are obtained under purely elastic conditions. If the response were elasto-plastic, the CB formulation would exhibit a softer response, as discussed in Section 2.2.2, while still preventing overshooting.

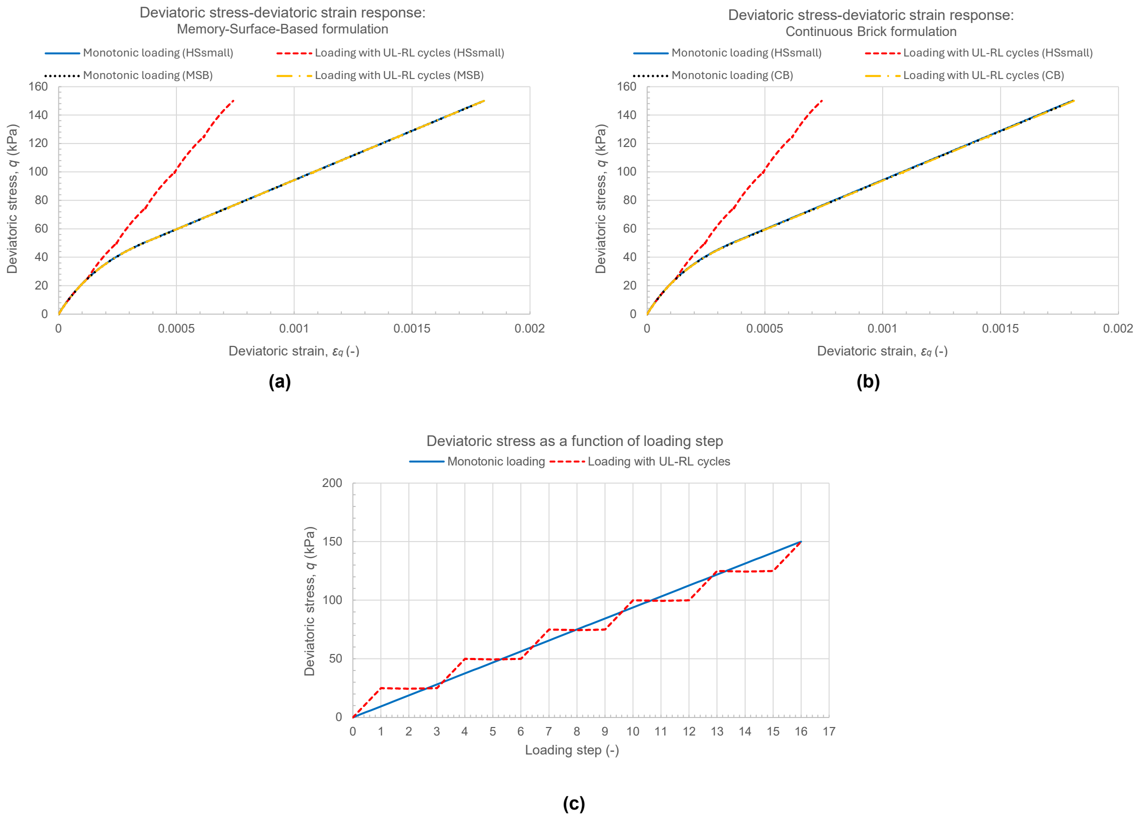

Figure 5.7: Comparison between the results obtained with the HSsmall model with the MSB formulation and the CB formulation for the CD triaxial compression test simulation.

5.2. Undrained direct simple shear test simulation

5.2.1. Results obtained with the Memory-Surface-Based formulation

The results obtained with the MSB formulation are presented in Figure 5.8. One unexpected aspect was identified, as detailed below.

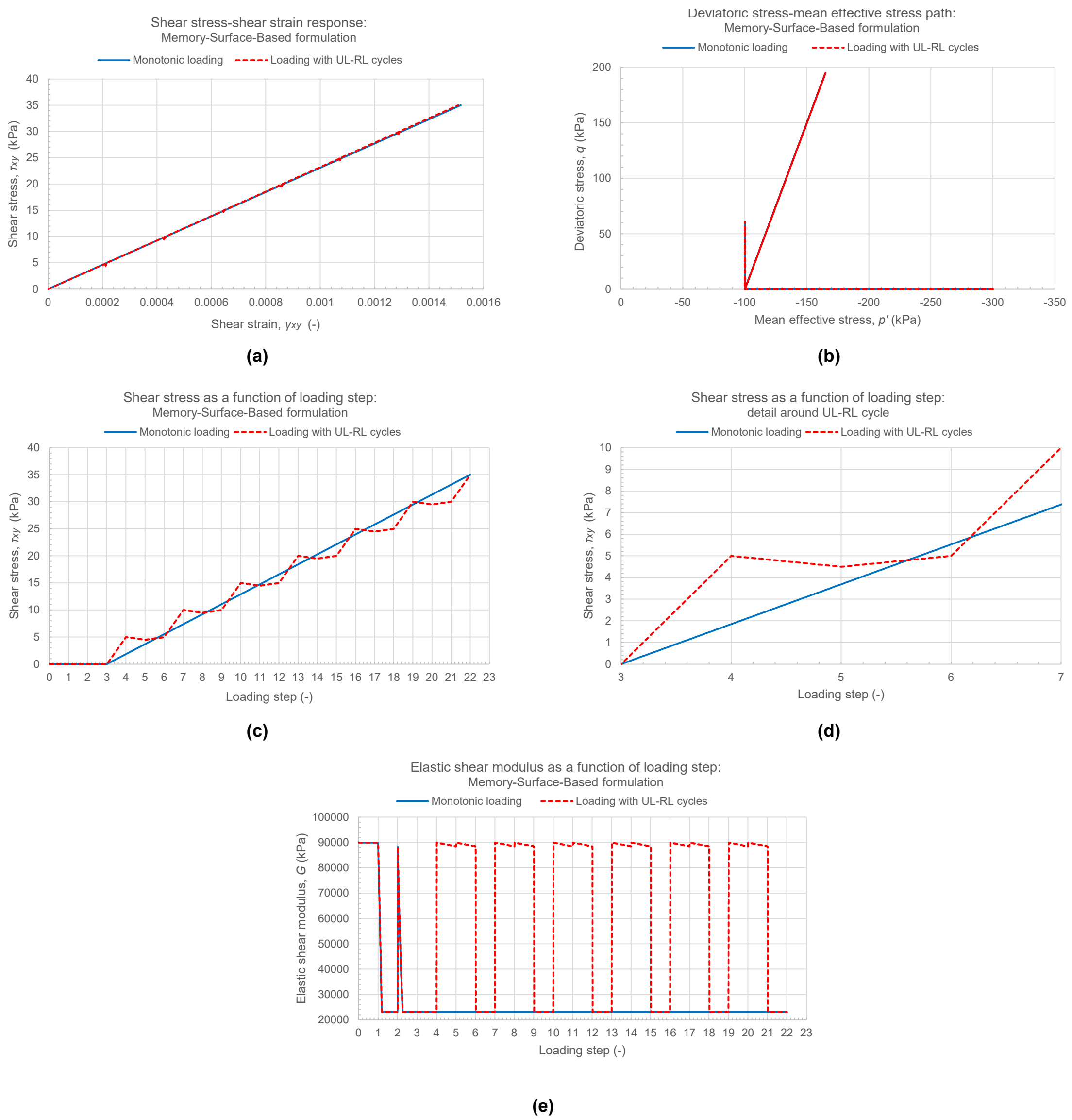

Figure 5.8: Results of the undrained DSS test simulation under stress-independent, purely elastic conditions obtained with the MSB formulation.

Unexpected results

The drained isotropic decompression and drained deviatoric triaxial compression pre-loading (note that these phases are not shown in Figures 5.8a and 5.8c) are followed by a shearing phase simulated under undrained DSS test conditions. The transition from triaxial decompression to DSS conditions at loading step 3 results in a change in the deviatoric loading direction, as illustrated in Figure 5.8b. However, this change in loading direction does not induce a SR,and consequently, the elastic shear modulus is not reset to its high initial value, as shown in Figure 5.8e.

Although no SR occurs, the change in loading direction affects the deviatoric strain loading direction, i.e., the direction of the current deviatoric strain increment $d\mathbf{e}$, which in turn affects the value of the shear strain measure γ_{Hist} and, consequently, the elastic shear modulus, as discussed in Section 2.1.2. As a result, a jump in the elastic shear modulus would be expected at loading step 3. Nonetheless, such a jump is not observed in Figure 5.8e.

Note that SRs in this study may refer to either full or partial SRs. If not specified, a full SR is implied. According to the SR detection algorithm proposed by Benz (2007), a SR is detected whenever a reversal occurs in any of the three eigen directions of $d\mathbf{e}$. The detected SR may be partial, when a reversal occurs in only one or two of the three eigen directions, or full, when a reversal occurs in all three eigen directions. In both cases, the SR results from a rotation of the deviatoric strain path.

The reason why a jump in the elastic shear modulus does not occur at loading step 3 was assessed by inspecting the values of γ_{Hist} at the end of the triaxial decompression and at the onset of the shearing phase. It was observed that, although γ_{Hist} decreases at loading step 3, it remains above the cut-off value (see Section 2.1.2), thereby retaining an elastic shear modulus equal to G_{UR}. This behaviour is consistent with the ingredients of the formulation, and no improvements are required.

Comparison between monotonic loading and loading with unloading–reloading cycles

According to Figure 5.8a, the shear stress-shear strain response obtained under monotonic loading conditions closely coincides with that obtained under loading with UL–RL cycles, indicating that overshooting does not occur.

5.2.2. Results obtained with the Continuous Brick formulation

The results obtained with the CB formulation are presented in Figure 5.9. One unexpected aspect was identified, as detailed below, followed by an explanation of the improvement implemented by PLAXIS.

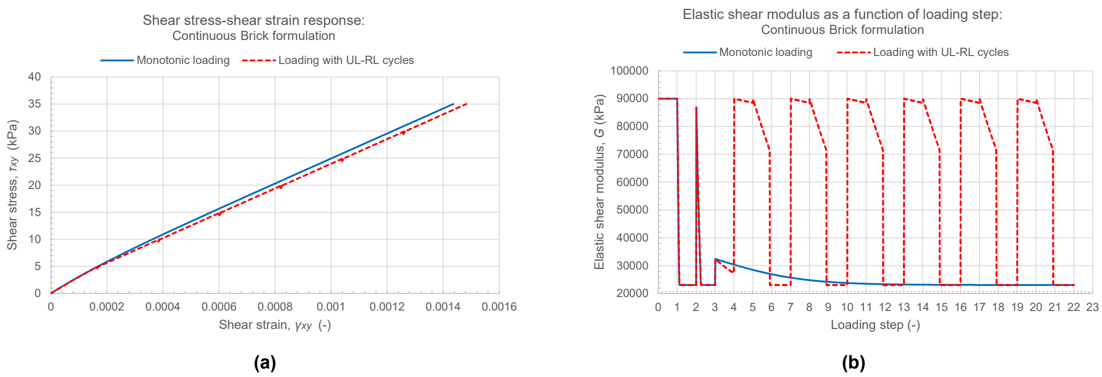

Figure 5.9: Results of the undrained DSS test simulation under stress-independent, purely elastic conditions obtained with the CB formulation.

Unexpected results

In contrast to the results obtained with the MSB formulation, Figure 5.9b shows a sudden increase in the elastic shear modulus at loading step 3, prior to which all bricks, including the cut-off brick, are active. This increase is unexpected, as no SR is detected. Consequently, all brick strings remain taut, i.e., all previously activated bricks remain active, implying that the elastic shear modulus should remain equal to its lower bound G_{UR}.

However, the elastic shear modulus increases because, similarly to the behaviour described in Section 5.2.1, the deviatoric strain loading direction changes at loading step 3. In the CB formulation, the elastic state variable $\Delta\gamma_{actv}$, which represents the shear strain measure accumulation required to activate the next brick, is updated upon such a change in deviatoric strain loading direction. (note that, if the deviatoric strain loading direction changes, it is only logical that the shear strain measure needed to activate the next brick changes).

As explained in Section 2.2.2, $\Delta\gamma_{actv}$ is a component of the formula used to determine γ_{hist} (Formula 2.4). Therefore, when $\Delta\gamma_{actv}$ is updated, γ_{hist} will also be updated, which in turn results in a new value for the elastic shear modulus according to Formula 2.5, also presented in Section 2.2.2.

The idea behind this approach (which, as explained later, was slightly redefined) was to induce a change in the elastic shear stiffness upon a change in deviatoric strain loading direction, similar to the behaviour in the HSsmall model and MSB formulation (recall the partial SRs discussed in Section 5.2.1).

However, it is illogical to continue accumulating shear strain measure required for the activation of the next brick when all bricks are already active. Thus, while the observed behaviour is consistent with the ingredients of the formulation, there remains room for improvement.

Additionally, this flaw resulted in inconsistent behaviour at loading step 6, where the elastic shear modulus at the start of the UL–RL cycle at loading step 4 is not recovered.

Improvements

To prevent this undesired update of the elastic shear modulus from occurring, an improvement was implemented: $\Delta\gamma_{actv}$ is now updated only if there is at least one brick remaining to be activated. The new results are consistent with the improved formulation and no longer exhibit a sudden increase in the elastic shear modulus at loading step 3, as illustrated in Figure 5.10b.

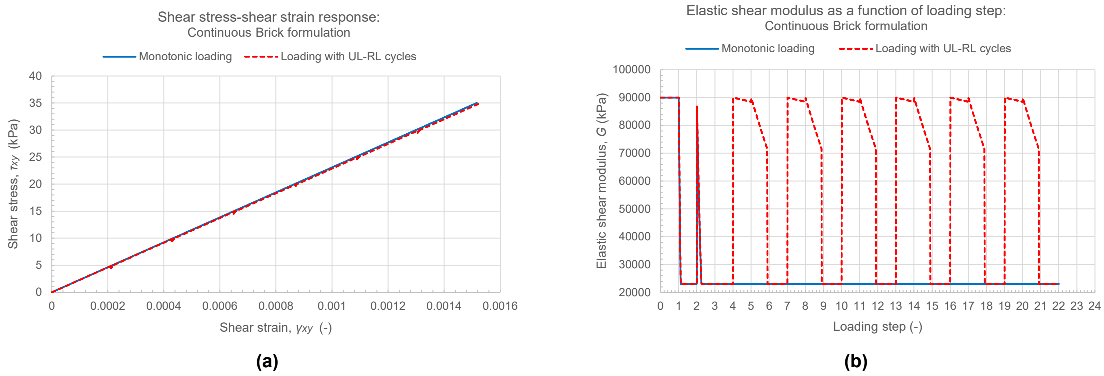

Figure 5.10: Results of the undrained DSS test simulation under stress-independent, purely elastic conditions obtained with the CB formulation after implementing the discussed improvement.

Comparison between monotonic loading and loading with unloading–reloading cycles

Figure 5.9a illustrates that the shear stress-shear strain response obtained under loading with small UL–RL cycles is softer than that under monotonic loading conditions. This behaviour is caused by the fact that a lower stiffness is obtained when closing the UL–RL cycle at loading step 6, instead of recovering the higher stiffness present at the onset of the UL–RL cycle. Figure 5.10a demonstrates that this “undershooting” no longer occurs after implementation of the discussed improvement.

5.2.3. Comparison between the results obtained with the HSsmall model, the Continuous Brick formulation and the Memory-Surface-Based formulation

Figures 5.11a and 5.11b show that both the MSB formulation and the CB formulation are able to prevent overshooting from happening, while the current version of the HSsmall model shows significant overshooting, as can be inferred from the deviation between the red dashed line and the other lines. Note that the red dashed, black dotted, and yellow dashed/dotted lines coincide in Figures 5.11a and 5.11b. Moreover, both the MSB formulation and the CB formulation are consistent with the monotonic response of the HSsmall model. The applied shear stress (Figure 5.11c throughout the simulation is independent of the model or formulation used. Note that the results were obtained using the improved version of the CB formulation.

In the UL–RL case of the HSsmall model, the initial part, up to a shear stress of $5\,\mathrm{kPa}$, has a stiffness equal to the UL–RL elastic shear modulus, as explained Sections 5.2.1 and 5.2.2. At $5\,\mathrm{kPa}$, the first UL–RL cycle occurs (see Figure 5.11c), and the stiffness at the onset of the UL–RL cycle is not restored upon its closure, i.e., overshooting, which explains the change in slope.

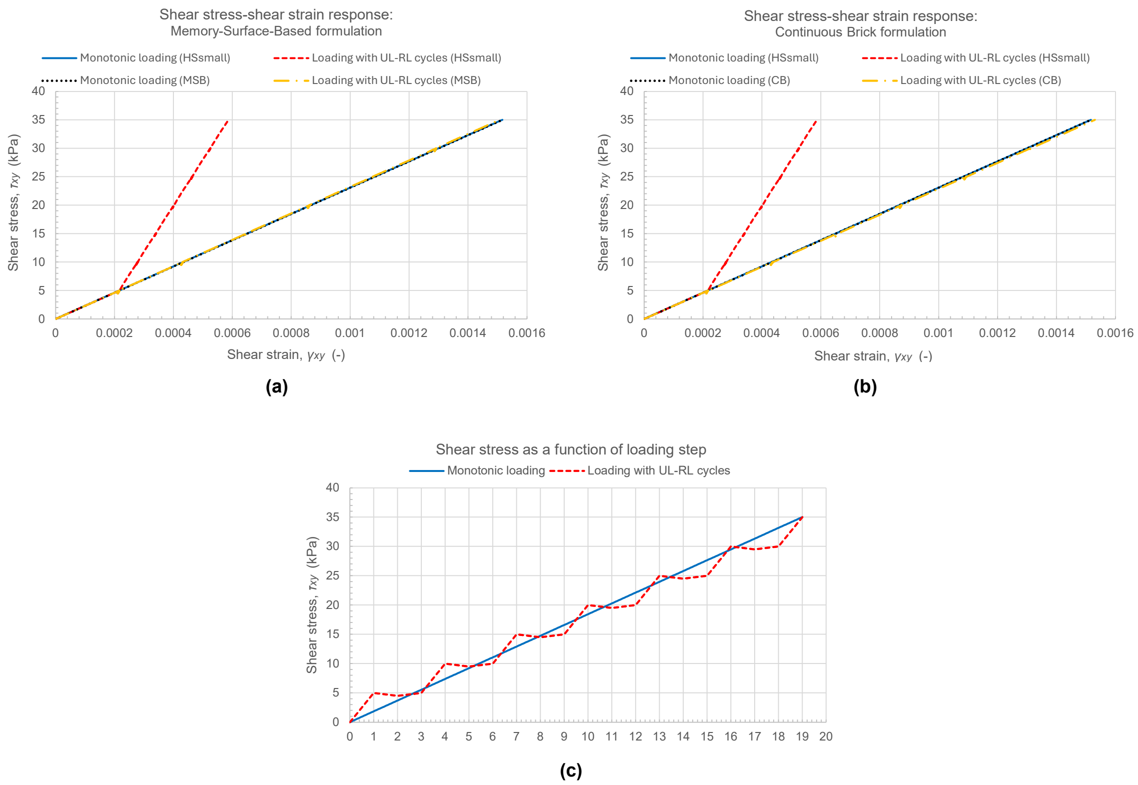

Figure 5.11: Comparison between the results obtained with the HSsmall model with the MSB formulation and the CB formulation for the undrained DSS test simulation.

5.3. Drained oedometer test simulation

5.3.1. Results obtained with the MSB formulation

The results obtained with the MSB formulation are presented in Figure 5.12. Figure 5.12e clearly demonstrates that the results are consistent with the ingredients of the formulation. At each SR, the high initial elastic shear modulus is recovered (at loading steps 2, 3, 4, 5, 7, etc.). Additionally, upon the closure of each UL–RL cycle, the elastic shear stiffness at the onset of the that cycle is recovered. For instance, the stiffness at loading step 4 and 6 is identical, as intended. Moreover, the axial stress-axial strain response obtained under monotonic loading conditions coincides with that under loading with UL–RL cycles, indicating that overshooting does not occur. Note that the axial strains shown in Figures 5.12a to 5.12d are deviatoric rather than total axial strains.

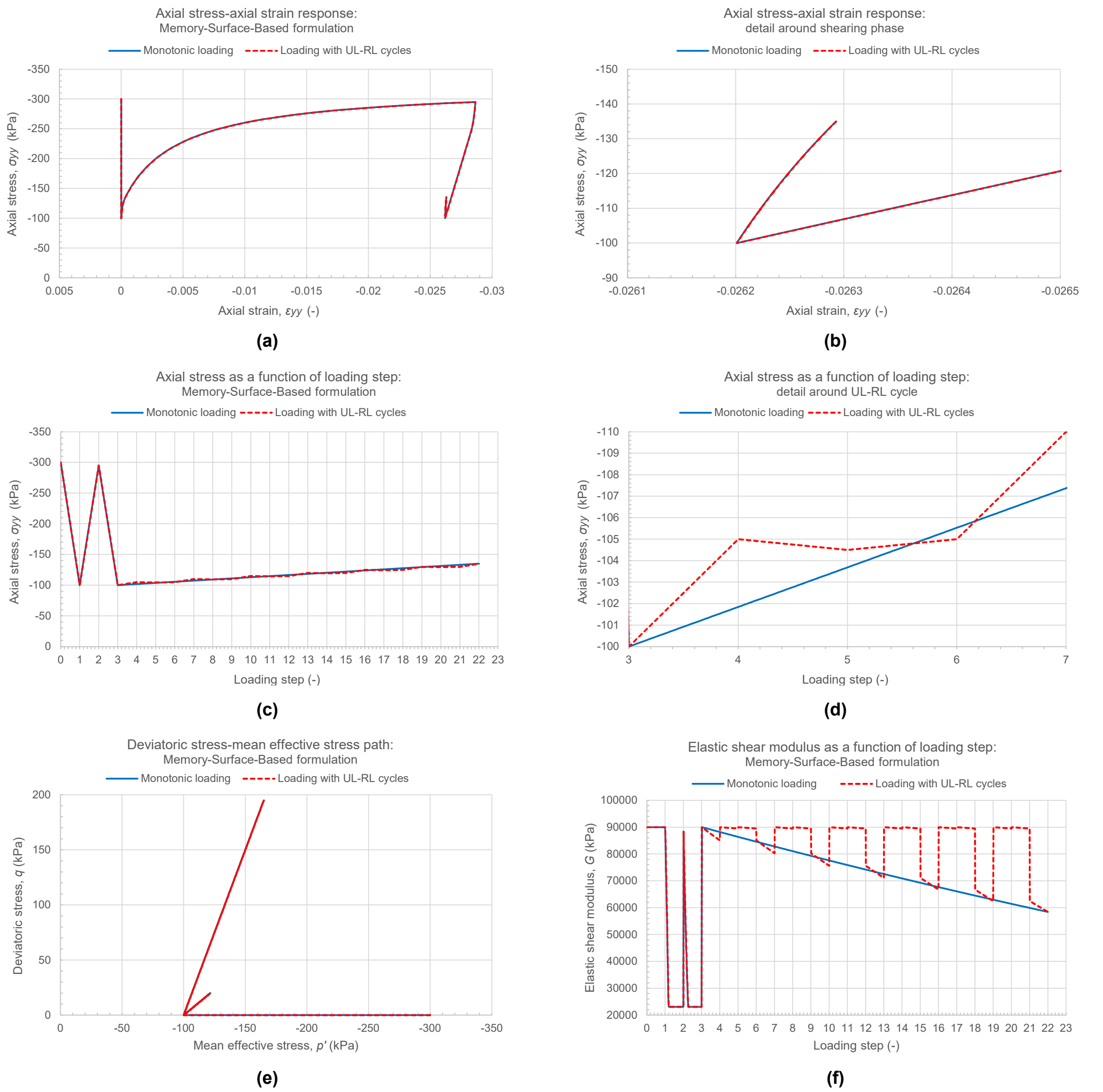

Figure 5.12: Results of the OED test simulation under stress-independent, purely elastic conditions obtained with the MSB formulation.

5.3.2. Results obtained with the CB formulation

The results obtained with the CB formulation are presented in Figure 5.13. One unexpected aspect was identified, as detailed below. The improvement implemented by PLAXIS is subsequently explained.

Unexpected results

Figure 5.13c shows a sudden decrease in the elastic shear modulus just after loading step 15. At this point, the first brick is activated during reloading. According to the formulation, the accumulated shear strain measure is then reset to the value stored at the last SR triggering unloading, as explained in Section 2.2.2. In this case, the value stored at loading step is used, because no brick was active between loading 3 and 15. In fact, when no brick is active upon a SR triggering unloading, the previously stored accumulated shear strain measure is retained, an assumption redefined, as detailed below. In such case, the shear strain measure accumulated prior to the larger UL–RL cycle (in this case, the cycle associated with the pre-loading) would be kept in memory. As a result, when the first brick would be finally activated, the current accumulated shear strain measure would be set equal to the large value stored in memory, therefore leading to a sudden drop in the elastic shear modulus. However, the larger UL–RL cycle has not yet been closed at that point, leading to a too small elastic shear stiffness. In conclusion, although the behaviour is consistent with the ingredients of the formulation, the formulation requires improvement.

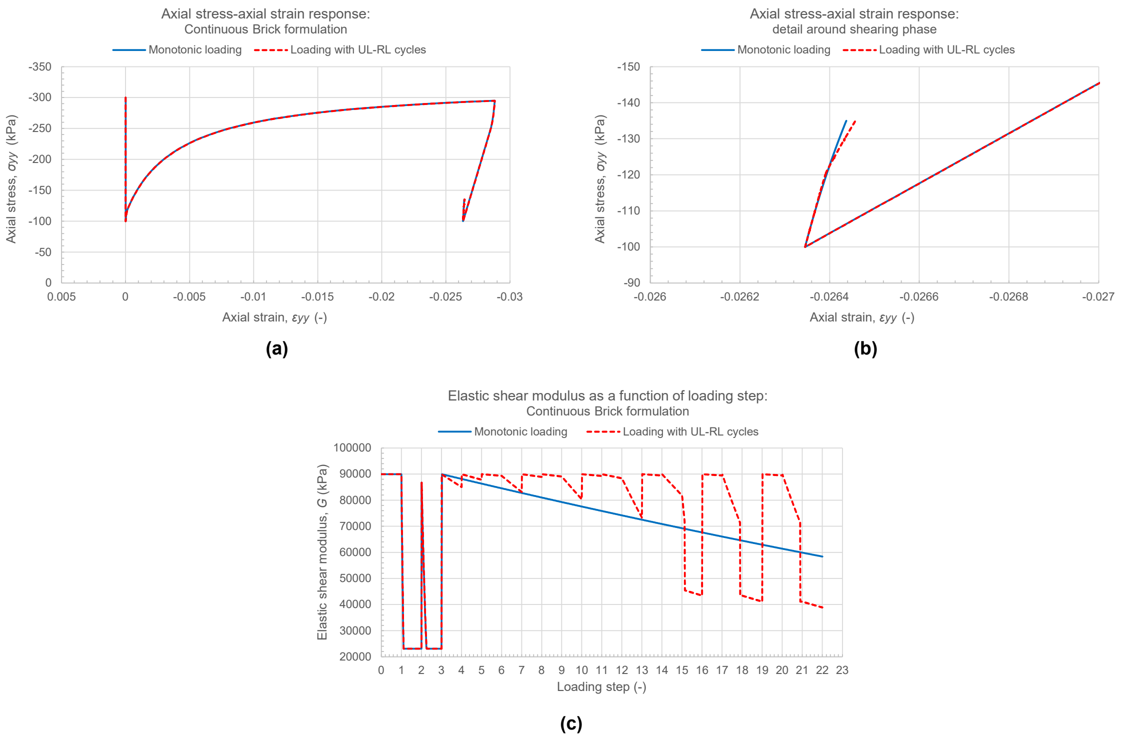

Figure 5.13: Results of the CD triaxial compression test simulation under stress-independent, purely elastic conditions obtained with the CB formulation after implementing the discussed improvements.

Improvements

Rather than retaining the previously stored accumulated shear strain measure at a SR triggering unloading when no brick is active, the stored value is now reset to zero. Consequently, when the first brick is activated just after loading step 15 in Figure 5.14c, a sudden decrease in the elastic shear modulus no longer occurs.

Note that before the activation of the first brick (just after loading step 15), the elastic shear modulus obtained at the onset of an UL–RL cycle is not restored upon its closure (for instance the stiffness at loading step 7 and 9 is not identical in Figure 5.14c). This is due to the fact that the shear strain measure at the last SR triggering unloading is no longer stored when no brick is activated. After activation of the first brick, the shear strain measure at a SR triggering unloading is stored and the elastic shear modulus at the onset of the UL–RL cycle is recovered upon its closure (see loading steps 16 and 18 in Figure 5.14c).

In conclusion, as a consequence of this needed improvement, the formulation no longer retains the shear strain measure corresponding to larger previous UL–RL cycles in memory, even when no brick is activated during a small UL–RL cycle. This may result in non-negligible overshooting under certain conditions. However, this drawback can easily be resolved by shortening the string length of the first brick, i.e., placing the first brick higher on the elastic modulus reduction curve. This will lead to an activation of the first brick at smaller shear strains. Testing this solution lies outside the scope of this study. Note that this improvement does not affect the previously obtained results.

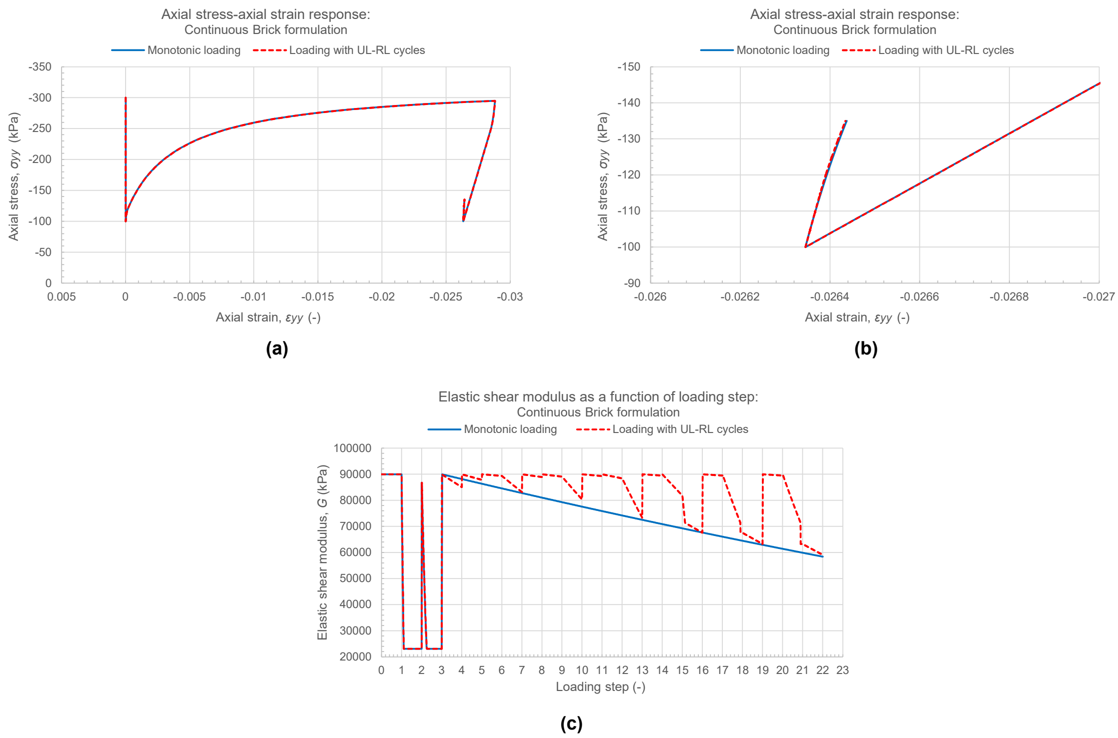

Figure 5.14: Results of the CD triaxial compression test simulation under stress-independent, purely elastic conditions obtained with the CB formulation after implementing the discussed improvements after implementing the discussed improvements.

Comparison between monotonic loading and loading with unloading–reloading cycles

Figure 5.13b shows that the axial stress-axial strain response obtained under loading with small UL–RL cycles is softer than that under monotonic loading when using the version of the CB formulation that does not include the discussed improvement. This behaviour is caused by the drop in the elastic shear modulus when activating the first brick, as discussed. Figure 5.14b demonstrates that this "undershooting" no longer occurs when using the improved version.

The improved results may show very slight overshooting caused by the drawback discussed in the previous paragraph: the elastic shear modulus at the onset of an UL–RL cycle is no longer recovered upon its closure when no brick is active (between loading steps 3 and 15). However, in this specific case, the extent of overshooting caused by this drawback is of a negligible level.

5.3.3. Comparison between results obtained with the Hardening Soil small-strain model, the Continuous Brick formulation and the Memory-Surface-Based formulation

Figure 5.15a shows that the results obtained with the MSB formulation are consistent with the monotonic response of the HSsmall model, as the blue solid, black dotted, and yellow dashed/dotted lines coincide. For the CB formulation (Figure 5.15b), only the black dotted and yellow dashed/dotted lines coincide, indicating that its response remains consistent with the HSsmall model under monotonic loading (this does not hold under elasto-plastic conditions, as discussed in Section 2.2.2), but that overshooting occurs, as the yellow dashed/dotted line deviates. The overshooting observed in the CB formulation results from the drawback described in Section 5.3.2. The applied (deviatoric) axial stress (Figure 5.15c) is independent of the model or formulation used. Note that the results were obtained using the improved version of the CB formulation.

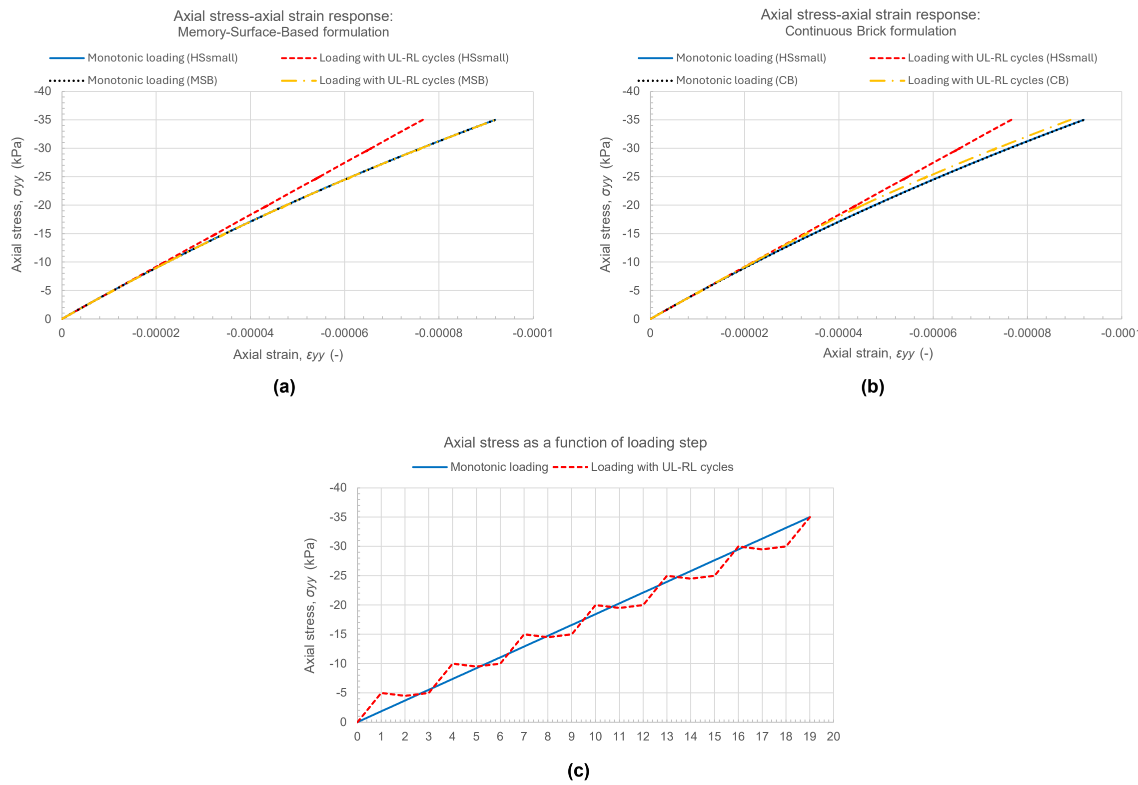

Figure 5.15: Comparison between the results obtained with the HSsmall model with the MSB formulation and the CB formulation for the OED test simulation.

5.4. Simulations under elasto-plastic, stress-dependent conditions

This section briefly presents the findings obtained from the simulations of the CD triaxial compression test, the undrained DSS test, and the drained OED test under stress-dependent, elasto-plastic conditions, i.e., without pre-loading. These simulations were performed using the final version of the proposed formulations, namely the version incorporating all previously discussed improvements. The figures presenting the results are provided in Appendix B.

For almost all test simulations, the deviatoric stress-deviatoric strain response under monotonic loading coincides with that of the loading case including UL–RL cycles, indicating that overshooting does not occur. This demonstrates that the formulations effectively mitigate overshooting under elasto-plastic, stress-dependent conditions at a single stress point level.

Unexpected behaviour was identified only in the CD triaxial compression test simulation using the MSB formulation. The formulation failed to recover the elastic shear modulus at the onset of the first UL–RL cycle upon its closure, which is inconsistent with the ingredients of the formulation. This inconsistency was resolved by reducing a numerical tolerance. The improved version no longer exhibits this inaccuracy. A more detailed explanation of the unexpected behaviour is provided in Appendix B.

5.5. Tailored consolidated drained triaxial compression test simulation with nested unloading–reloading cycles to assess the formulations' ability to retain memory

This section presents the results of the tailored CD triaxial compression test simulations that include nested UL–RL cycles, specifically designed to assess whether the formulations are capable of retaining the memory of more than a single cycle. Recall from Section 3.3.1 that stress-independent, purely elastic (i.e., including pre-loading) conditions apply.

In Section 3.3.1, the modelling sequence was briefly introduced. However, it is discussed here in more detail to provide a clearer understanding of the test setup and the obtained findings. Figure 5.16 shows the applied deviatoric loading throughout the simulation.

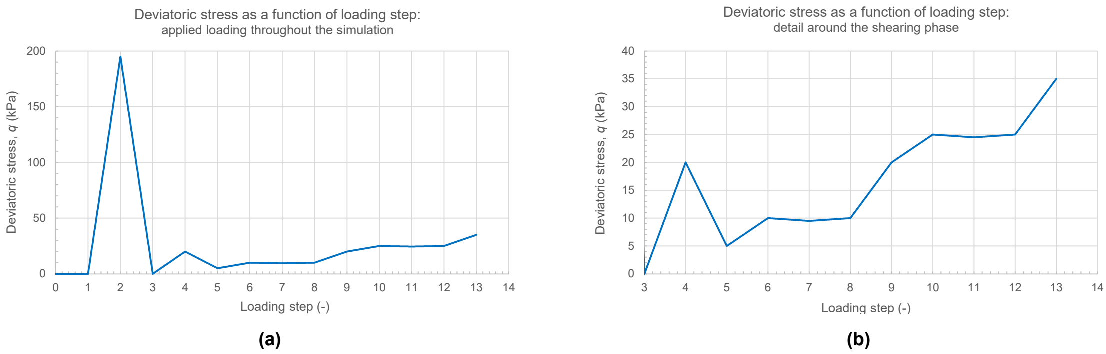

Figure 5.16: Applied deviatoric loading throughout the simulations.

Pre-loading occurs from loading steps 0 to 3, followed by a shearing phase. A SR triggering unloading occurs at loading step 4. At this point, both formulations store the variable required to reproduce the corresponding elastic shear modulus upon closure of the corresponding cycle, either the accumulated shear strain measure in the CB formulation, or the deviatoric strain history tensor in the MSB formulation. Reloading begins at loading step 5. From loading steps 6 to 8, a smaller UL–RL cycle occurs before the larger cycle is closed at loading step 9. Note that when referring to the larger UL–RL cycle in this section, the cycle starting at loading step 4 is meant, rather than the one associated with the pre-loading (starting at loading step 2).

Figures 5.17 and 5.18 show the test results obtained with the MSB formulation and the CB formulation, respectively. For both formulations, the results demonstrate that, when the larger cycle is closed, the elastic shear modulus at the onset of that UL–RL cycle is not restored. This is inferred from the fact that the stiffness at loading steps 4 and 9 is not identical (see Figures 5.17d and 5.18d. This behaviour results from the overwriting of the previously stored memory (that at loading step 4) when a new SR triggering unloading occurs (in this case, the one at loading step 6). In conclusion, neither formulation is capable of retaining the memory of more than a single cycle, which can potentially result in non-negligible overshooting.

For the MSB formulation, a slight difference in the slope of the deviatoric stress-deviatoric strain response is observed between overloading and initial loading, i.e., when the larger cycle is closed, at a deviatoric stress of $20\,\mathrm{kPa}$ (see the point indicated with the black arrow in Figures 5.17b and 5.17c). This occurs because the stiffness at the onset of the cycle is not recovered upon its closure, as previously explained, indicating overshooting. If overshooting did not occur, overloading would continue to follow the same trend as the initial loading.

For the CB formulation, no difference in the slope of the deviatoric stress-deviatoric strain response is observed when closing the larger cycle (see the point indicated with the black arrow in Figures 5.18b and 5.18c). However, if the formulation were able to memorise the larger cycle, the deviatoric stress-deviatoric strain response would show a reduction in the slope at that point, as the lower stiffness at the onset of the UL–RL cycle would then be recovered.

Although the difference in stiffness between the onset and closure of the larger UL–RL cycle is small in this specific case for both the MSB formulation and the CB formulation, it could become more pronounced under different test conditions, potentially leading to more significant overshooting effects.

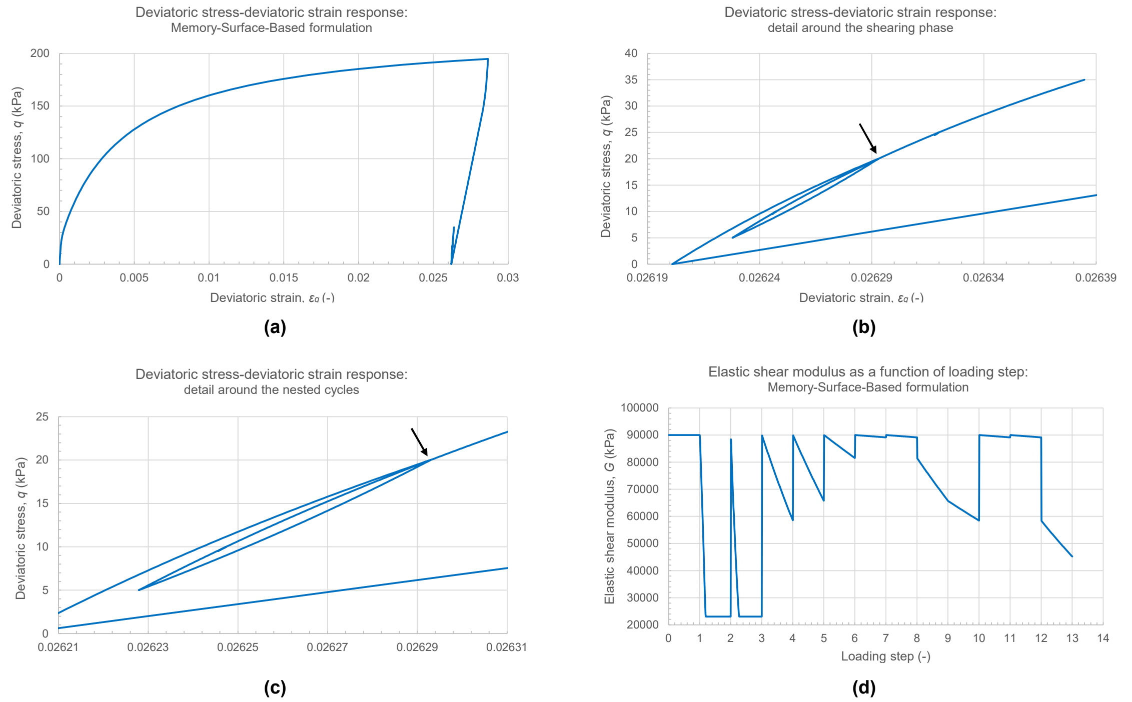

Figure 5.17: Results of the tailored CD triaxial compression test with nested UL-RL cycles obtained with the MSB formulation.

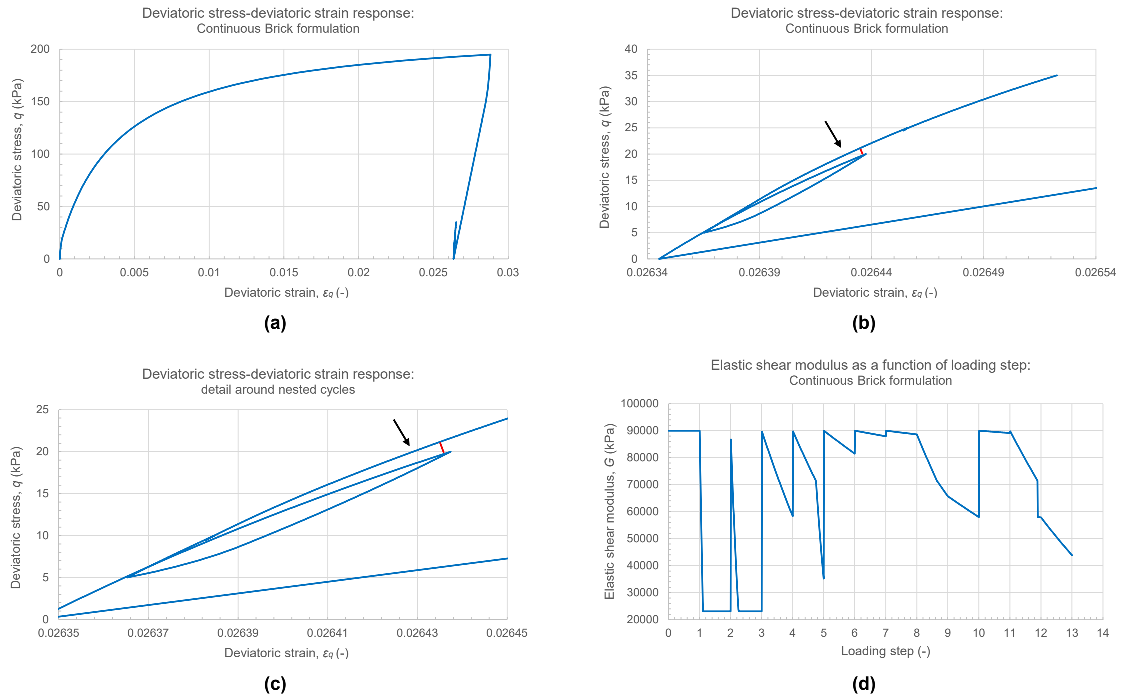

Figure 5.18: Results of the tailored CD triaxial compression test with nested UL-RL cycles obtained with the CB formulation.

Looking more closely at the smaller UL–RL cycle (from loading steps 6 to 8):

1. In the MSB formulation, the elastic shear modulus at loading step 6 is identical to that at loading step 8 (see Figure 5.17d), indicating that the stiffness at the onset of the smaller UL–RL cycle is restored upon its closure. Therefore, this cycle does not result in overshooting.

2. In the CB formulation, the shear moduli at loading steps 6 and 8 are not identical (see Figure 5.18d). This difference was expected to result from the drawback within the CB formulation explained in Section 5.3.2, namely that the shear strain measure accumulated prior to a cycle is not stored when no brick is active at its onset, resulting in overshooting. The overshooting caused by this drawback is clearly visible in Figures 5.18b and 5.18c as the difference between the overloading (top line) and the initial loading (second line from top), indicated by the red line. It should be noted that this overshooting is therefore not caused by the drawback addressed in this section, i.e., the inability to retain the memory of more than a single cycle, but rather by the drawback discussed in Section 5.3.2.

5.6. Tailored consolidated drained triaxial test simulation to investigate the detection of strain reversals in triaxial extension and compression

Since no unexpected behaviour was identified in this test, the detailed interpretation of the results is provided in Appendix C for conciseness. However, the main findings are briefly discussed in this Section.

Under triaxial compression conditions, a decreasing deviatoric stress indicates loading/reloading, whereas an increasing value indicates unloading. Under triaxial extension conditions, these interpretations are reversed. Both the MSB formulation and the CB formulation correctly capture this behaviour by accurately classifying SRs as triggering unloading or reloading in triaxial compression and extension.

Note that the criterion for this classification was refined for the CB formulation in Section 5.1.2. For the MSB formulation, the criterion remains unchanged from that described in Section 2.2.1.

5.7. Sub-conclusion

At the single stress point level, both formulations are effective in preventing or minimising overshooting under both stress-independent, purely elastic conditions and stress-dependent, elasto-plastic conditions. Moreover, under purely elastic conditions, they yield a response consistent with that of the HSsmall model under monotonic loading. No noticeable difference in computational efficiency between the two formulations was observed in terms of runtime.

However, differences were identified in their robustness and the simplicity of their frameworks. In addition, in both formulations a drawback related to retaining the memory of only a single UL–RL was identified, along with a second drawback that applies only to the CB formulation.

A summary of all the issues encountered in the single stress point simulations together with their solutions is provided in Appendix D, except for the two drawbacks as no solution is implemented.

Finally, it was observed that both formulations adjust their elastic shear modulus upon a change in the deviatoric strain loading direction, which will become of greater importance in Chapter 6.

Robustness and simplicity

The MSB formulation appears to be more robust and easier to interpret than the CB formulation. While almost no improvements were required for the MSB formulation, improvements were necessary for the CB formulation at each fundamental laboratory soil test simulation. This suggests that the CB formulation is more sensitive to specific test conditions, likely due to its more complex framework.

Drawback: nested UL–RL cycles

Both the CB formulation and the MSB formulation are capable of memorising only a single UL–RL cycle: the one associated with the most recent SR triggering unloading.

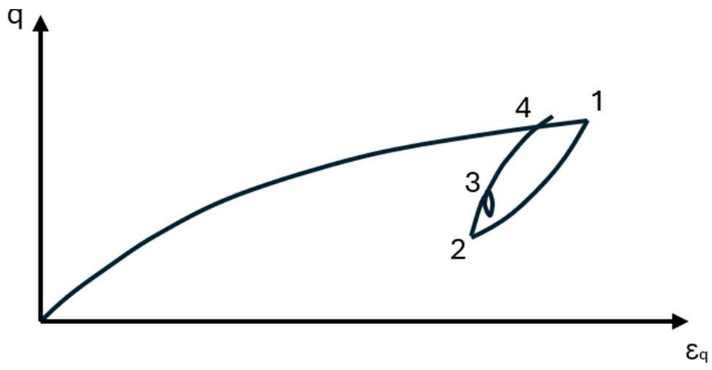

Figure 5.19: Visualisation of the drawback exhibited by both formulations: inability to retain the memory of more than a single cycle.

Under specific circumstances, this memory constraint can result in overshooting, as illustrated in Figure 5.19. In this figure, monotonic loading is interrupted by an UL–RL cycle at point 1. At point 2, a SR triggering reloading occurs, and the high initial elastic shear modulus is restored. At point 3, reloading is interrupted by a smaller UL–RL cycle. As a result, the memory stored at the reversal at point 1 is overwritten by that at point 3. When the smaller UL–RL cycle is closed (i.e., when the deviatoric stress-deviatoric strain response returns to point 3), the formulation restores the stiffness corresponding to that at the onset of this smaller cycle. Consequently, the formulation can no longer restore the elastic shear modulus associated with the onset the larger cycle (i.e., starting at point 1) upon its closure. Nevertheless, the response is still improved compared to the original HSsmall model, where overshooting would already occur at point 3 (and therefore earlier than point 4), which would mean that the response at point four would be even stiffer.

The described behaviour becomes more problematic when the UL–RL cycle starting at point 1 has a small magnitude (see Section 4), as only minimal reduction could have occurred during reloading. Consequently, the difference between the stiffness at the onset of the larger UL–RL cycle (at point 1) and upon its closure (at point 4) becomes larger. In other words, when a situation such as that shown in Figure 5.19 occurs when using the MSB or CB formulation, overshooting behaviour similar to that of the HSsmall model would be observed if, in that case, the smaller UL–RL cycle were absent. The nested cycle therefore effectively counteracts the intended improvement. Moreover, the issue becomes more pronounced when multiple nested cycles occur.

While this problem could theoretically be resolved by memorising multiple cycles, doing so would require a substantial increase in the number of elastic state variables, consequently in computer memory consumption.

An advantage of the CB formulation is that this approach has already been implemented, as a user option, in its source code. The number of UL–RL cycles for which the formulation can retain memory is governed by a model parameter that specifies the number of bricks to be used, which was hard-coded as 2 in this study: the cut-off brick and one additional brick. Six elastic state variables are introduced per each additional brick. However, the effectiveness of this approach in mitigating the identified drawback has not yet been assessed.

For the MSB formulation, the drawback could be addressed by introducing multiple Memory Surfaces. However, its source code would firstly need to be generalised to be able to use any user-defined number of Memory Surfaces. Moreover, note that per each additional Memory Surface, more than just six elastic state variables would be needed, which means that adding additional memory is more expensive for the MSB formulation than for the CB formulation.

In conclusion, for the MSB formulation, the solution would still need to be both generalised and tested, whereas for the CB formulation, only testing is still required. Before doing so, it should first be assessed, by performing additional test cases, whether this drawback can not be considered negligible in practical geotechnical analyses.

Drawback: overshooting due to inactive brick during UL–RL cycles
Within the CB formulation, at least one brick must be active for the formulation to store the memory when a SR triggering unloading occurs. Consequently, overshooting arises when UL–RL cycles occur while no brick is active. This is not considered a major drawback, as it can theoretically be resolved by shortening the string length of the first brick, i.e., by positioning the first brick higher on the elastic modulus reduction curve. This adjustment would lead to the activation of the first brick at smaller shear strains. However, it should be verified whether this proposed approach effectively resolves the issue, and the optimal string length of the first brick should be determined.

6

Boundary value problem

This chapter presents and discusses the results of the BVP introduced in Section 3.3.2. The first section examines the results obtained with the original HSsmall model, with the aim of identifying the cause of the UL–RL cycles responsible for overshooting. The second and third sections discuss the results obtained with the MSB formulation and the CB formulation, respectively. The fourth section demonstrates the impact of nested UL–RL cycles on the extent of overshooting in the BVP. These nested cycles reveal a limitation of both formulations, as discussed in Section 5.7. The chapter concludes with final remarks on the BVP.

6.1. Cause of the unloading–reloading cycles

The BVP involves two physical processes that occur simultaneously. However, they are described separately below, with each process considered independently:

1. **Excavation**

   Excavation on the left side of the sheet pile wall removes part of the overburden, thereby reducing the load on the subsoil. More specifically, the total stress distribution in the subsoil changes: the total stresses in the underlying soil decrease, leading to unloading of the surrounding soil. When soil is unloaded, it tends to expand. However, due to the extremely low permeability of the glacial till, this expansion is partly constrained because the availability of water is required for soil to swell. The tendency to expand is counteracted by a decrease in pore water pressure. From a physical perspective, the pore water effectively exerts a tensile force on the soil skeleton. Because the hydraulic boundary conditions remain unchanged, the steady-state pore pressure profile does not change. Consequently, when the pore water pressure decreases, a deviation from the steady-state profile is introduced. This deviation is referred to as *excess pore water suction*, i.e., positive excess pore water stress. Note that compression is negative in PLAXIS 2D.

   Part of the reduction in total stress is directly transferred to the soil skeleton, leading to a reduction in effective stress and resulting in some instantaneous heave.

   Over time, water may flow towards areas prone to swelling, leading to an increase in pore water pressure and a gradual restoration of the steady-state profile. This increase in pore water pressure reduces the effective stress, which in turn causes additional heave. In other words, the portion of the total stress reduction that was initially carried by the pore water is gradually transferred to the effective stress over time.

   The evolution of stresses due to excavation can be expressed by the following equations:

$$\boldsymbol{\sigma} = \boldsymbol{\sigma}' + \boldsymbol{u} \tag{6.1}$$
$$\boldsymbol{\sigma} - \Delta\boldsymbol{\sigma} = (\boldsymbol{\sigma}' - \beta\Delta\boldsymbol{\sigma}) + (\boldsymbol{u} - \eta\Delta\boldsymbol{\sigma}) \tag{6.2}$$
$$\boldsymbol{\sigma} - \Delta\boldsymbol{\sigma} = (\boldsymbol{\sigma}' - (\eta + \beta)\Delta\boldsymbol{\sigma}) + \boldsymbol{u} \tag{6.3}$$
$$\eta + \beta = 1 \tag{6.4}$$

where:

$\boldsymbol{\sigma}$	total stress vector [kPa]
$\Delta\boldsymbol{\sigma}$	total stress change due to excavation [kPa]
$\boldsymbol{\sigma}'$	effective stress vector [kPa]
$\boldsymbol{u}$	pore water pressure [kPa]
η, β	dimensionless coefficients satisfying $\eta + \beta = 1$

Equation 6.1 represents the initial stress state prior to excavation. Although a *fully coupled flow-deformation analysis* in PLAXIS uses Bishop's definition of effective stress , Terzaghi's definition is used in this explanation for simplicity (Bentley Systems, 2024). Although in a Equation 6.2 describes the stress state immediately after excavation. The parameter η denotes the portion of the total stress reduction that is instantaneously carried by the pore water, whereas β denotes the portion carried by the soil skeleton. Equation 6.3 represents the stress state at the end of consolidation, when the portion of the total stress reduction initially carried by the pore water has been fully transferred to the soil skeleton. Finally, Equation 6.4 provides the condition that the parameters η and β must satisfy.

2. **Dewatering**
As explained in Section 3.3.2, the excavation is simulated as dry by prescribing the hydraulic head at the bottom of the excavation corresponding to the current excavation phase such that the pore water pressure equals $0\,\mathrm{kPa}$. In other words, the water level inside the excavation is lowered, thereby modifying the hydraulic boundary conditions and establishing a new steady-state pore water pressure distribution. Due to the very low permeability of the glacial till, the soil requires time to adjust to this new steady-state profile, which results in temporary negative excess pore water pressures. Over time, these excess pore water pressures gradually dissipate and are transferred to the soil skeleton. Consequently, the effective stresses increase, leading to settlement.

The evolution of stresses due to dewatering can be expressed by the following equations:

$$\boldsymbol{\sigma} = \boldsymbol{\sigma}' + \boldsymbol{u} \tag{6.5}$$
$$\boldsymbol{\sigma} = (\boldsymbol{u}_{\text{steady-state}} + \boldsymbol{u}_{\text{excess}}) + \boldsymbol{\sigma}' \tag{6.6}$$
$$\boldsymbol{\sigma} = \boldsymbol{u}_{\text{steady-state}} + (\boldsymbol{\sigma}' + \boldsymbol{u}_{\text{excess}}) \tag{6.7}$$

where:

$\boldsymbol{u}_{\textbf{steady state}}$	steady-state pore water pressure [kPa]
$\boldsymbol{u}_{\textbf{excess}}$	excess pore water pressure [kPa]

Equation 6.5 represents the initial stress state prior to dewatering. Equation 6.6 describes the stress state immediately after dewatering. Finally, Equation 6.7 represents the stress state at the end of consolidation, when the negative excess pore pressures have been fully transferred to the soil skeleton.

During the intermediate consolidation phases, the hydraulic boundary conditions remain unchanged and no additional overburden is removed from the subsoil, allowing the soil to adjust to the new equilibrium. To assess whether consolidation induced by dewatering could be responsible for the minor settlements observed during the intermediate consolidation phases, it must be verified whether the development of negative excess pore water pressures caused by dewatering outweighs the positive excess pore water pressures generated by excavation. If this condition is not met, only heave will occur during the intermediate consolidation phases, as the effective stress keeps decreasing.

Figure 6.1 shows that the excess pore water pressure is positive during the calculation step in which one of the minor settlements is observed at node 225 (indicated with the red arrow in Figure 6.1). The excess pore water pressure is positive not only at node 225 but also throughout the entire domain on the left side of the sheet pile wall. This demonstrates that the development of negative excess pore water pressures due to dewatering does not dominate over the positive excess pore water pressures generated by excavation. Therefore, it is highly unlikely that dewatering-induced consolidation is the cause of the UL–RL cycles.

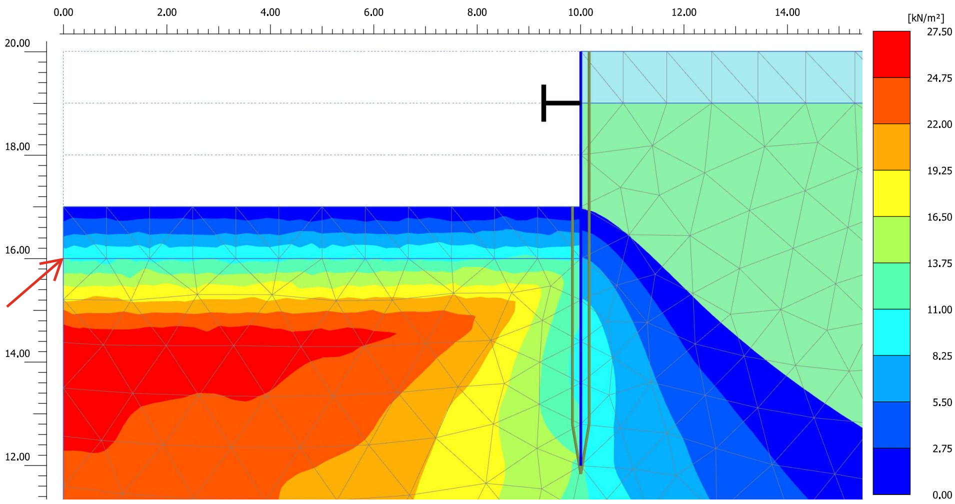

Figure 6.1: Excess pore water pressure for the calculation step associated with the minor settlement at node 225 (scaled up 0.02 times, pressure = negative, $t = 3.23\,\mathrm{d}$).

Several simulations were performed to further investigate the origin of the UL–RL cycles. By applying different types of analysis and model configurations, the factors that have the greatest influence on the extent of overshooting, and thus are likely responsible for the UL–RL cycles, could be identified.

Three types of analysis available in PLAXIS 2D were considered:

1. **Fully coupled flow-deformation (FCFD) analysis**
   If the excavation phases are simulated using a *fully coupled flow-deformation* analysis, the intermediate consolidation phases and the final consolidation phase are simulated using a *fully coupled flow-deformation* analysis as well. A short description of a *fully coupled flow-deformation* analysis is provided in Section 3.3.2.
2. **Plastic undrained (PU) analysis**
   The excavation phases are simulated using a *Plastic* undrained analysis. In a *Plastic* analysis, elasto-plastic deformations are calculated while time-dependent changes in pore water pressures are not considered. Because the analysis is undrained, excess pore water pressures are generated instantaneously and no volume change is allowed.
3. **Consolidation (C) analysis**
   If the excavation phases are simulated using a *Plastic* undrained analysis, the intermediate consolidation phases and the final consolidation phase are simulated using a *Consolidation* analysis. In a *consolidation* analysis, the generation and dissipation of excess pore water pressures are calculated over time for soils whose behaviour lies between fully drained and fully undrained conditions.

For a more detailed description of each type of analysis, the reader is referred to Bentley Systems (2024).

The analysis types were combined with two sets of modifications: (i) to the construction sequence, namely excavation and dewatering or excavation only, and (ii) to the sheet pile wall behaviour, namely a fixed wall or a wall that can deform.

Table 6.1: Simulations performed to identify the cause of the UL–RL cycles.

Type of analysis	Construction sequence	Sheet pile wall behaviour	Overshooting [%]
FCFD	Excavation and dewatering	Free	14.0
FCFD	Excavation	Free	10.7
FCFD	Excavation and dewatering	Fixed	3.1
PU + C	Excavation and dewatering	Free	10.9
PU + C	Excavation and dewatering	Fixed	0.7

Table 6.1 summarises the applied combinations and the corresponding extents of overshooting. The extent of overshooting is quantified as a percentage: the difference in vertical displacement at node 225 (see Figure 3.2) between the monotonic loading case and the loading case including intermediate consolidation phases, after a final consolidation phase of $50\,000\,\mathrm{d}$, divided by the vertical displacement of the monotonic loading case, multiplied by 100%.

It should be noted that differences in the extent of overshooting cannot be solely attributed to the number of UL–RL cycles, as they also depend on the amplitude and the timing of the cycles along the deviatoric stress-deviatoric strain response (see Section 4. The timing matters because the soil exhibits elasto-plastic rather than purely elastic behaviour. As discussed in Section 4, overshooting becomes less pronounced further along the deviatoric stress-deviatoric strain response, where the plastic component increasingly dominates over the elastic component. This is because, overshooting is associated with the elastic part of the response. Even so, the simulations reveal several interesting trends.

The main trend identified is the significant reduction in overshooting when the sheet pile wall is fixed. Since consolidation during the intermediate consolidation phases does not cause the UL–RL cycles, as demonstrated in this section, and newly imposed loading or hydraulic conditions cannot be responsible because both dewatering and excavation are paused, and the model conditions therefore remain unchanged, the UL–RL cycles are most likely caused by numerical redistributions of stresses. This effect appears to become more pronounced as model complexity increases, for instance when both excavation and dewatering are simulated instead of excavation only, when flow and deformation are coupled, and when deformation of the wall is allowed. Among these factors, it is evident that deformation of the wall has the strongest influence.

In general, these stress redistributions become apparent when the model is allowed time to resolve stress imbalances and adjust to a new equilibrium, i.e., when no changes to the model conditions are imposed.

This indicates that these stress redistributions, and consequently UL–RL cycles, are not confined to the intermediate consolidation phases but may also occur during the final consolidation phase, which is included in both the monotonic modelling sequence and the modelling sequence with intermediate consolidation phases.

6.2. Results obtained with the Memory-Surface-Based formulation

This section presents the results of the BVP simulated with the MSB formulation.

6.2.1. Vertical displacement at node 225

Figure 6.2 illustrates how the vertical displacement at node 225 evolves over time for both the monotonic loading case and the loading case with intermediate consolidation phases. Figure 6.2a presents the results over a period of $100\,\mathrm{d}$, while Figure 6.2b provides a detailed view of the excavation period starting at $1.5\,\mathrm{d}$. The monotonic excavation is completed at $t = 3.5\,\mathrm{d}$, whereas the excavation with intermediate consolidation phases reaches completion at $t = 3.8\,\mathrm{d}$.

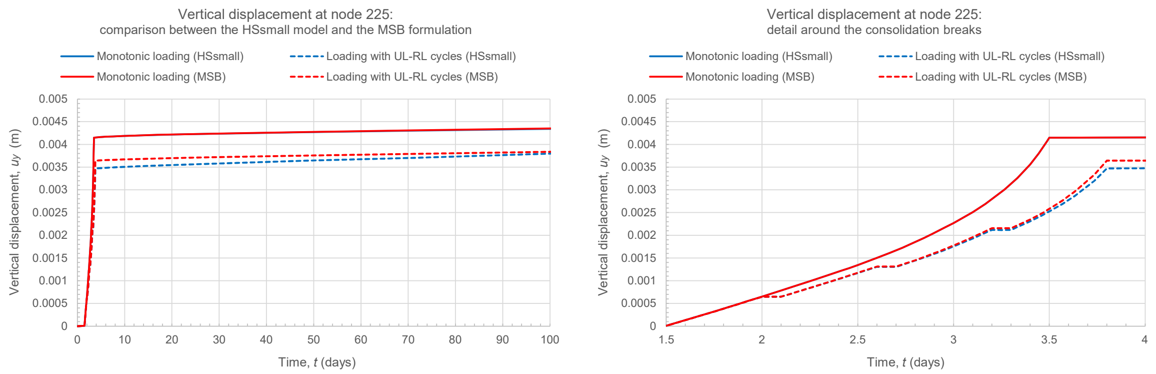

(a) Results presented up to 100 days.

(b) Results presented up to 4 days.

Figure 6.2: Evolution of the vertical displacement at the centre of the final excavation bottom (node 225) simulated with the HSsmall model and MSB formulation, for both the monotonic loading case and the loading case with UL–RL cycles.

It has been demonstrated in Section 6.1 that the UL–RL cycles are not necessarily confined to the intermediate consolidation phases but may also occur during the final consolidation phase, as they result from numerical redistribution of stresses. Consequently, additional overshooting can arise during the final consolidation phase, not only in the loading case with intermediate consolidation phases but also in the monotonic loading case. The more UL–RL cycles occur in the monotonic loading case, the less suitable it becomes as a reference case. This provides an additional justification for limiting the time span to $100\,\mathrm{d}$, which is nevertheless sufficient to evaluate whether the MSB formulation improves the results, alongside the ability to make a comparison with the work of Cudny and Truty (2020), as already discussed in Section 3.3.2. The same reasoning applies to the results presented in Section 6.3.

Figures 6.2a and 6.2b clearly demonstrate that overshooting is still observed in the MSB formulation, as the monotonic loading case and the loading case with UL–RL cycles deviate significantly from one another. The results are comparable to those obtained with the original HSsmall model, indicating that only limited improvement has been achieved. However, the response under monotonic loading obtained with the MSB formulation coincides with that obtained with HSsmall model.

To investigate why the MSB formulation did not produce the desired outcome, the deviatoric stress-deviatoric strain response at stress point 10083 during the first intermediate consolidation phase is analysed in combination with the debug files. The location of stress point 10083 is shown in Figure 3.2 in Section 3.3.2. Figure 6.3 indicates the position of the first intermediate consolidation phase on the stress-strain response. Figure 6.4a presents the stress-strain response during the first intermediate consolidation phase, while Figures 6.4b, 6.4c, and 6.4d each provide a detailed view of one of the three points highlighted in 6.4a.

Recall from Section 5.2.1 that, according to the SR detection algorithm proposed by Benz (2007), a SR is detected whenever a reversal occurs in any of the three eigen directions of the current deviatoric strain increment d**e**, and that the detected SR may be partial, when a reversal occurs in only one or two of the three eigen directions, or full, when a reversal occurs in all three eigen directions. In both cases, the SR arises from a rotation of the deviatoric strain path.

The MSB formulation adopts the same SR detection algorithm as proposed by Benz (2007) (Plaxis, 2025a). This implies that the Memory Surface also evolves when a partial SR is detected during reloading, and that the deviatoric strain history tensor **H** is stored when a partial SR is detected during unloading 2.2.1.

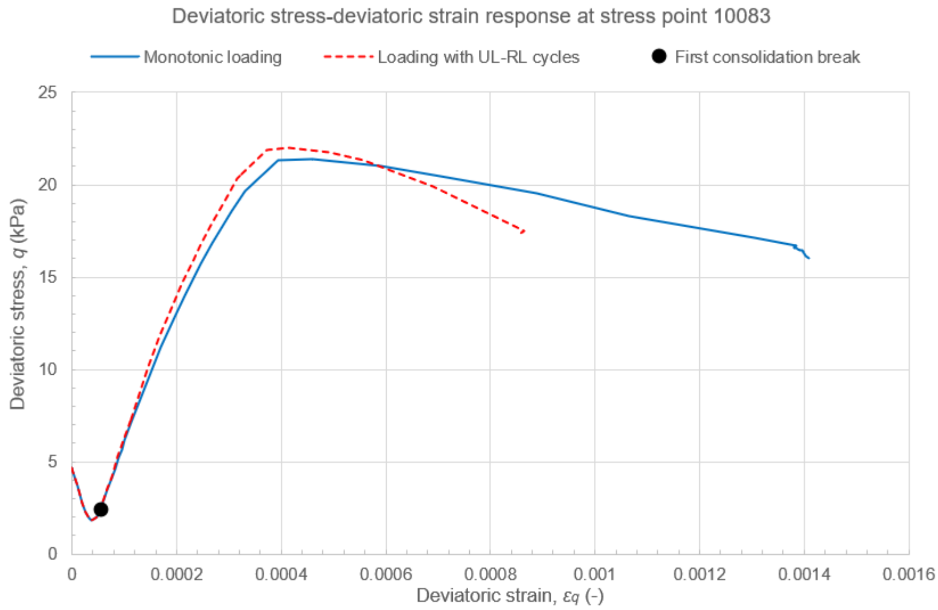

Figure 6.3: Deviatoric stress-deviatoric strain response at stress point 10083.

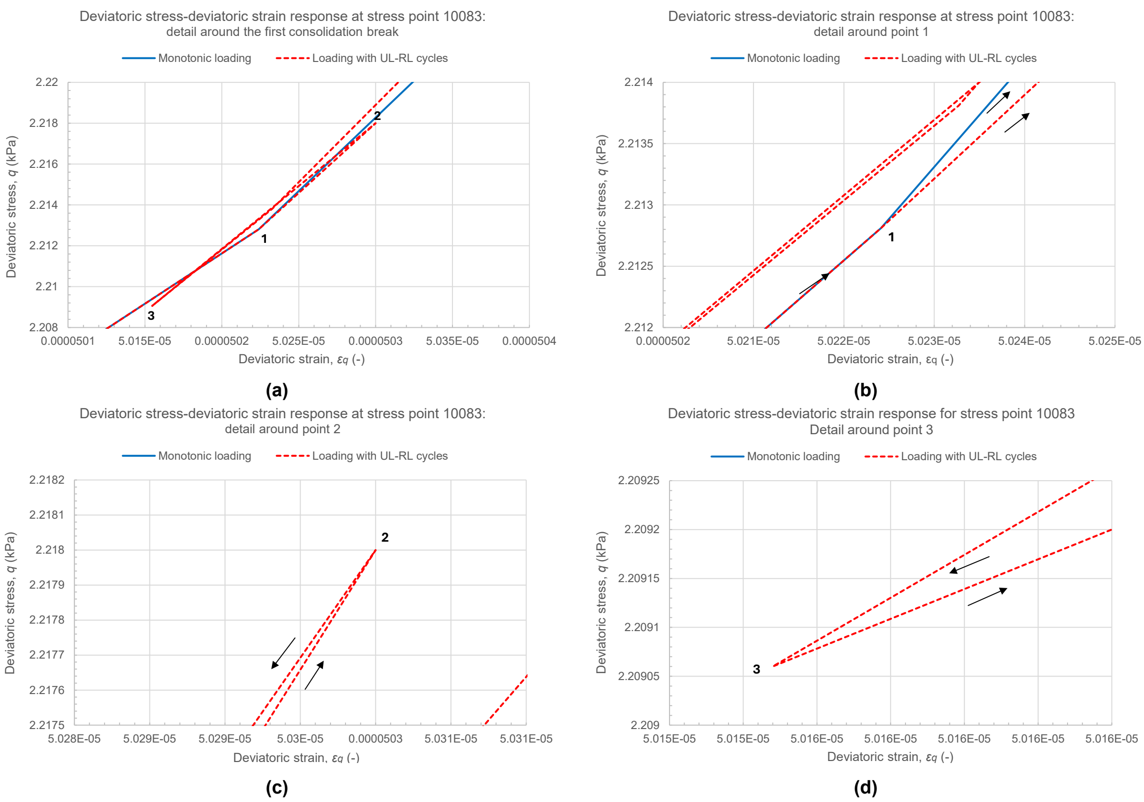

Figure 6.4: Deviatoric stress-deviatoric strain response at stress point 10083 during the first intermediate consolidation phase for both monotonic loading and loading with UL–RL cycles.

At point 1 in Figure 6.4, a partial SR is detected. Following the criterion used to determine whether the SR corresponds to unloading or reloading, as described in Section 2.2.1, reloading conditions apply. These reloading conditions were already applicable prior to this partial SR, as can be verified from Figure 6.3. Therefore, no UL–RL cycle is initiated at this point, and no update of the Memory Surface should be required. Even though, such an update does occur. At points 2 and 3, full SRs occur, triggering unloading and reloading, respectively. In these cases, the loading conditions do change after the SR, and consequently an UL–RL cycle occurs, resulting in a correct update of **H** in memory and of the Memory Surface.

Thus, adopting the SR detection algorithm proposed by Benz (2007) in the MSB formulation results either in an excessive number of relocations and size readjustments of the Memory Surface, or in wrongfully overwriting **H**, and consequently in an incorrect memory. This behaviour is consistent with the ingredients of the formulation, however, their is room for improvement.

To avoid such incorrect updates, a different SR detection algorithm is implemented in the MSB formulation. This algorithm builds on ideas originally proposed by Papadimitriou and Bouckovalas (2002). The check for a SR compares the distance between the deviatoric strain point at the last SR, $\mathbf{e_{SR}}$, and the deviatoric strain point at the start of the step, $\mathbf{e_0}$, i.e. $||\mathbf{e_0} - \mathbf{e_{SR}}||$, with the distance between $\mathbf{e_{SR}}$ and the deviatoric strain point at the end of the step, $\mathbf{e}$, i.e. $||\mathbf{e} - \mathbf{e_{SR}}||$. A deviatoric SR is detected if

$$\|\mathbf{e} - \mathbf{e}_{SR}\| < \|\mathbf{e}_0 - \mathbf{e}_{SR}\| \tag{6.8}$$

Here, $\mathbf{e_{SR}}$ serves as a reference point. A schematic representation of the algorithm is provided in Figure 6.5.

By employing this algorithm, only full SRs are detected in the MSB formulation. It should be noted that this adjustment only applies to the MSB formulation. The existing small-strain component of the HSsmall model, of which the MSB formulation is an extension, remains unchanged and continues to use the algorithm proposed by Benz (2007). As a result, partial SRs, resulting from changes in the direction of the deviatoric strain path, still lead to sudden changes of the elastic shear modulus, as explained in Section 5.2.1.

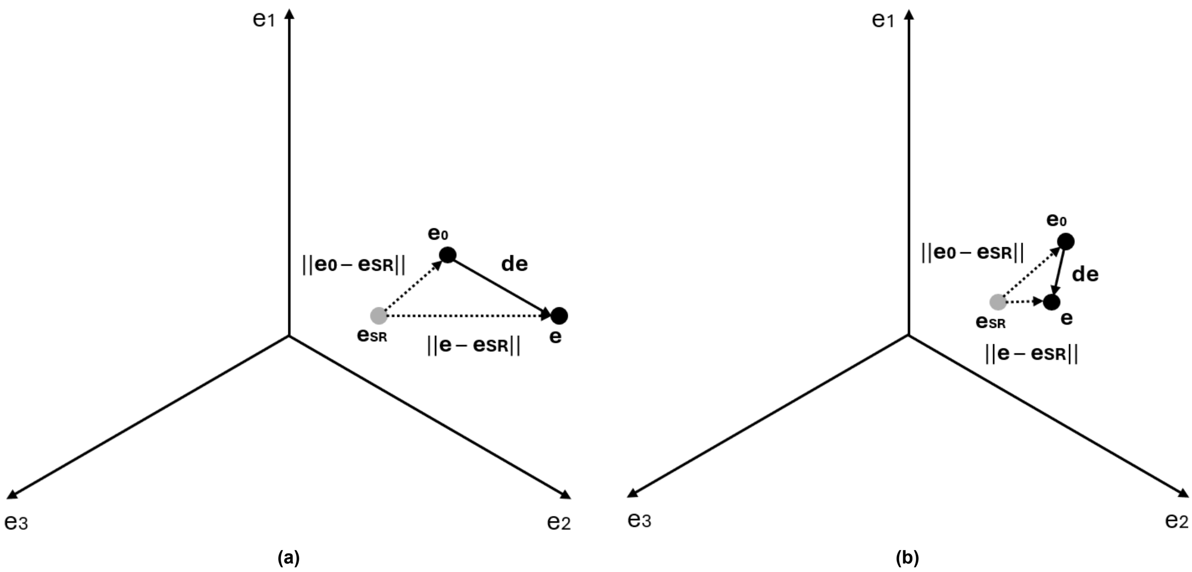

Figure 6.5: Proposed SR detection algorithm applied to the MSB formulation: (a) No SR detected and (b) SR detected.

Figure 6.6a compares the results obtained before and after implementing the improved SR detection algorithm. Although the results show improvement, a substantial extent of overshooting is still observed. The original MSB formulation is defined in the deviatoric stress space (see Section 2.2.1), however, it was found that the formulation performs more effectively when formulated in the deviatoric strain space (see Figure 6.6b). Therefore, unless stated otherwise, the MSB formulation defined in the strain space, including the new SR detection algorithm, is used from this point onwards. Chapter 7 discusses the results of an investigation into the underlying cause of this improvement.

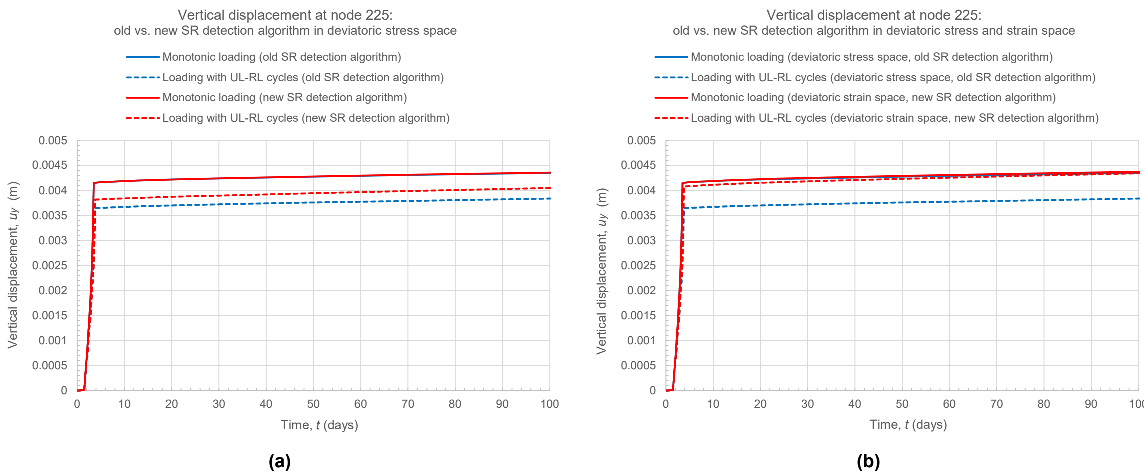

Figure 6.6: Evolution of the vertical displacement at the centre of the final excavation bottom (node 225): (a) comparison between the MSB formulation in the deviatoric stress space with and without the new SR detection algorithm, and (b) comparison between the MSB formulation in the stress space using the old SR detection algorithm and the MSB formulation in the strain space using the new algorithm.

6.2.2. Assessment of overshooting at three stress points

Figure 6.7 shows the deviatoric stress-deviatoric strain response at three stress points selected in the model. The locations of these stress points are shown in Figure 3.3 in Section 3.3.2. By plotting each graph on the same scale, it becomes evident that at some stress points the stress-strain response reaches relatively small stress and strain levels, and the overshooting observed in the original HSsmall model can therefore be regarded as negligible.

The entire final consolidation phase of $50\,000\,\mathrm{d}$ is included in the graph, as explained in Section 3.3.2. Although a counterargument was presented in 6.2.1 against showing the entire phase, it is nevertheless displayed here in order to illustrate its impact. The irregularity observed during the final consolidation phase, caused by the numerical redistribution of stresses (see Section 6.1) becomes especially evident in Figure 6.7a, where the final consolidation phase begins at the point where the response exhibits an abrupt change. This irregularity occurs in both the monotonic loading cases and the loading cases with intermediate consolidation phases. The same reasoning applies to the results presented in Section 6.3.

Figure 6.7a demonstrates a significant improvement in the results, as the extent of overshooting is considerably reduced when using the MSB formulation compared to the HSsmall model. However, overshooting is still observed to some extent, the origin of which is investigated in Section 6.2.3. In Figure 6.7b, the attained stress and strain levels are so limited that overshooting can be considered negligible, although closer inspection still reveals improvements. Figure 6.7c shows a small but nonetheless clearly visible improvement in the results.

The stress-strain response under monotonic loading at each node obtained with the MSB formulation coincides with that obtained with the original HSsmall model (except for the final consolidation phase).

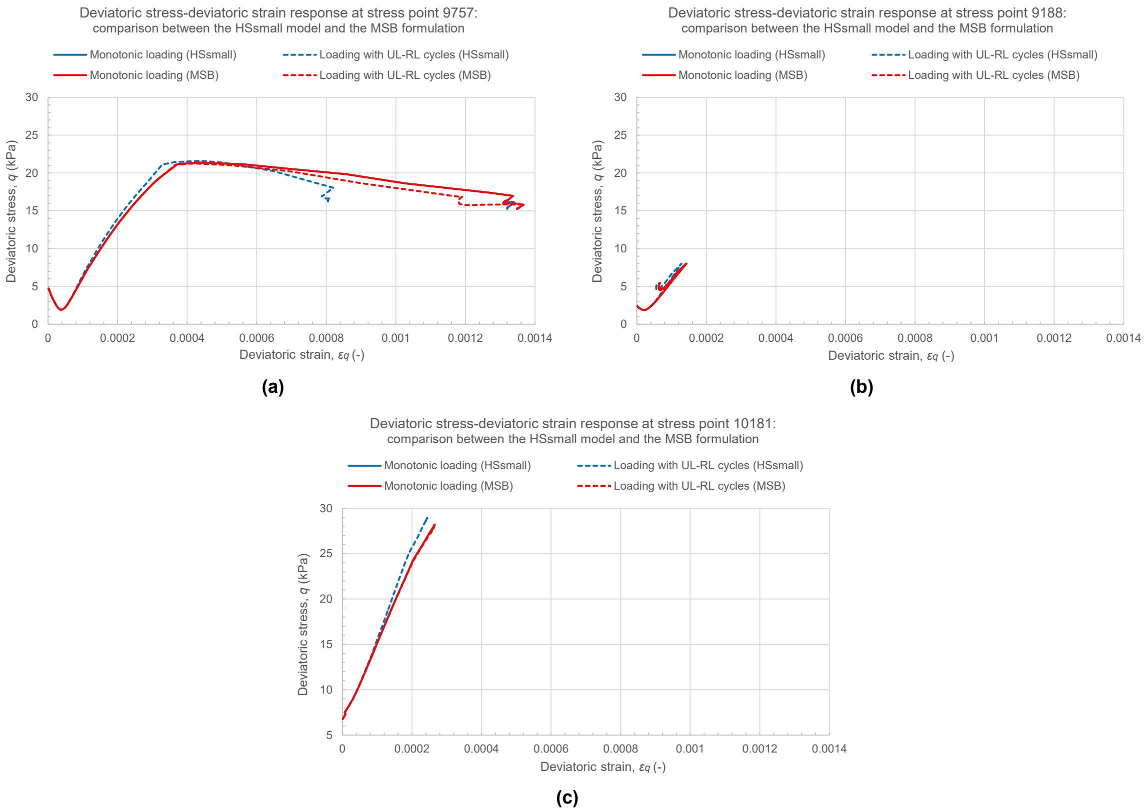

Figure 6.7: Comparison between the deviatoric stress-deviatoric strain response obtained with the MSB formulation and the original HSsmall model.

6.2.3. Detailed analysis of stress point 9757

Figure 6.8 shows the evolution of the elastic shear modulus and the deviatoric strain at stress point 9757 over time, for both the monotonic loading case and the loading case with intermediate consolidation phases. Figures 6.8a and 6.8b include the intermediate consolidation phases, whereas Figures 6.8c and 6.8d omit them while maintaining a continuous time axis. The intermediate consolidation phases, each with a duration of $0.1\,\mathrm{d}$, occur at $t = 2\,\mathrm{d}$, $t = 2.6\,\mathrm{d}$, and $t = 3.2\,\mathrm{d}$. Figures 6.8c and 6.8d show a similar evolution up to approximately $t = 3.1\,\mathrm{d}$, which corresponds to the end of the first calculation step of the fourth excavation phase ($t = 3.4\,\mathrm{d}$ in Figures 6.8a and 6.8b). This indicates that the error originates in the third intermediate consolidation phase.

A detailed view of the third intermediate consolidation phase is provided in Figure 6.9. It was found that the full SR triggering reloading at $t = 3.3\,\mathrm{d}$ was not detected (Figure 6.9b). As a result, the Memory Surface was neither relocated nor readjusted. Consequently, the reset of the deviatoric strain history tensor **H** was based on the location and size of the Memory Surface at the last deviatoric SR triggering unloading, which in this case coincides with $t = 3.2\,\mathrm{d}$ (see Figure 6.9b).

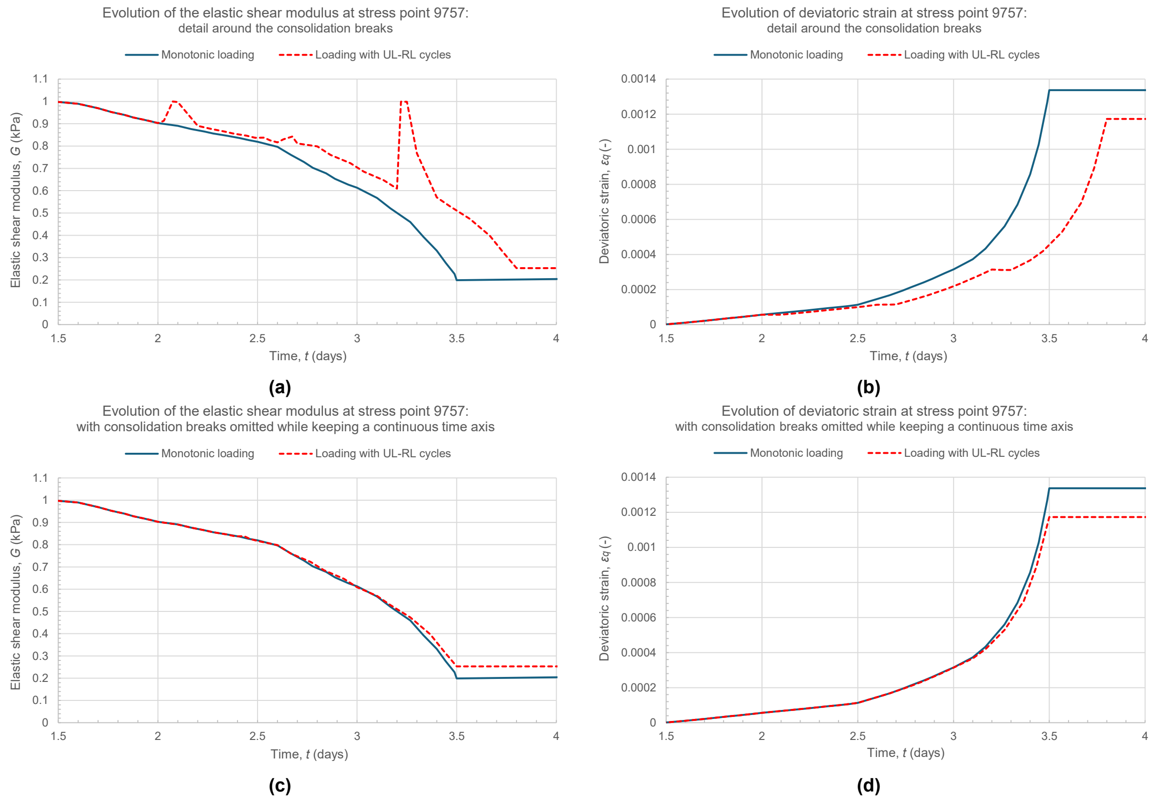

Figure 6.8: Evolution of the elastic shear modulus and the deviatoric strain at stress point 9757 for both monotonic loading and loading with UL–RL cycles.

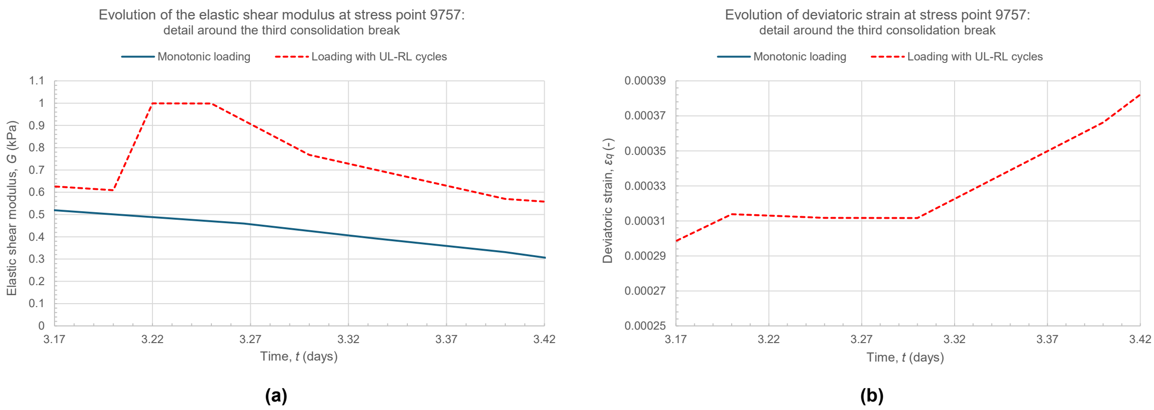

Figure 6.9: Detailed view of the evolution of the elastic shear modulus and the deviatoric strain at stress point 9757 during the third intermediate consolidation phase, for both monotonic loading and loading with UL–RL cycles.

The SR detection algorithm is described by Formula 6.8 in Section 6.2.1. Figure 6.10 illustrates a situation in which this algorithm fails to detect the SR. Although a SR occurs, the current deviatoric strain increment $d\mathbf{e}$ is sufficiently large that the algorithm fails to capture the interval where the criterion described by Formula 6.8 is satisfied.

The observed behaviour is consistent with the ingredients of the formulation but their is room for improvement.

To address this shortcoming, the algorithm is modified to evaluate whether fractions of $d\mathbf{e}$ satisfy the criterion described by Formula 6.8. In this way, a SR can still be detected if one occurs but is missed due to the situation shown in Figure 6.10.

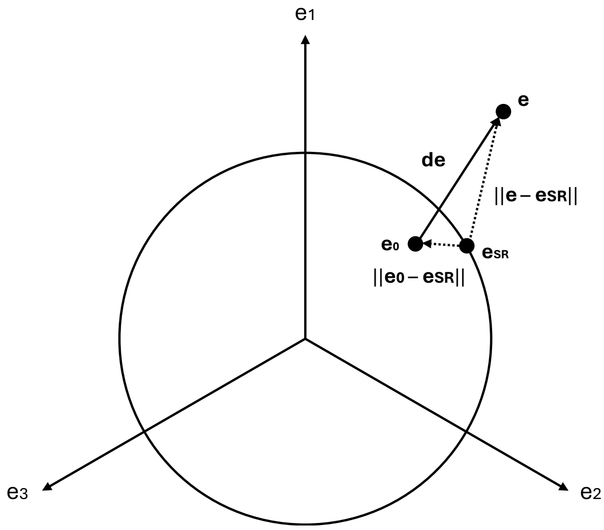

Figure 6.10: Failed detection of deviatoric SR

Figure 6.11 presents a comparison between the results obtained using the MSB formulation, with and without the implemented modification. *MSB0* corresponds to the original version without the modification, while *MSB1* corresponds to the modified version. When using the modified version, less overshooting is observed: the evolution of the elastic shear modulus, deviatoric strain, and stress-strain response all align more closely with the monotonic reference case. Unless stated otherwise, all subsequent analyses use the improved formulation.

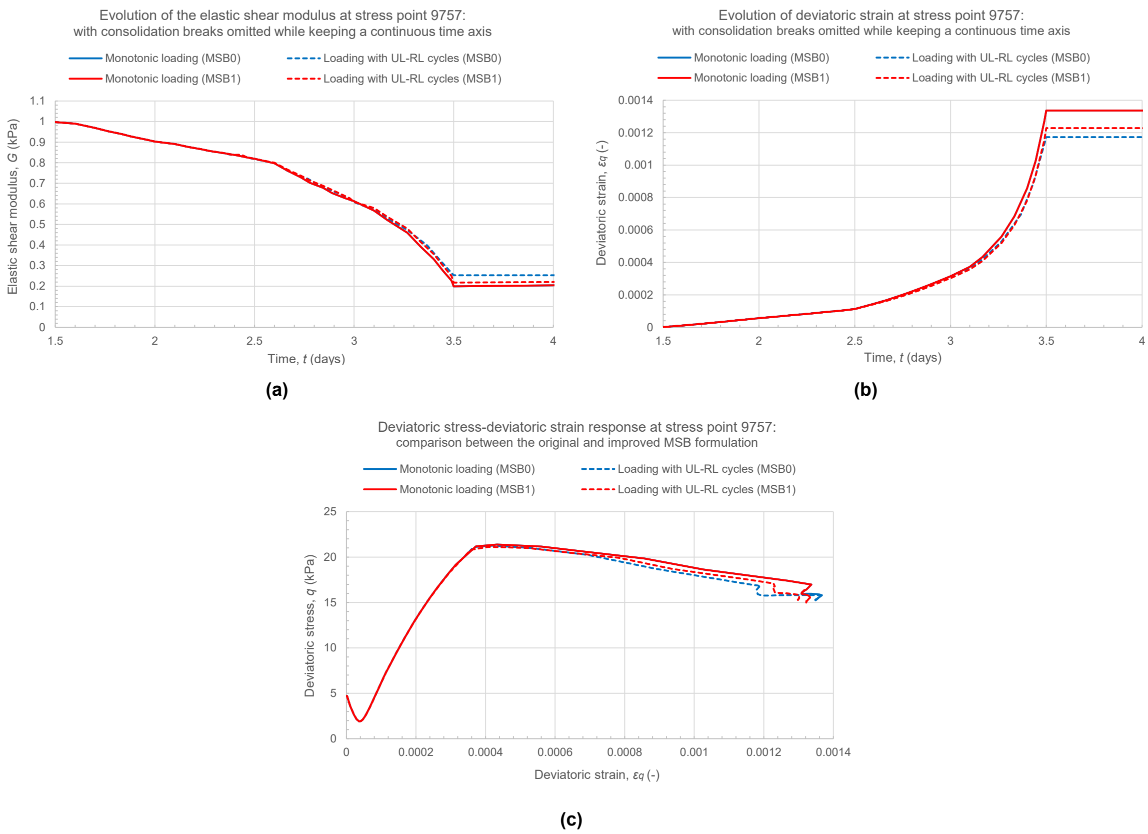

Figure 6.11

6.2.4. Comparison with the results reported by Cudny and Truty (2020)

Figure 6.12a presents the results reported by Cudny and Truty (2020), whereas Figure 6.12b shows the results obtained with the MSB formulation analysed in this study. It is evident that the MSB formulation produces results of a similar quality to those obtained with the model proposed by Cudny and Truty (2020), since the monotonic loading case and the loading case with UL–RL cycles show close agreement.

Furthermore, the results of the Hardening Soil Brick model proposed by Cudny and Truty (2020), deviate more from the monotonic loading case of the HSsmall model (referred to as HSS in Cudny and Truty (2020)) than those of the MSB formulation. A smaller deviation is preferred, as it implies less consequences for the end user of the model.

It should be noted that Figure 6.12b was obtained using the version of the MSB formulation without the modification discussed in Section 6.2.3. Although implementing this modification improved the results at stress point 9757, it negatively affected the results at other stress points and nodes, including node 225. For brevity of the presentation, figures illustrating this decline in performance are not included. The investigation into the cause of the observed degradation in the results at other stress points and nodes is ongoing and is not regarded as part of this thesis.

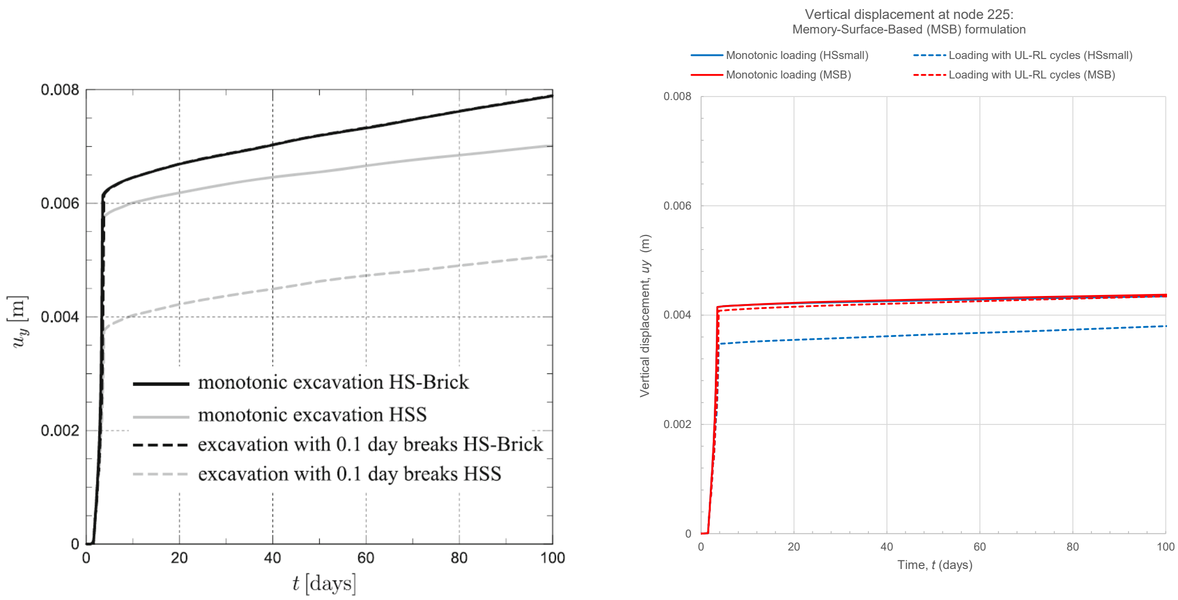

(a) (b)

Figure 6.12: Comparison between the results reported by Cudny and Truty (2020) and those obtained with the MSB formulation.

6.3. Results obtained with the Continuous Brick formulation

This section presents the results of the BVP simulated with the CB formulation.

6.3.1. Vertical displacement at node 225

Figure 6.13 illustrates the evolution of the vertical displacement at node 225 over time for both the monotonic loading case and the loading case with intermediate consolidation phases. Figure 6.13a presents the results over a period of $100\,\mathrm{d}$, while Figure 6.13b provides a detailed view of the excavation period starting at $1.5\,\mathrm{d}$. The monotonic excavation is completed at $t = 3.5\,\mathrm{d}$, whereas the excavation with intermediate consolidation phases reaches completion at $t = 3.8\,\mathrm{d}$.

Figures 6.13a and 6.13b demonstrate that the monotonic loading case and the loading case with intermediate consolidation phases nearly coincide, indicating that the extent of overshooting is reduced to a negligible level. However, the monotonic case differs from that obtained with the original HSsmall model.

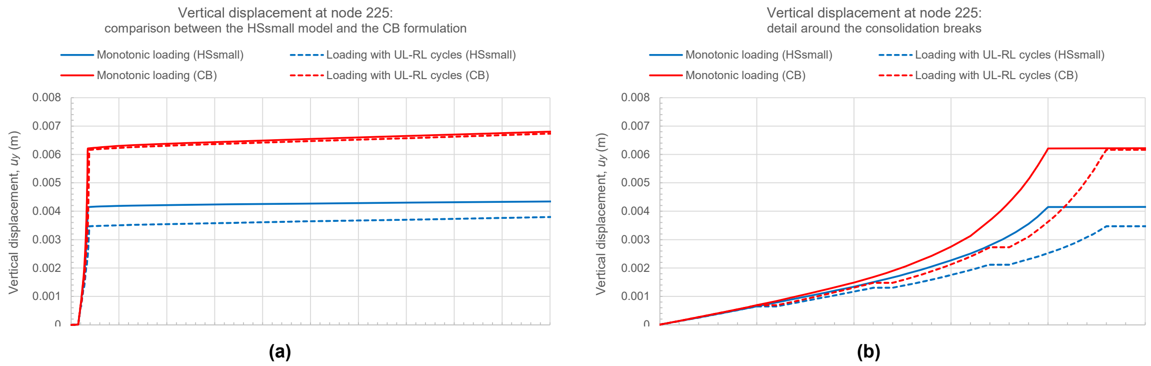

Figure 6.13: Evolution of the vertical displacement at the centre of the final excavation bottom (node 225) simulated using the HSsmall model and CB formulation, for both the monotonic loading case and the loading case with UL–RL cycles)

As explained in Section 2.2.2, the primary (elasto-plastic) response is softer than that of the HSsmall model, as shown in Figures 6.13a and 6.13b, because the backbone curve used in the CB formulation is not scaled by a factor of two. Recall that this softer response can be partially compensated by doubling the model parameter $\gamma_{0.7}$, as shown in Figures 6.14a and 6.14b. From this point onwards the results are shown for a doubled $\gamma_{0.7}$.

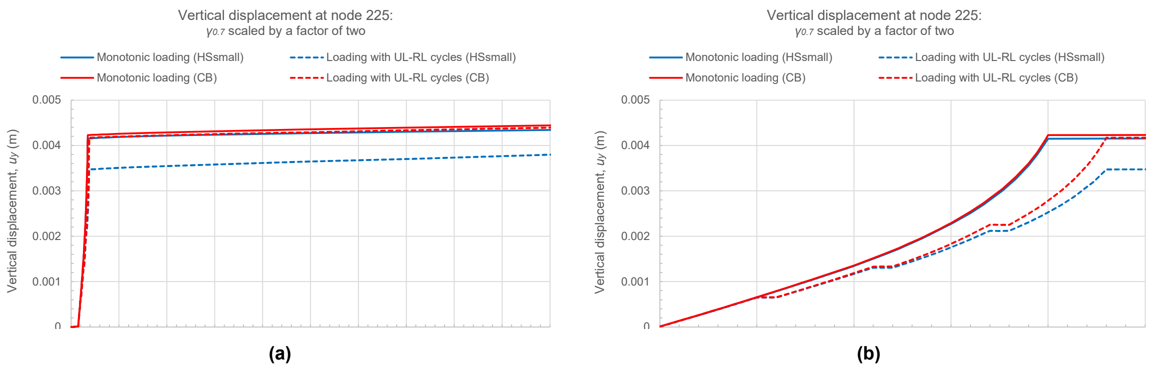

Figure 6.14: Evolution of the vertical displacement at the centre of the final excavation bottom (node 225) simulated using the HSsmall model and CB formulation with $\gamma_{0.7}$ scaled by a factor of two, for both the monotonic loading case and the loading case with UL–RL cycles

6.3.2. Assessment of overshooting at three stress points

Figure 6.15 shows the deviatoric stress-deviatoric strain response at three stress points selected in the model. The locations of these stress points are shown in Figure 3.3 in Section 3.3.2. Results are provided for both the CB formulation and the HSsmall model. By plotting each graph on the same scale, it becomes evident that at some stress points the stress-strain response reaches relatively small stress and strain levels, and the overshooting observed in the original HSsmall model can therefore be regarded as negligible.

Figure 6.15a demonstrates that the extent of overshooting is reduced to a negligible level. In Figure 6.15b, the attained stress and strain levels are so limited that overshooting can be considered negligible, although closer inspection still reveals improvements. Figure 6.15c shows a small but nonetheless clearly visible improvement in the results.

In each case, the results obtained under monotonic loading using the CB formulation differ from those of the HSsmall model, as expected given the explanation in 2.2.2, concerning the application of a different scaling factor.

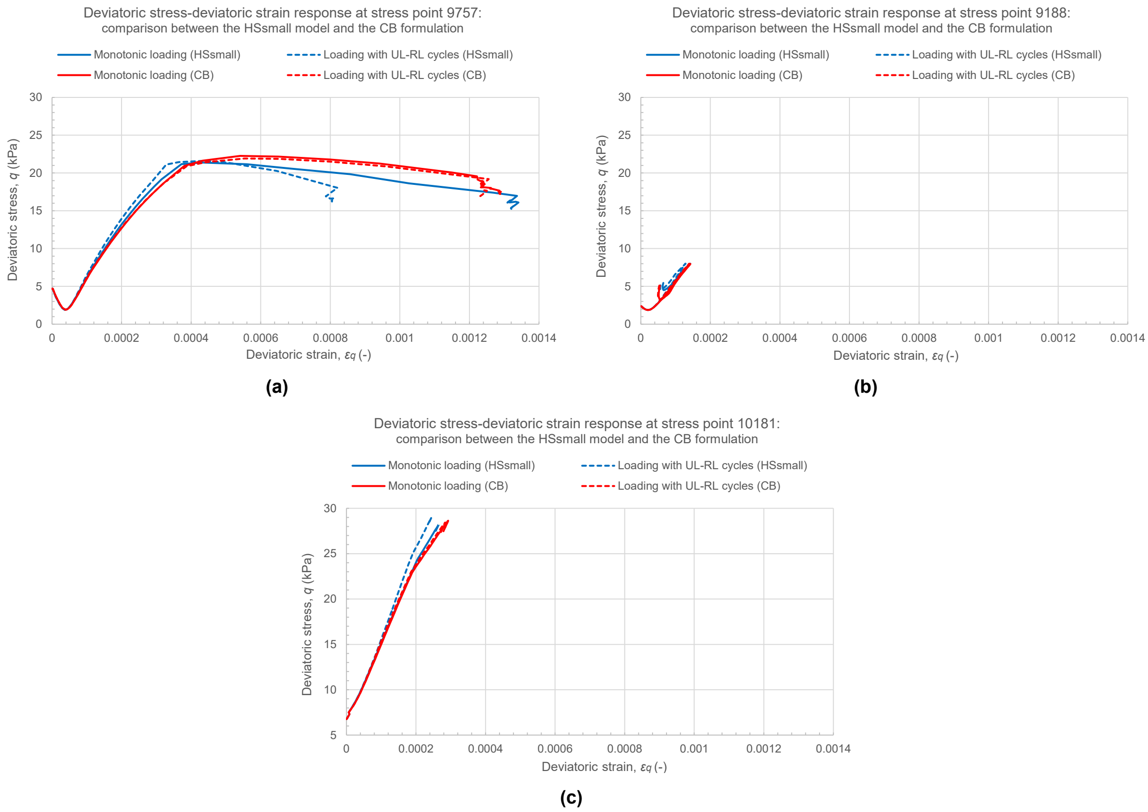

Figure 6.15: Deviatoric stress-deviatoric strain response at three stress points in the model simulated using the original HSsmall model and the CB formulation, for both the monotonic loading case and the case with UL–RL cycles.

6.3.3. Detailed analysis of stress point 9757

Figure 6.16 illustrates the evolution of the elastic shear modulus and the deviatoric strain at stress point 9757 over time, for both the monotonic loading case and the loading case with intermediate consolidation phases. Figures 6.16a and 6.16b include the intermediate consolidation phases, whereas Figures 6.16c and 6.16d omit them while maintaining a continuous time axis. The intermediate consolidation phases, each with a duration of $0.1\,\mathrm{d}$, occur at $t = 2.0\,\mathrm{d}$, $t = 2.6\,\mathrm{d}$, and $t = 3.2\,\mathrm{d}$. Figures 6.16c and 6.16d show an error over the interval $t = 2.0\,\mathrm{d}$ to $2.4\,\mathrm{d}$. Since $t = 2.0\,\mathrm{d}$ corresponds to the onset of the first intermediate consolidation phase (corresponding to $t = 2.0\,\mathrm{d}$ in Figures 6.16a and 6.16b as well), this indicates that the error originates in that break.

A detailed view of the first intermediate consolidation phase is provided in Figure 6.17. It was found that no brick was active during the SR triggering unloading at $t = 2.03\,\mathrm{d}$ (Figure 6.17b). As discussed in Section 5.3.2, the formulation does not store the memory upon a SR triggering unloading when no brick is active. Consequently, the elastic shear modulus at the onset of an UL–RL cycle cannot be restored upon its closure, which may lead to overshooting, although in this simulation being of a negligible level. This behaviour is consistent with the ingredients of the formulation.

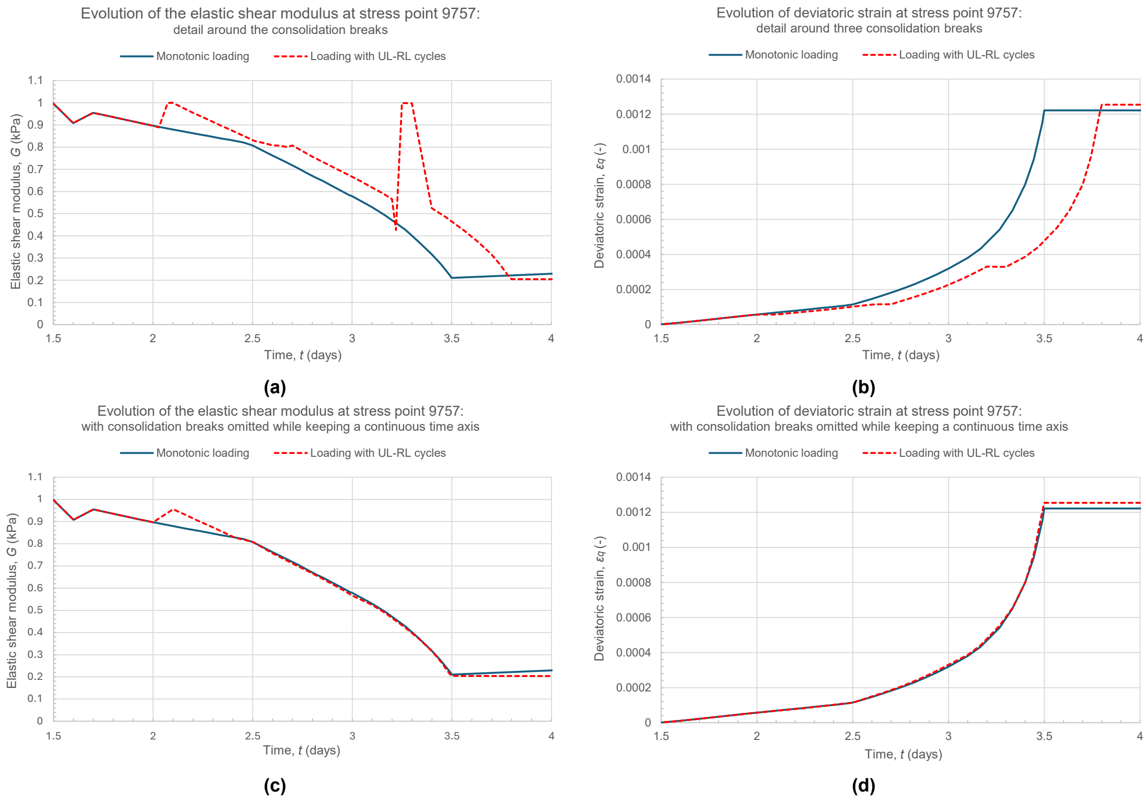

Figure 6.16: Evolution of the elastic shear modulus and the deviatoric strain at stress point 9757 for both the monotonic loading case and the loading case with UL–RL cycles using the CB formulation.

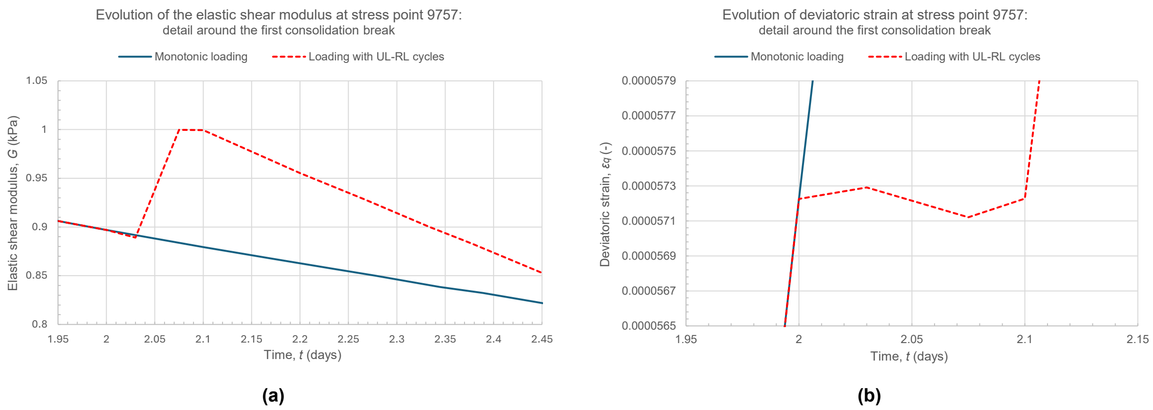

Figure 6.17: Detailed view of the evolution of the elastic shear modulus and the deviatoric strain at stress point 9757 during the first intermediate consolidation phase, for both the monotonic loading case and the loading case with UL–RL cycles.

6.3.4. Comparison with the results reported by Cudny and Truty (2020)

Figure 6.18a presents the results reported by Cudny and Truty (2020), whereas Figure 6.18b shows the results obtained using the CB formulation analysed in this study. The monotonic loading case and the loading case with UL–RL cycles of the CB formulation do not coincide exactly, but the difference is negligible. Therefore, it is evident that the CB formulation produces results of comparable quality to those obtained with the model proposed by Cudny and Truty (2020).

Furthermore, the results of the Hardening Soil Brick model proposed by Cudny and Truty (2020), deviate more from the monotonic loading case of the HSsmall model (referred to as HSS in Cudny and Truty (2020)) than those of the CB formulation. A smaller deviation is preferred, as it implies less consequences for the end user of the model.

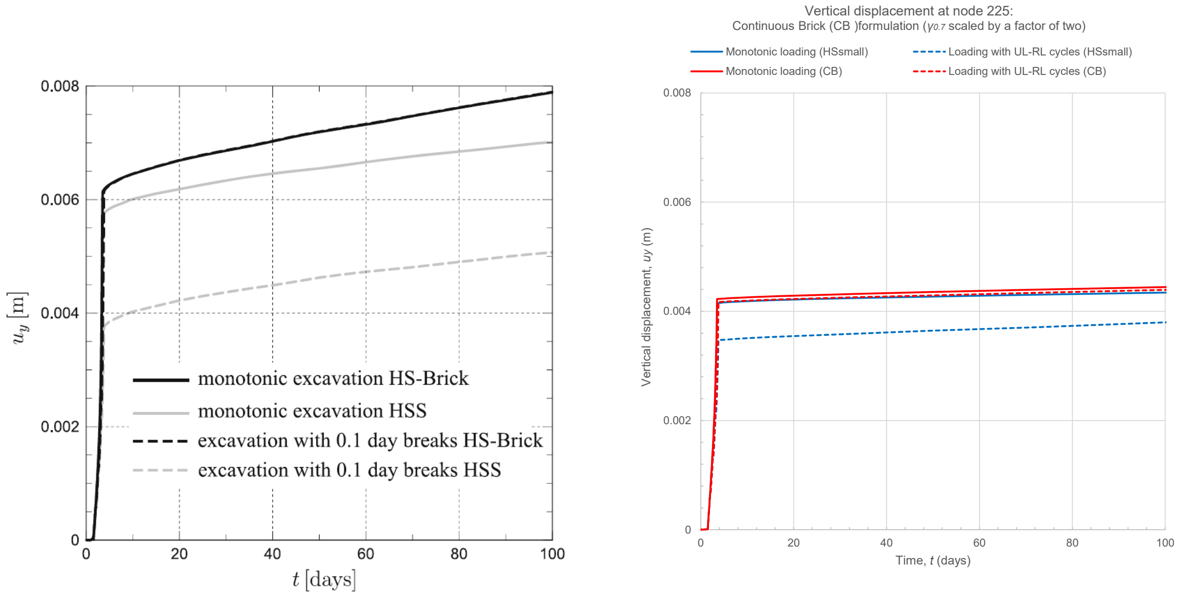

(a) **(b)**

Figure 6.18: Comparison between the results reported by Cudny and Truty (2020) and those obtained with the CB formulation.

6.3.5. Bending moments in the sheet pile wall

Figure 6.19 shows the bending moments in the sheet pile wall along its length for both the MSB formulation and the CB formulation. In both Figures, the results obtained with the HSsmall model are also presented.

As explained in Section 3.3.2, overshooting in the HSsmall model causes the soil to behave stiffer in the loading case with UL–RL cycles compared to the monotonic loading case, which results in a larger portion of the load being carried by the soil. This hypothesis is confirmed in Figure 6.19, where, over a large part of the sheet pile wall, the bending moment is smaller in the loading case with UL–RL cycles than in the monotonic loading case. Note that the monotonic loading case of the HSsmall model coincides with that of the CB formulation. It should be noted that in this specific case this difference is not extremely large. According to Cudny and Truty (2020), this difference may become larger in more complicated real-world scenarios.

For both the MSB formulation (Figure 6.19a) and the CB formulation (Figure 6.19b), the bending moments are no longer smaller in the loading case with UL–RL cycles, indicating that overshooting reduced to a negligible level.

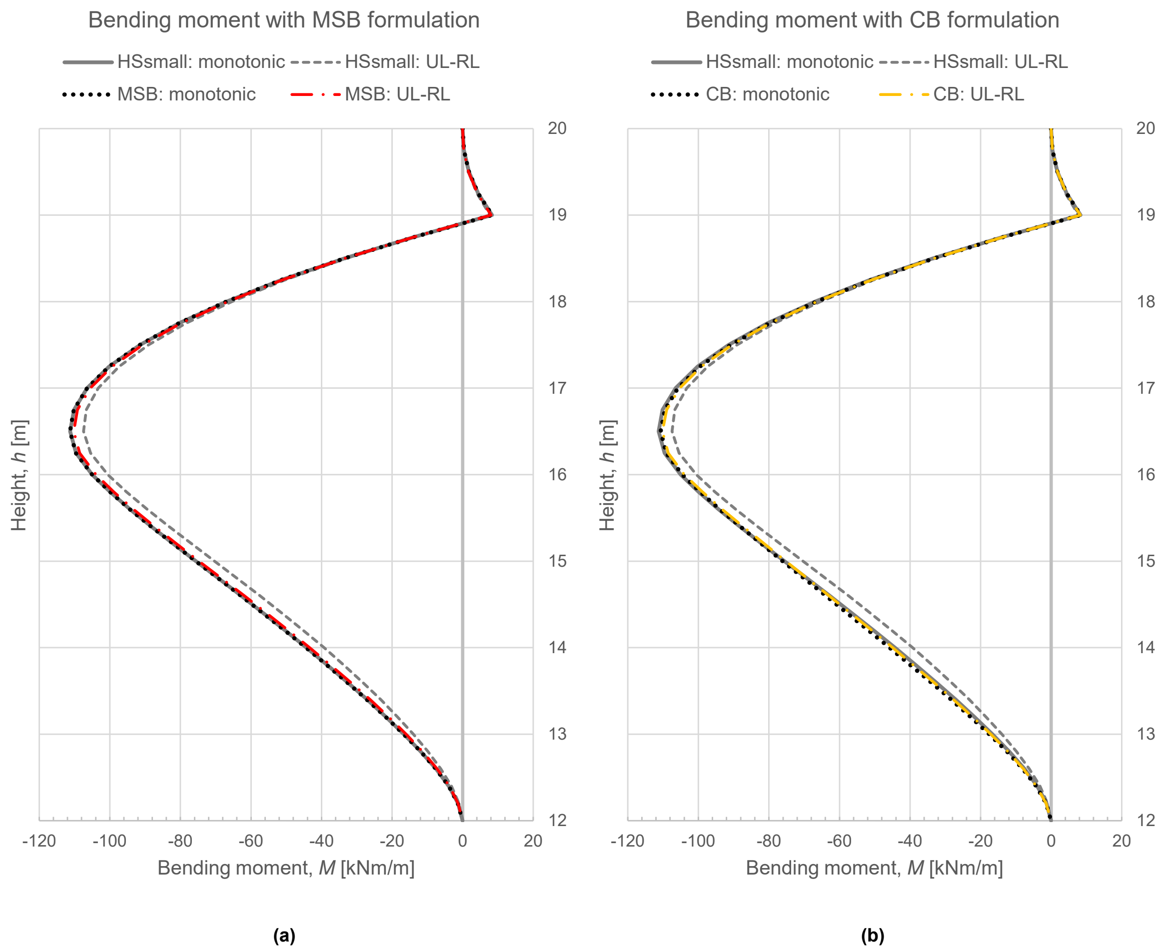

Figure 6.19: Bending moment in the sheet pile wall for both the MSB formulation and the CB formulation, compared to the HSsmall model

6.4. Drawback: nested cycles

It was found in Section 5.7 that both the MSB formulation and the CB formulation exhibit a drawback: both formulations are unable to memorise more than a single UL–RL cycle. If a smaller UL-RL cycle occurs within a larger one, the memory associated with the larger cycle is overwritten by that of the smaller cycle. Consequently, when closing the larger, initial cycle, the formulations are unable to restore the corresponding elastic shear modulus.

In the simulation presented in this section, numerous nested UL–RL cycles appeared unintentionally in the deviatoric stress-deviatoric strain response due to poorly specified numerical control parameters: the load step of the numerical calculation scheme had been reduced by a great amount. Reducing the load step was neither part of the original plan nor a methodological refinement adopted during the investigation, and the fact that it leads to numerous nested UL–RL cycles was discovered by accident. This behaviour does not occur when the default numerical control settings are used, which are applied throughout the remainder of the BVP analysis.

Figures 6.20a and 6.20b show the deviatoric stress-deviatoric strain response at stress point 9757 for the MSB and CB formulation, respectively. In the reference case, the load step is not reduced. Therefore, nested cycles are most likely absent. It is evident that, when nested cycles occur, the extent of overshooting is much larger for both formulations. However, it should still be assessed whether such nested cycles also occur in practical geotechnical analyses, since the ones in this simulation are not that likely to occur.

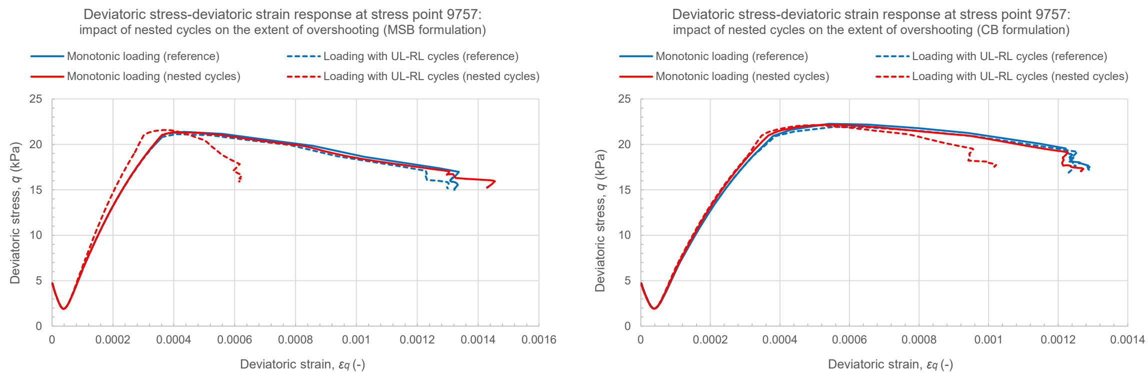

(a) (b)

Figure 6.20: Deviatoric stress-deviatoric strain response at stress point 9757 to assess the impact of nested cycles on the extent of overshooting: (a) MSB formulation and (b) CB formulation.

Figure 6.21a illustrates the extent of overshooting introduced during the first intermediate consolidation phase for both the reference case and the case with nested cycles obtained using the MSB formulation. In the reference case, the monotonic loading curve and the curve with UL–RL cycles nearly coincide, indicating that no overshooting occurs. In contrast, for the case with nested cycles, a clear deviation is observed, demonstrating the occurrence of overshooting. As mentioned earlier, this overshooting is introduced during the first intermediate consolidation phase. Figure 6.21b shows the nested cycles occurring during this phase. At points 1, 2, 3, and 4 SRs triggering unloading occur successively, respectively. Each time, the memory stored at the previous point is overwritten by that of the next.

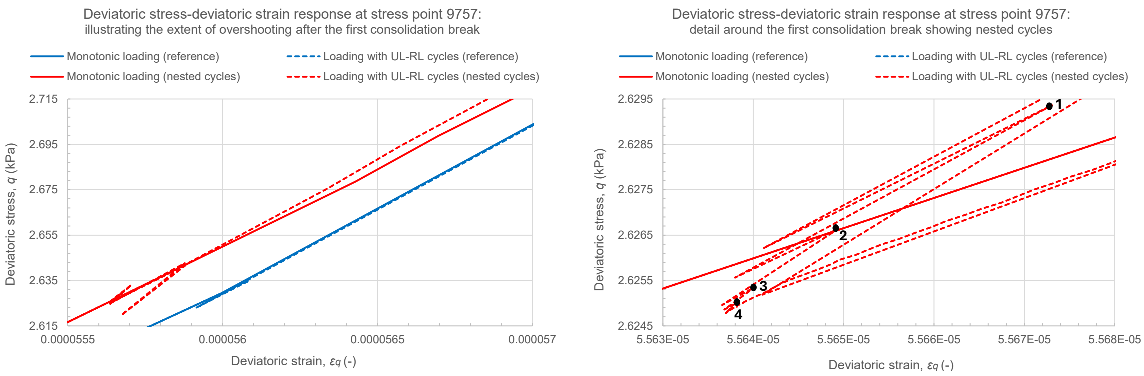

(a) (b)

Figure 6.21: Detail around the first intermediate consolidation phase showing the extent of overshooting and nested cycles for the MSB formulation.

6.5. Sub-conclusion

The UL–RL cycles observed in the BVP presented in this study are mainly caused by numerical redistributions of stresses triggered by physical deformation mechanisms and increased model complexity, leading to stress imbalances that are resolved when the model is allowed time to adjust to a new equilibrium, i.e., when no additional changes to the model conditions are imposed. This insight is highly valuable, as it implies that such cycles may occur in any numerical analysis of practical two-dimensional geotechnical problems, especially when deformation mechanisms greatly disturb the soil, i.e., strong plastic straining.

It was found that the MSB formulation required two improvements before overshooting was significantly reduced: (i) the SR detection algorithm had to be changed, and (ii) the formulation had to be defined in the deviatoric strain space rather than in the deviatoric stress space. At a later stage, an extension was added to the SR detection algorithm to improve the results even further. This improvement is, however, still under investigation, as the results either improved or worsened at different stress points and nodes.

The response of the MSB formulation under monotonic loading coincides with that of the original HSsmall model, except for the deviatoric stress-deviatoric strain response of the final consolidation phase, which is due to numerical redistributions of stresses occurring during this phase.

Overall, the MSB formulation can effectively reduce overshooting. When compared with the results reported by Cudny and Truty (2020), the results are of similar quality.

The CB formulation did not require any improvements, and overshooting was significantly reduced. When compared with the results reported by Cudny and Truty (2020), the results are of similar quality. However, the response of the CB formulation does not coincide with that of the original HSsmall model under monotonic loading, due to the use of a different scaling factor in the backbone curve that describes the deviatoric stress-deviatoric strain response. This discrepancy can be partially counteracted by multiplying the model parameter $\gamma_{0.7}$ by a factor of two. Nevertheless, this adjustment does not reproduce an identical response.

A summary of all the issues encountered in the boundary value problem together with their solutions is provided in Appendix D.

Both the MSB formulation and the CB formulation exhibit a drawback which was identified in the single stress point simulations: they are unable to memorise more than a single UL–RL cycle. However, the severity of this drawback was not yet established. Although the nested cycles observed in the BVP analysed in Section 6.4 were the result of numerical instabilities due to poorly specified numerical control parameters, it is evident that they have a significant impact on the extent of overshooting. A realistic scenario in which nested cycles are more likely to occur and could therefore increase the extent of overshooting, thereby leading to inaccurate deformation predictions, is dynamic loading.

As a final note, no noticeable difference in computational efficiency between the two formulations was observed in terms of run time.

7

Why the Memory-Surface-Based formulation performs better in the deviatoric strain space than in the deviatoric stress space

In Section 6.2.1, it was shown that the MSB formulation performs more effectively when defined in the deviatoric strain space than in the deviatoric stress space, as less overshooting was observed. The first part of this chapter clarifies the underlying reason for the formulation's improved performance in the deviatoric strain space. This chapter does not aim to make the formulation work in the stress space, but rather to highlight and explain the differences between the two spaces. The second part summarises the main findings in a brief sub-conclusion.

7.1. Underlying mechanism

7.1.1. Differences between the deviatoric stress and strain space

Defining the formulation in the deviatoric strain space rather than in the deviatoric stress space means that the evolution of the Memory Surface is governed by deviatoric strains instead of deviatoric stresses. As explained in Section 2.2.1, the radius of the Memory Surface, m, is used to establish when an UL–RL cycle is closed. Upon a SR triggering reloading, the radius is set equal to the distance between the SR triggering unloading and SR triggering reloading corresponding to that UL–RL cycle. One of the main implications of defining the formulation in the strain space is that this distance is expressed in terms of strains rather than stresses. Consequently, the closure of an UL–RL cycle is now defined in terms of strains. For a detailed explanation of the Memory Surface formulated in the deviatoric stress space, the reader is referred to 2.2.1.

Figure 7.1 shows the evolution of the shear stiffness reduction factor, R_g over time for both the MSB formulation defined in the stress space and in the strain space, using the same BVP as in Section 6. The shear stiffness reduction factor represents the current shear modulus normalised by its initial value, G_0. The figure provides a detailed view of the three intermediate consolidation phases, and includes a monotonic loading case that serves as a reference. During the first and third intermediate consolidation phases, an UL–RL cycle occurred. It is evident that both versions of the formulation capture these UL–RL cycles, as the elastic shear modulus suddenly increases to its high initial value and is subsequently reset to a lower value at a specific time instance, i.e., when the formulation detects that the Memory Surface has been reached. However, a clear trend is observed: the formulation in the stress space lags one step behind in resetting the elastic shear modulus (specifically, resetting the deviatoric strain history tensor **H**) compared to the formulation in the strain space.

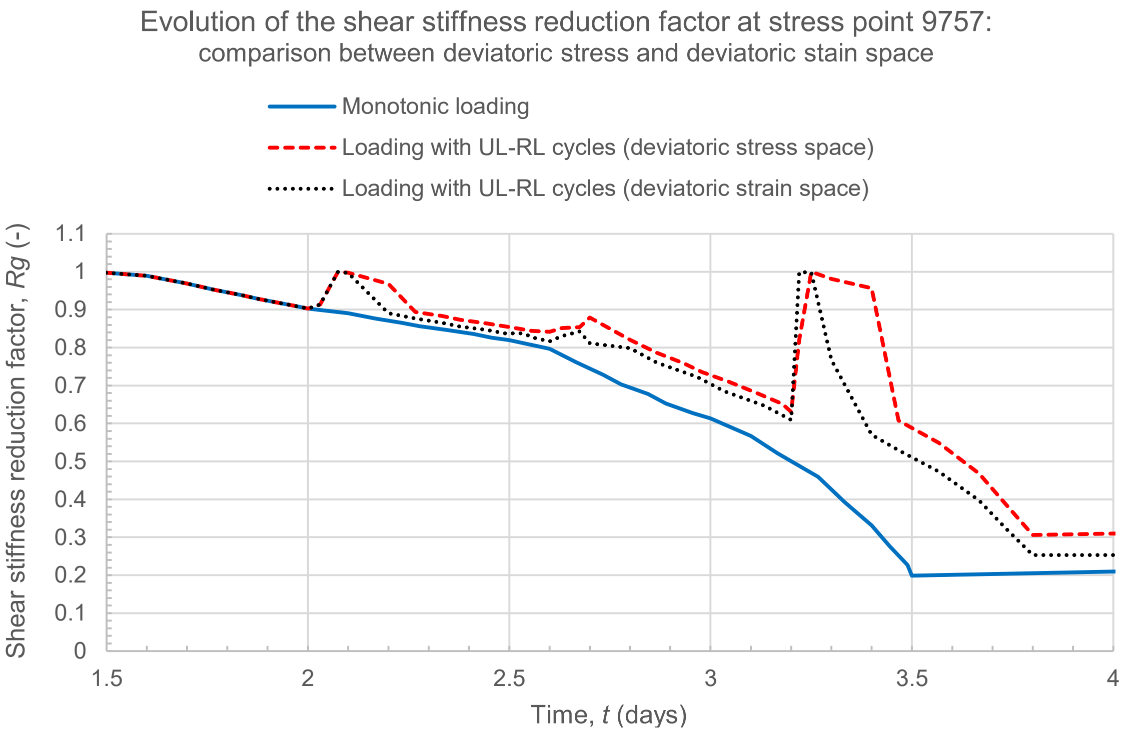

Figure 7.1: Evolution of the shear stiffness reduction factor over time during the excavation period for both the MSB formulation defined in the deviatoric stress space and defined in the deviatoric strain space.

7.1.2. Origin of the one-step lag in the deviatoric stress space

The HSsmall model employs an implicit integration scheme (Benz, 2007). As a consequence, an elastic trial is performed to estimate the stress state at the end of each calculation step based on elasticity. This may result in stress states beyond the shear and cap hardening yield surfaces, which is physically impossible. Therefore, a plastic correction is applied to return the stress state to the yield surfaces. For further information on the yield surfaces, the reader is referred to Section 2.1.1 and Schanz et al. (1999).

Because the elastic state variables are updated during the elastic trial, the final deviatoric stress state at the end of the calculation step is not yet known during this update. An example of such an elastic state variable is m, the radius of the Memory Surface, which is used to determine whether the Memory Surface has been reached and, consequently, whether the deviatoric strain history tensor **H** must be reset (Plaxis, 2025a).

To address this issue, the elastic state variables could, in principle, be updated during the plastic correction. However, this approach is complex and computationally demanding. Therefore, a simpler approach is adopted: the position of the Memory Surface is updated based on the stress state of the previous calculation step rather than that of the current one, i.e., the Memory-Surface lags one step (Plaxis, 2025a).

7.1.3. Explanation of the one-step lag approach

During each calculation step, a check is performed to determine whether the Memory Surface has been reached and, consequently, whether it is necessary to reset **H**. The one-step lag approach is illustrated in Figure 7.2. During calculation step 2, the Memory Surface values from calculation step 1 are used. Recall that the Memory Surface value is defined as the distance between the centre of the Memory Surface and the current deviatoric stress point, minus the radius of the Memory Surface. When this value is approximately equal to one, the Memory Surface has been reached. To make it possible to use the values from the previous step, the Memory Surface value at the start of calculation step 1 is stored (F_{StVar}), and the stress state at the start of calculation step 2 is used to compute the Memory Surface value at the end of calculation step 1 ($F = f(s_0)$) (note that the stress state at the end of calculation step 1 is equal to that at the start of calculation step 2). Hence, if a reset should have occurred during calculation step 1 because an UL–RL cycle was closed, it is only detected during calculation step 2,thereby introducing a one-step lag.

Such an approach is not required when the MSB formulation is defined in the deviatoric strain space, since the deviatoric strain increment **de**, corresponding to a calculation step, and consequently the deviatoric strain state at the end of the calculation step, is known.

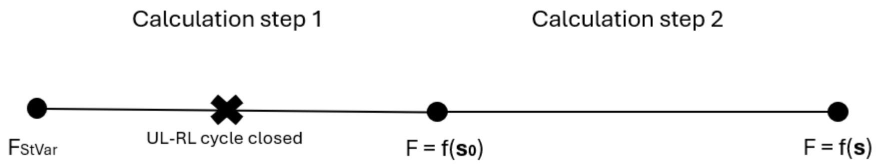

Figure 7.2: Schematisation of the "lag" approach implemented in the MSB formulation in the stress space.

7.1.4. Effect of the one-step lag approach on overshooting

The one-step lag approach introduces an additional step (calculation step 1 in Figure 7.2) before resetting **H**, during which the elastic shear modulus reduces. During this step, the elastic shear modulus of the monotonic response also decreases, but this additional decrease is not stored in the memory of the response with UL–RL cycles. As a result, when **H** is reset upon closure of the UL–RL cycle in an attempt to continue following the monotonic response, the monotonic response is already further along the elastic modulus reduction curve, which leads to overshooting. This additional step will be referred to as the *extra step* in the remainder of this study.

To support this explanation, a simple stress-controlled CD triaxial compression test is simulated, incorporating a single UL–RL cycle of $0.5\,\mathrm{kPa}$, using both the MSB formulation defined in the deviatoric stress space and in the deviatoric strain space. Preloading is applied and stress-dependency is deactivated to ensure that only elastic, strain-dependent behaviour is captured. The *extra step*, discussed in the previous paragraph, is simulated with three magnitudes: $0.25\,\mathrm{kPa}$, $5\,\mathrm{kPa}$, and $15\,\mathrm{kPa}$ (note that these steps are not extra when the formulation is defined in the strain space). A monotonic loading case is included in the figures as a reference. Figures 7.3a and 7.3b present the results including the UL–RL cycle, whereas Figures 7.3c and 7.3d present the results with the UL–RL cycle omitted while maintaining a continuous loading step sequence. The loading steps are defined such that each loading step corresponds to $1\,\mathrm{kPa}$.

At loading step 43, a SR triggering unloading occurs, causing the elastic shear modulus to increase to its high initial value and the current deviatoric strain history tensor **H** to be stored. At loading step 43.5, a SR triggering reloading occurs, again increasing the elastic shear modulus to its high initial value, this time with the Memory Surface relocated and its size readjusted. The subsequent step in the modelling sequence is 43.75, after which the extra step begins. At loading step 44 (note that this is not a loading step explicitly defined in the modelling sequence when the extra step is $5\,\mathrm{kPa}$ or $15\,\mathrm{kPa}$, and therefore occurs within a calculation step), the UL–RL cycle is closed, i.e., the Memory Surface has been reached. For the formulation defined in the strain space (7.3b), **H** is reset during the step in which the cycle is closed, whereas for the formulation in the stress space (7.3a), **H** is reset in the following step.

From Figures 7.3a and 7.3b, the one-step lag inherent to the formulation in the stress space becomes evident. It is clear that **H** resets one step later compared to the formulation in the strain space, for instance, at loading step 53.75 for the black dotted case in Figure 7.3a and at loading step 48.75 for the black dotted case in Figure 7.3b. It is also apparent that, during the extra step, the elastic shear modulus of the monotonic loading case continues to decrease.

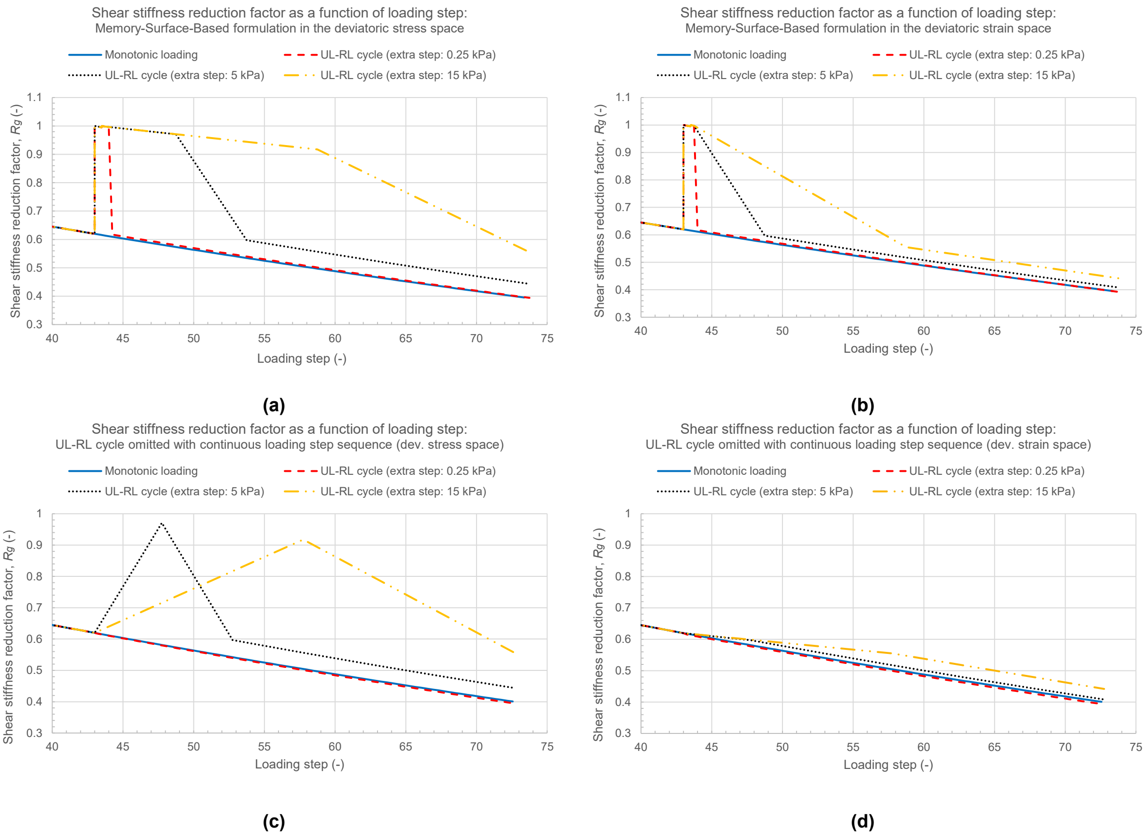

Figure 7.3: Evolution of the shear stiffness reduction factor over time for the MSB formulation defined in both the deviatoric stress space and in the deviatoric strain space involving one UL–RL cycle for different different magnitudes of the extra step: (a) formulation defined in the stress space (b) formulation defined in the strain space (c) formulation defined in the stress space. The UL–RL cycle is omitted in the figure, while maintaining a continuous loading step sequence (d) formulation defined in the strain space. The UL–RL cycle is omitted in the figure, while maintaining a continuous loading step sequence.

Figure 7.3c clearly shows that the elastic shear modulus obtained upon resetting **H** (at loading step 44 for the red dashed case, 48 for the black dotted case and, 58 for the orange dotted/dashed line) deviates from the monotonic loading case. In Figure 7.3d, this deviation is much smaller. The cause of the remaining deviation lies outside the scope of this study.

This lag, when the MSB formulation is defined in the deviatoric stress space, was difficult to identify in the single stress point simulations presented in Chapter 5, since the magnitude of the extra step was very small and the UL–RL cycles were always closed at the end of a step. For instance, in Figure 7.3c, the results are of good quality when the extra step is equal to $0.25\,\mathrm{kPa}$ (red dashed line). When the UL–RL cycle is closed at the end of a step, the peak observed in Figure 7.3c for the yellow dashed/dotted case and black dotted case does not appear (as illustrated by the red dashed case). In BVPs, however, these conditions are generally not met, thereby revealing the drawback.

The impact of the lag on the extent of overshooting becomes more pronounced (a) when the magnitude of the extra step increases, allowing for more reduction of the elastic shear modulus of the monotonic loading case, (b) when multiple UL–RL cycles occur, as the effect is cumulative, and (c) when the extra step occurs at deviatoric strain levels corresponding to the part of the elastic modulus reduction curve where the elastic shear modulus decreases more rapidly, leading to greater reduction of the elastic shear modulus in the monotonic loading case during the extra step.

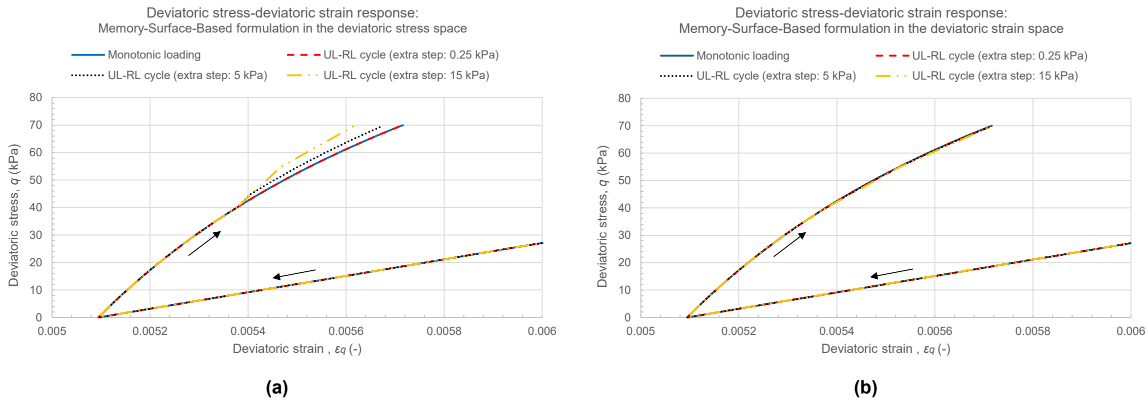

Figure 7.4: Comparison of the extent of overshooting when using the MSB formulation defined in the deviatoric stress space and in the deviatoric strain space.

As overshooting is most effectively evaluated through the deviatoric stress-deviatoric strain response (see 2), Figure 7.4 presents these responses. Figure 7.4a shows the results obtained with the MSB formulation defined in the stress space, whereas Figure 7.4b those obtained with the formulation defined in the strain space. The black arrows indicate the direction of the response. It is evident that overshooting is observed when the formulation is defined in the stress space, as the attained deviatoric strain is smaller. Moreover, the results confirm once again that a larger extra step amplifies overshooting. When the extra step is $0.25\,\mathrm{kPa}$, no overshooting is observed, as its magnitude is sufficiently small and the cycle closes at the end of a calculation step.

7.2. Sub-conclusion

When the MSB formulation is defined in the deviatoric stress space, the position of the Memory Surface lags one step behind the current deviatoric stress state. This is because, the stress states of the previous step are used to check whether the Memory Surface has been reached, i.e., whether an UL–RL cycle has been closed. Therefore, although an UL–RL cycle is actually closed in the previous step, it is only detected in the current step. The stress states of the previous step are used because the deviatoric stress state at the end of the current calculation step is unknown.

Due to this lag, an extra step is introduced during which the elastic shear modulus of the monotonic loading case continues to decrease. Since this additional decrease is not stored in the memory of the response with the UL–RL cycles, the elastic shear modulus obtained upon resetting **H** is larger than that of the monotonic loading case at the same time instance, resulting in overshooting. To prevent this overshooting, a formulation defined in the deviatoric strain space is a better approach, as the deviatoric strain state at the end of a calculation step is known.

This one-step lag was not identified in the single stress point simulations presented in Chapter 5, since the magnitude of the extra step was very small and the UL–RL cycles were always closed at the end of a calculation step. In BVPs, however, these conditions are generally not met, thereby revealing the drawback.

One could argue why a formulation in the stress space was considered in the first place. The reason for this stems from the early stages of the formulation's development and falls outside the scope of this study.

8
Discussion

This chapter first discusses difficulties encountered in the interpretation of overshooting in the presented BVP. The final part of the chapter considers factors that, while not directly affecting the obtained results, should be taken into account when interpreting the conclusions of this study.

Difficulties in the interpretation of overshooting in the BVP

Reference case
In this study, overshooting is assessed by comparing the material response under monotonic loading conditions with that under loading including small UL–RL cycles. The monotonic response serves as a reference, as no overshooting is assumed to occur in the absence of UL–RL cycles. Overshooting is quantified as the deviation between the monotonic response and the response including UL–RL cycles.

This paragraph explains why the monotonic response cannot strictly be considered a reference. Nonetheless, it is regarded as sufficiently reliable to serve as a reference in this study and is therefore used to draw conclusions on overshooting behaviour. Two factors limit the suitability of the monotonic loading case as an ideal reference:

1. **Adjustment of the elastic shear modulus upon a change in the deviatoric strain loading direction**
   Both the MSB formulation and the CB formulation adjust the elastic shear modulus upon a change in the deviatoric strain loading direction. Such changes in direction may occur in both the monotonic loading case and the case with UL–RL cycles. Once a change occurs in one of these cases, its deviatoric strain loading history, and consequently its material response, begins deviating from that of the other case (assuming that an exact same change in deviatoric strain loading direction does not occur at the exact same time instance in both cases). This has two implications:
   (a) A deviation between the responses under monotonic loading and loading with small UL–RL cycles can no longer be attributed solely to overshooting once a change in the deviatoric strain loading direction occurs in either the monotonic loading case or the loading case with UL-RL cycles.
   (b) When a change in deviatoric strain loading direction occurs in the monotonic loading case, it can no longer strictly serve as a reference for the assessment of overshooting.
2. **The occurrence of UL–RL cycles during the final consolidation phase**
   In this study, it was found that the UL–RL cycles observed in the BVP are mainly caused by numerical redistributions of stresses, especially when deformation mechanisms greatly disturb the soil. These stress redistributions occur not only during the intermediate consolidation phases, as initially expected, but also during the final consolidation phase, which is included in both the monotonic loading sequence and the sequence with short intermediate consolidation phases. Once a small UL–RL cycle occurs during the final consolidation phase of the monotonic loading sequence, it can no longer strictly serve as a reference, as overshooting could potentially also

occur in this case. Prior to this cycle, however, the monotonic loading case could serve as an ideal reference if the first factor limiting its suitability as a reference is disregarded.

The first limitation cannot easily be resolved, as it is inherent to both the MSB formulation and the CB formulation. However, its consequences are assumed to be minor. Nonetheless, it complicates the assessment of whether the potentially remaining difference between the monotonic response and the response including UL–RL cycles is caused solely by overshooting, which would indicate that the formulations could still be improved, by this limitation, suggesting that overshooting may no longer occur, or by a combination of both.

The second limitation cannot be resolved either, as numerical stress redistributions cannot be prevented. However, this limitation can partly be mitigated by showing only a small part of the final consolidation phase in the presented results, a strategy that was also adopted in some analyses in this study.

In the single stress point simulations, these limitations were not evident due to the following two reasons: (i) numerical redistributions of stresses did not occur in either the monotonic case or the case with UL–RL cycles, and (ii) changes in the deviatoric strain loading direction mainly occur in multi-directional stress paths, which are not present in the single stress point simulations performed in this study.

Extent of overshooting dependent on location and time in the BVP
The observed extent of overshooting in the BVP depends on the location within the model and time instance during the simulation. Stress paths and deviatoric stress-deviatoric strain responses can vary significantly between different stress points. Only a limited number of stress points (and nodes) were considered in this study. Therefore, stress points (and nodes) may have been missed where overshooting still occurs when using the MSB formulation and the CB formulation. However, the analysed stress points (and node) were selected because they were either located at practically relevant positions or at a location where overshooting was expected to be most significant.

Node and stress point chosen on the axis of symmetry for analysis purposes
For the analysis of the BVP presented in this study, nodes and stress points were selected in the model to evaluate their vertical displacement over time and deviatoric stress-deviatoric strain response. Two of these points, one node and one stress point, were selected at and very close to the axis of symmetry of the model. The axis of symmetry is a model boundary where boundary conditions are imposed. It is undesirable to select nodes or stress points on the axis of symmetry for analysis purposes, since they are forced to exhibit behaviour corresponding to the imposed boundary conditions rather than behaviour that follows from the physical principles on which the model is based.

However, this limitation only concerns the sections related to the evaluation of the vertical displacement at the centre of the final excavation bottom and the comparison with the results reported by Cudny and Truty (2020). The centre of the final excavation bottom was chosen to enable a comparison with the results reported by Cudny and Truty (2020).

Applicability of the drawn conclusions

Study part of ongoing research
This study is part of ongoing research into optimisation of the MSB formulation and the CB formulation. This implies that the final version of the formulations used in this study is not necessarily the same as the version that will eventually be released. Therefore, the findings presented in this study are only applicable to the versions considered here.

Limited number of tests and BVPs
Due to the limited time available for this study, only a limited number of tests and BVPs could be considered. This inherently means that the formulations were not tested under all possible conditions. Clearly, it is not realistic to perform an infinite number of tests and BVPs. Nonetheless, only one BVP was considered: a static, two-dimensional, dewatering excavation case. Some potentially detrimental loading conditions were not included, such as dynamic (cyclic) loading or a three-dimensional analysis. Therefore, it should be kept in mind that the conclusions drawn in this study cannot necessarily be considered true for all other cases.

9 Conclusions

The purpose of this chapter is to present the conclusions drawn from this study. The first section addresses the main research question by reflecting on the corresponding sub-questions. The second section discusses which of the two formulations provides the most suitable approach to mitigate overshooting. The third and final section summarises additional findings obtained from this study.

9.1. Main research question

The main research question addressed in this study was as follows:

To what extent do the Continuous Brick formulation, as a new formulation for small-strain stiffness, and the Memory-Surface-based formulation, as an extension to the existing small-strain stiffness formulation within the Hardening Soil small-strain model, reduce the overshooting observed in the current formulation?

This question is addressed by reflecting on the corresponding sub-questions, which are discussed below.

What factors influence the extent of overshooting, and how?
Among other factors, it was found that both the amplitude of an UL–RL cycle and the degree of elasto-plastic behaviour influence the extent of overshooting. Specifically, a larger amplitude results in a smaller extent of overshooting, and the more dominant the plastic component of the HSsmall model becomes, the smaller the extent of overshooting.

To what extent do the numerical implementations of the two proposed formulations correctly reproduce their underlying analytical formulation?
In order to assess whether the proposed formulations are effective in reducing overshooting, it was first verified that their numerical implementations correctly reproduce their underlying analytical formulations. If this is not the case, the observed material response could be the result of an error in the source code, making it difficult to determine whether any observed overshooting is inherent to the formulations themselves.

In the single stress point simulations, the numerical implementation of the MSB formulation was found to correctly reproduce the underlying analytical formulation in almost all cases. Only in the CD triaxial compression test simulation under stress-dependent, elasto-plastic conditions an inconsistency was identified. In principle, this inconsistency could lead to overshooting, however it was negligible in this specific simulation and was easily resolved. In the numerical implementation of the CB formulation, two inconsistencies became apparent. Although these inconsistencies did not cause overshooting, they resulted in an incorrect material response and therefore had to be resolved.

In the BVP, no inconsistencies were encountered for the CB formulation, whereas one was identified for the MSB formulation. The formulation was implemented such that the elastic shear modulus would reset one step later than the actual closure of an UL–RL cycle, in order to avoid complex and computationally demanding procedures to obtain the deviatoric stress state at the end of a calculation step. However, in the BVP it became evident that this strategy may result in overshooting. This issue was not identified in the single stress point simulations because the calculation step sizes were too small and because each UL–RL cycle always closed at the end of a calculation step. Conditions that are generally not met in a BVP, thereby revealing the limitation. The problem was resolved by defining the formulation in the deviatoric strain space, where the deviatoric strain state at the end of a calculation step is known.

In conclusion, both the MSB formulation and the CB formulation correctly reproduce their underlying analytical formulations once the identified inconsistencies were resolved, based on the laboratory test simulations and BVP performed in this study.

What potential changes can be identified to improve or refine the two proposed formulations?
When unexpected behaviour was observed in the material response, and the underlying analytical formulation was confirmed to be correctly reproduced, it was assessed whether there was room for improvement, either to make it more consistent with the expected physical behaviour or to reduce overshooting. The latter directly contributes to the main research question.

In the single stress point simulations, no potential improvements were identified for the MSB formulation, whereas several were identified and subsequently implemented for the CB formulation: (i) the criterion for classifying a SR as corresponding to either unloading or reloading conditions was improved. Previously, this criterion could result in loading conditions being detected opposite to what they actually were. This could have a detrimental effect on the memory, as the current elastic shear modulus is stored upon a SR triggering unloading, which should correspond to the onset of an UL–RL cycle, (ii) it was ensured that, upon the activation of a brick, the elastic shear modulus is reset only when an UL–RL cycle is closed. Previously, the reset could occur too soon, which is inconsistent with the expected physical behaviour where the monotonic material response is continued after an UL–RL cycle is closed, (iii) it was ensured that the elastic shear modulus was no longer updated upon a change in the strain loading direction when all bricks were are already activated, thereby correctly retaining its lower bound, the UL–RL elastic shear modulus, and (iv) it was ensured that the formulation would no longer retain the memory of a larger cycle when a sequence of smaller cycles occurs within it during which no brick is active. Otherwise, when the first brick is activated, the memory of the larger cycle would be used. Although it could be desirable for the formulation to memorise the larger cycle, it would not be possible to determine whether this larger cycle would actually be closed when the first brick is activated. As a result, the elastic shear modulus could be reset before the larger UL–RL cycle being closed.

In the BVP, the situation was reversed. No potential changes were identified for the CB formulation, whereas two were identified and implemented for the MSB formulation: (i) the SR detection algorithm was modified to ensure that only full SRs are captured by the MSB formulation and, (ii) an extension was added to the SR detection algorithm to ensure that SRs are detected when they are masked by large deviatoric strain increments.

How do the results obtained with the two proposed formulations differ from those obtained with the original Hardening Soil small-strain model?
The monotonic response, both purely elastic and elasto-plastic, obtained with the MSB formulation coincides with that of the original HSsmall model. For the CB formulation, the monotonic elasto-plastic response was observed to be softer, while the elastic response coincides with that of the original HSsmall model. This softer response can be counteracted to a large extent by multiplying the model parameter $\gamma_{0.7}$ by a factor of two. However, in some simulations, a softer response was still observed.

The responses with UL–RL cycles differ, as expected, since overshooting is inherent to the HSsmall model, whereas both the MSB formulation and the CB formulation were specifically designed to mitigate this behaviour.

To what extent do the two proposed formulations effectively reduce overshooting at a single stress point level?
The MSB formulation and the CB formulation reduce overshooting to a negligible level in the laboratory test simulations performed in this study, both under purely elastic, stress-independent conditions and under elasto-plastic, stress-dependent conditions. In all cases, the material response under monotonic loading approximately coincides with that under loading with UL–RL cycles, demonstrating that

overshooting has been effectively reduced.

Two drawbacks were identified that can potentially result in overshooting: (i) both formulations are capable of memorising only a single UL-RL cycle, which could become problematic when nested cycles occur, and (ii) the CB formulation stores the memory of an UL-RL cycle only if a brick was active at the onset of that cycle.

The second drawback could potentially be resolved by shortening the string length of the first brick. However, this was not tested in this study. The first drawback is more difficult to address, as resolving it would require a substantial increase in the number of elastic state variables and consequently in computational memory usage, and is therefore considered a significant limitation that should be taken into account.

How effective are the two proposed formulations in reducing overshooting when applied to a boundary value problem?
Both the MSB formulation and the CB formulation were found to effectively reduce overshooting. When compared with the results reported by Cudny and Truty (2020), the results are of similar quality.

The two drawbacks identified in the single stress point simulations also became apparent in the analysis of the BVP. It was observed that the first drawback can result in a substantial amount of overshooting, whereas the overshooting caused by the second drawback was negligible.

Returning to the main research question

The main research question can now be answered as follows: both the MSB formulation and the CB formulation effectively reduce overshooting to a negligible level, provided that nested cycles do not occur. The occurrence of nested cycles in simulations reduces the effectiveness of both formulations. Further research is needed to determine whether the consequences of these nested cycles can be neglected in practical geotechnical analyses, and to identify the conditions, both numerical and physical, under which such nested cycles arise. If their consequences cannot be considered negligible, the formulations are not sufficiently robust and a further improvement to the formulations would be required. If their consequences can be regarded as negligible, both formulations can be considered sufficiently robust, and there is no need to consult additional literature for alternative approaches to mitigate overshooting; instead, a choice must be made between the two formulations.

9.2. Most suitable approach

A summary of the main advantages and disadvantages of both formulations is presented in Table 9.1. Both formulations have comparable runtimes in both the single stress point simulations and the BVP, and both share the limitation of retaining the memory of only a single UL-RL cycle. Therefore, these aspects are omitted from the table, as they do not lead to any differences between the two formulations. From the table, it is evident that the MSB formulation offers considerably more advantages than the CB formulation. Therefore, based on the performed simulations, this study concludes that the MSB formulation is the most suitable approach to mitigate overshooting in the HSsmall model. If a follow-up study demonstrates that the limitation exhibited by both formulations to retain the memory of only a single UL–RL cycle cannot be considered negligible in practical geotechnical analyses, the adoption of the CB formulation may be reconsidered, since a potential solution has already been implemented in its source code.

	MSB formulation	CB formulation
Advantages	• Easier to interpret • Seems more robust • Retains the small-strain component of the HSsmall model	• Slightly less elastic state variables • Easily extendable to potentially address the memory limitation of a single UL–RL cycle (by using more bricks)
Disadvantages		• Only stores the previous memory if at least one brick is active at the onset of the corresponding UL–RL cycle • Results may differ from those obtained with the current version of HSsmall under elasto-plastic conditions

Table 9.1: Comparison between the MSB formulation and the CB formulation.

9.3. Additional findings

Influence of overshooting on the sheet pile wall

This study shows that overshooting in the HSsmall model affects not only the soil but also the sheet pile wall. It leads to smaller calculated bending moments and, consequently, smaller horizontal deformations. This is caused by the fact that the soil behaves stiffer due to overshooting, and a stiffer material carries a larger share of the load, resulting in less load being transferred to the sheet pile wall. When using the MSB or CB formulation, a reduced bending moment is no longer observed.

Cause of the UL–RL cycles in the boundary value problem

The UL–RL cycles observed in the BVP presented in this study are mainly caused by numerical redistributions of stresses triggered by physical deformation mechanisms and increased model complexity, leading to stress imbalances that are resolved when the model is allowed time to adjust to a new equilibrium, i.e., when no additional changes to the model conditions are imposed.

10 Recommendations

From a practical perspective, extending the HSsmall model with the MSB formulation will lead to more accurate deformation estimations in geotechnical problems especially within the pre-failure range (serviceability limit states). Specifically, deformations will no longer be underestimated, which is quite significant in practical applications, at no cost of additional model parameters. This is true not only for the soil itself but also for structural elements such as a sheet pile wall. By implementing the MSB formulation, less load is transferred to the soil and a larger portion to the structural element, as the soil behaviour is no longer overly stiff due to overshooting.

Furthermore, the material response under monotonic loading conditions obtained with the MSB formulation does not deviate from that of the original HSsmall model. Therefore, adopting this formulation will not have major implications for the end user, as previously obtained results will remain unchanged, except for those that exhibit overshooting.

Finally, since the UL–RL cycles observed in the BVP presented in this study were found to be mainly caused by numerical redistributions of stresses, a phenomenon that can occur in any numerical simulation, especially where deformation mechanisms greatly disturb the soil, the MSB formulation could potentially improve the results in many numerical simulations of geotechnical problems.

This study suggests several possibilities for follow-up research:

1. **Dynamic loading case**
   In this study, the ability of the two proposed formulations to reduce overshooting was not evaluated under dynamic loading conditions. However, as became evident in this study, such conditions could result in overshooting, since both formulations retain the memory of only one UL–RL cycle, and nested cycles are more likely to occur under these loading conditions. Therefore, a follow-up study is recommended to evaluate the performance of both formulations under such conditions, for instance, in a seismic loading case. If this limitation proves to cause a significant extent of overshooting, versions of the MSB and CB formulations that are capable of memorising more than a single cycle should be tested and it should be assessed whether they do not require excessive computer memory storage.
2. **Three-dimensional simulation**
   Only 1D and 2D cases were considered in this study. It is recommended to perform also a 3D analysis, as such an analysis would include the influence of the out-of-plane conditions and therefore yield a more realistic stress path. Since the computational efficiency of both formulations appeared to be similar, a 3D analysis may reveal whether one formulation is computationally less efficient than the other.
3. **Validation**
   Both the MSB formulation and the CB formulation were not validated in this study. Validation is recommended to assess whether their results are consistent with real physical behaviour, particularly for the CB formulation, as its monotonic response under elasto-plastic conditions deviates

from that of the original HSsmall model.

4. **Partial SRs in the MSB formulation**
   A follow-up study could investigate whether adjusting the elastic shear modulus upon changes in the strain loading direction is consistent with physical behaviour. Furthermore, it could be examined whether the results of the MSB formulation align more closely with physical reality if the Memory Surface tracks UL–RL cycles separately for each of the three eigen directions of the current deviatoric strain increment.

References

Amorosi, A., Boldini, D., & di Lernia, A. (2016). Seismic ground response at lotung: Hysteretic elasto-plastic-based 3d analyses. *Soil Dynamics and Earthquake Engineering*, *85*, 44–61. https://doi.org/10.1016/j.soildyn.2016.03.001

Bentley Systems. (2024, May). *Plaxis 2d 2024.2 reference manual* [Last updated: May 07, 2024]. https://www.bentley.com/en/products/brands/plaxis

Benz, T. (2007). *Small-strain stiffness of soils and its numerical consequences* [Doctoral dissertation]. Universität Stuttgart.

Burland, J. B. (1989). Ninth laurits bjerrum memorial lecture: “small is beautiful”—the stiffness of soils at small strains. *Canadian Geotechnical Journal*, *26*, 499–516.

Cudny, M., & Truty, A. (2020). Refinement of the hardening soil model within the small strain range. *Acta Geotechnica*, *15*, 2031–2051. https://doi.org/10.1007/s11440-020-00945-5

Hardin, B. O., & Drnevich, V. P. (1972). Shear modulus and damping in soils: Design equations and curves. *Journal of the Soil Mechanics and Foundations Division, ASCE*, *98*(SM7), 667–692. https://doi.org/10.1061/JSFEAQ.0001760

Kan, M. E., & Taiebat, H. A. (2014). On implementation of bounding surface plasticity models with no overshooting effect in solving boundary value problems. *Computers and Geotechnics*, *55*, 103–116. https://doi.org/10.1016/j.compgeo.2013.08.006

Li, Z., & Liu, H. (2020). An isotropic-kinematic hardening model for cyclic shakedown and ratcheting of sand. *Soil Dynamics and Earthquake Engineering*, *138*, 1–17.

Masing, G. (1926). Eigenspannungen und verfestigung beim messing. *Proceedings of the Second International Congress of Applied Mechanics*.

Niemunis, A., & Cudny, M. (2018). Discussion on “dynamic soil-structure interaction: A three-dimensional numerical approach and its application to the lotung case study”. poor performance of the hss model. *Computers and Geotechnics*. https://doi.org/10.1016/j.compgeo.2018.02.003

Papadimitriou, A. G., & Bouckovalas, G. D. (2002). Plasticity model for sand under small and large cyclic strains: A multiaxial formulation. *Soil Dynamics and Earthquake Engineering*, *22*(3), 191–204.

Plaxis. (2025a). Internal documentation: A memory surface-enhanced small strain model [Unpublished internal documentation, Plaxis, part of Seequent, the Bentley Subsurface company].

Plaxis. (2025b). Internal documentation: Continuous brick model [Unpublished internal documentation, Plaxis, part of Seequent, the Bentley Subsurface company].

Plaxis. (2025c). Internal documentation: Original formulation of the small strain stiffness [Unpublished internal documentation, Plaxis, part of Seequent, the Bentley Subsurface company].

Santos, J., & Correia, A. (2001). Reference threshold shear strain of soil: Its application to obtain a unique strain-dependent shear modulus curve for soil. *Proceedings of the 15th International Conference on Soil Mechanics and Geotechnical Engineering (ISSMGE)*, *1*, 267–270.

Schanz, T., Vermeer, P. A., & Bonnier, P. G. (1999). The hardening soil model: Formulation and verification. *Beyond 2000 in Computational Geotechnics – 10 Years of PLAXIS*, 1–16.

Seed, H. B., & Idriss, I. M. (1970, December). *Soil moduli and damping factors for dynamic response analyses* (tech. rep.). Earthquake Engineering Research Center, University of California, Berkeley. https://ntrl.ntis.gov/NTRL/dashboard/searchResults/titleDetail/PB197869.xhtml

Simpson, B. (1992). Retaining structures: Displacement and design (32nd rankine lecture). *Géotechnique*, *42*(4), 541–576. https://doi.org/10.1680/geot.1992.42.4.541

Tafili, M., Duque, J., Mašín, D., & Wichtmann, T. (2024). Repercussion of overshooting effects on elemental and finite-element simulations [Technical Note]. *International Journal of Geomechanics*, *24*(3), 06024001. https://doi.org/10.1061/IJGNAI.GMENG-8842

A

Test specifications single stress point simulations

This appendix provides an overview of the input used for the single stress point simulations. An example lay-out is shown below:

100						= number of steps in phase 1
1						= phase duration for phase 1
0	0	0	0	0	0	= strain increments for phase 1
200	200	200	0	0	0	= stress increments for phase 1
1	1	1	1	0	0	= boundary conditions

Each row corresponds to a stress or strain vector in the following order:

$$\begin{array}{cccccc} \sigma_{xx} & \sigma_{yy} & \sigma_{zz} & \sigma_{xy} & \sigma_{yz} & \sigma_{zx} \\ \varepsilon_{xx} & \varepsilon_{yy} & \varepsilon_{zz} & \varepsilon_{xy} & \varepsilon_{yz} & \varepsilon_{zx} \end{array}$$

The boundary condition value determines whether, in a specific simulation phase, the stress or strain component is controlled:

(a) A value of 0 means the strain is being controlled

(b) A value of 1 means the stress is being controlled

The input for the elasto-plastic simulations is not provided, as it is nearly identical to that of the elastic simulations. The only differences are:

(a) Phases 1, 2, and 3 (pre-loading) are omitted

(b) The initial stresses are defined as follows:

-100 -100 -100 0 0 0

Consolidated drained triaxial compression test simulation – monotonic loading

-300	-300	-300	0	0	0	= initial stresses
4						= number of phases
100						= number of steps in phase 1
1						= phase duration for phase 1
0	0	0	0	0	0	= strain increments for phase 1
200	200	200	0	0	0	= stress increments for phase 1
1	1	1	1	0	0	= boundary conditions
100						= number of steps in phase 2
1						= phase duration for phase 2
0	0	0	0	0	0	= strain increments for phase 2
0	-195	0	0	0	0	= stress increments for phase 2
1	1	1	1	0	0	= boundary conditions
100						= number of steps in phase 3
1						= phase duration for phase 3
0	0	0	0	0	0	= strain increments for phase 3
0	195	0	0	0	0	= stress increments for phase 3
1	1	1	1	0	0	= boundary conditions
600						= number of steps in phase 4
16						= phase duration for phase 4
0	0	0	0	0	0	= strain increments for phase 4
0	-150	0	0	0	0	= stress increments for phase 4
1	1	1	1	0	0	= boundary conditions

Consolidated drained triaxial compression test simulation – loading with small unloading–reloading cycles

-300	-300	-300	0	0	0	= initial stresses
19						= number of phases
100						= number of steps in phase 1
1						= phase duration for phase 1
0	0	0	0	0	0	= strain increments for phase 1
200	200	200	0	0	0	= stress increments for phase 1
1	1	1	1	0	0	= boundary conditions
100						= number of steps in phase 2
1						= phase duration for phase 2
0	0	0	0	0	0	= strain increments for phase 2

0	-195	0	0	0	0	= stress increments for phase 2
1	1	1	1	0	0	= boundary conditions
100						= number of steps in phase 3
1						= phase duration for phase 3
0	0	0	0	0	0	= strain increments for phase 3
0	195	0	0	0	0	= stress increments for phase 3
1	1	1	1	0	0	= boundary conditions
100						= number of steps in phase 4
1						= phase duration for phase 4
0	0	0	0	0	0	= strain increments for phase 4
0	-25	0	0	0	0	= stress increments for phase 4
1	1	1	1	0	0	= boundary conditions
100						= number of steps in phase 5
1						= phase duration for phase 5
0	0	0	0	0	0	= strain increments for phase 5
0	0.5	0	0	0	0	= stress increments for phase 5
1	1	1	1	0	0	= boundary conditions
100						= number of steps in phase 6
1						= phase duration for phase 6
0	0	0	0	0	0	= strain increments for phase 6
0	-0.5	0	0	0	0	= stress increments for phase 6
1	1	1	1	0	0	= boundary conditions
100						= number of steps in phase 7
1						= phase duration for phase 7
0	0	0	0	0	0	= strain increments for phase 7
0	-25	0	0	0	0	= stress increments for phase 7
1	1	1	1	0	0	= boundary conditions

The last three phases are repeated four more times

Undrained direct simple shear test simulation – monotonic loading

-300	-300	-300	0	0	0	= initial stresses
4						= number of phases
100						= number of steps in phase 1
1						= phase duration for phase 1
0	0	0	0	0	0	= strain increments for phase 1
200	200	200	0	0	0	= stress increments for phase 1

1	1	1	0	0	0	= boundary conditions
100						= number of steps in phase 2
1						= phase duration for phase 2
0	0	0	0	0	0	= strain increments for phase 2
0	-195	0	0	0	0	= stress increments for phase 2
1	1	1	0	0	0	= boundary conditions
100						= number of steps in phase 3
1						= phase duration for phase 3
0	0	0	0	0	0	= strain increments for phase 3
0	195	0	0	0	0	= stress increments for phase 3
1	1	1	0	0	0	= boundary conditions
700						= number of steps in phase 4
19						= phase duration for phase 4
0	0	0	0	0	0	= strain increments for phase 4
0	0	0	35	0	0	= stress increments for phase 4
0	0	0	1	0	0	= boundary conditions

Undrained direct simple shear test simulation – loading with small unloading–reloading cycles

-300	-300	-300	0	0	0	= initial stresses
22						= number of phases
100						= number of steps in phase 1
1						= phase duration for phase 1
0	0	0	0	0	0	= strain increments for phase 1
200	200	200	0	0	0	= stress increments for phase 1
1	1	1	0	0	0	= boundary conditions
100						= number of steps in phase 2
1						= phase duration for phase 2
0	0	0	0	0	0	= strain increments for phase 2
0	-195	0	0	0	0	= stress increments for phase 2
1	1	1	0	0	0	= boundary conditions
100						= number of steps in phase 3
1						= phase duration for phase 3
0	0	0	0	0	0	= strain increments for phase 3
0	195	0	0	0	0	= stress increments for phase 3
1	1	1	0	0	0	= boundary conditions
100						= number of steps in phase 4

1						= phase duration for phase 4
0	0	0	0	0	0	= strain increments for phase 4
0	0	0	5	0	0	= stress increments for phase 4
0	0	0	1	0	0	= boundary conditions
100						= number of steps in phase 5
1						= phase duration for phase 5
0	0	0	0	0	0	= strain increments for phase 5
0	0	0	-0.5	0	0	= stress increments for phase 5
0	0	0	1	0	0	= boundary conditions
100						= number of steps in phase 6
1						= phase duration for phase 6
0	0	0	0	0	0	= strain increments for phase 6
0	0	0	0.5	0	0	= stress increments for phase 6
0	0	0	1	0	0	= boundary conditions
100						= number of steps in phase 7
1						= phase duration for phase 7
0	0	0	0	0	0	= strain increments for phase 7
0	0	0	5	0	0	= stress increments for phase 7
0	0	0	1	0	0	= boundary conditions

The last three phases are repeated for five more times

Drained oedometer test simulation – monotonic loading

-300	-300	-300	0	0	0	= initial stresses
4						= number of phases
100						= number of steps in phase 1
1						= phase duration for phase 1
0	0	0	0	0	0	= strain increments for phase 1
200	200	200	0	0	0	= stress increments for phase 1
1	1	1	0	0	0	= boundary conditions
100						= number of steps in phase 2
1						= phase duration for phase 2
0	0	0	0	0	0	= strain increments for phase 2
0	-195	0	0	0	0	= stress increments for phase 2
1	1	1	0	0	0	= boundary conditions
100						= number of steps in phase 3
1						= phase duration for phase 3
0	0	0	0	0	0	= strain increments for phase 3

0	195	0	0	0	0	= stress increments for phase 3
1	1	1	0	0	0	= boundary conditions
700						= number of steps in phase 4
22						= phase duration for phase 4
0	0	0	0	0	0	= strain increments for phase 4
0	-35	0	0	0	0	= stress increments for phase 4
0	1	0	0	0	0	= boundary conditions

Drained oedometer test simulation – loading with small unloading–reloading cycles

-300	-300	-300	0	0	0	= initial stresses
22						= number of phases
100						= number of steps in phase 1
1						= phase duration for phase 1
0	0	0	0	0	0	= strain increments for phase 1
200	200	200	0	0	0	= stress increments for phase 1
1	1	1	0	0	0	= boundary conditions
100						= number of steps in phase 2
1						= phase duration for phase 2
0	0	0	0	0	0	= strain increments for phase 2
0	-195	0	0	0	0	= stress increments for phase 2
1	1	1	0	0	0	= boundary conditions
100						= number of steps in phase 3
1						= phase duration for phase 3
0	0	0	0	0	0	= strain increments for phase 3
0	195	0	0	0	0	= stress increments for phase 3
1	1	1	0	0	0	= boundary conditions
100						= number of steps in phase 4
1						= phase duration for phase 4
0	0	0	0	0	0	= strain increments for phase 4
0	-5	0	0	0	0	= stress increments for phase 4
0	1	0	0	0	0	= boundary conditions
100						= number of steps in phase 5
1						= phase duration for phase 5
0	0	0	0	0	0	= strain increments for phase 5
0	0.5	0	0	0	0	= stress increments for phase 5
0	1	0	0	0	0	= boundary conditions

100						= number of steps in phase 6
1						= phase duration for phase 6
0	0	0	0	0	0	= strain increments for phase 6
0	-0.5	0	0	0	0	= stress increments for phase 6
0	1	0	0	0	0	= boundary conditions
100						= number of steps in phase 7
1						= phase duration for phase 7
0	0	0	0	0	0	= strain increments for phase 7
0	-5	0	0	0	0	= stress increments for phase 7
0	1	0	0	0	0	= boundary conditions

The last three phases are repeated five more times.

Tailored consolidated drained triaxial compression test simulation with nested UL-RL cycles

-300	-300	-300	0	0	0	= initial stresses
13						= number of phases
100						= number of steps in phase 1
1						= phase duration for phase 1
0	0	0	0	0	0	= strain increments for phase 1
200	200	200	0	0	0	= stress increments for phase 1
1	1	1	1	0	0	= boundary conditions
100						= number of steps in phase 2
1						= phase duration for phase 2
0	0	0	0	0	0	= strain increments for phase 2
0	-195	0	0	0	0	= stress increments for phase 2
1	1	1	1	0	0	= boundary conditions
100						= number of steps in phase 3
1						= phase duration for phase 3
0	0	0	0	0	0	= strain increments for phase 3
0	195	0	0	0	0	= stress increments for phase 3
1	1	1	1	0	0	= boundary conditions
100						= number of steps in phase 4
1						= phase duration for phase 4
0	0	0	0	0	0	= strain increments for phase 4
0	-20	0	0	0	0	= stress increments for phase 4
1	1	1	1	0	0	= boundary conditions
100						= number of steps in phase 5

1						= phase duration for phase 5
0	0	0	0	0	0	= strain increments for phase 5
0	15	0	0	0	0	= stress increments for phase 5
1	1	1	1	0	0	= boundary conditions
100						= number of steps in phase 6
1						= phase duration for phase 6
0	0	0	0	0	0	= strain increments for phase 6
0	-5	0	0	0	0	= stress increments for phase 6
1	1	1	1	0	0	= boundary conditions
100						= number of steps in phase 7
1						= phase duration for phase 7
0	0	0	0	0	0	= strain increments for phase 7
0	0.5	0	0	0	0	= stress increments for phase 7
1	1	1	1	0	0	= boundary conditions
100						= number of steps in phase 8
1						= phase duration for phase 8
0	0	0	0	0	0	= strain increments for phase 8
0	-0.5	0	0	0	0	= stress increments for phase 8
1	1	1	1	0	0	= boundary conditions
100						= number of steps in phase 9
1						= phase duration for phase 9
0	0	0	0	0	0	= strain increments for phase 9
0	-10	0	0	0	0	= stress increments for phase 9
1	1	1	1	0	0	= boundary conditions
100						= number of steps in phase 10
1						= phase duration for phase 10
0	0	0	0	0	0	= strain increments for phase 10
0	-5	0	0	0	0	= stress increments for phase 10
1	1	1	1	0	0	= boundary conditions
100						= number of steps in phase 11
1						= phase duration for phase 11
0	0	0	0	0	0	= strain increments for phase 11
0	0.5	0	0	0	0	= stress increments for phase 11
1	1	1	1	0	0	= boundary conditions
100						= number of steps in phase 12
1						= phase duration for phase 12
0	0	0	0	0	0	= strain increments for phase 12
0	-0.5	0	0	0	0	= stress increments for phase 12
1	1	1	1	0	0	= boundary conditions

100						= number of steps in phase 13
1						= phase duration for phase 13
0	0	0	0	0	0	= strain increments for phase 13
0	-10	0	0	0	0	= stress increments for phase 13
1	1	1	1	0	0	= boundary conditions

Tailored consolidated drained triaxial test simulation to investigation the detection of strain reversal in triaxial extension and compression

-300	-300	-300	0	0	0	= initial stresses
13						= number of phases
100						= number of steps in phase 1
1						= phase duration for phase 1
0	0	0	0	0	0	= strain increments for phase 1
200	200	200	0	0	0	= stress increments for phase 1
1	1	1	1	0	0	= boundary conditions
100						= number of steps in phase 2
1						= phase duration for phase 2
0	0	0	0	0	0	= strain increments for phase 2
0	-195	0	0	0	0	= stress increments for phase 2
1	1	1	1	0	0	= boundary conditions
100						= number of steps in phase 3
1						= phase duration for phase 3
0	0	0	0	0	0	= strain increments for phase 3
0	195	0	0	0	0	= stress increments for phase 3
1	1	1	1	0	0	= boundary conditions
100						= number of steps in phase 4
1						= phase duration for phase 4
0	0	0	0	0	0	= strain increments for phase 4
0	-20	0	0	0	0	= stress increments for phase 4
1	1	1	1	0	0	= boundary conditions
100						= number of steps in phase 5
1						= phase duration for phase 5
0	0	0	0	0	0	= strain increments for phase 5
0	10	0	0	0	0	= stress increments for phase 5
1	1	1	1	0	0	= boundary conditions
100						= number of steps in phase 6
1						= phase duration for phase 6

0	0	0	0	0	0	= strain increments for phase 6
0	-0.5	0	0	0	0	= stress increments for phase 6
1	1	1	1	0	0	= boundary conditions
100						= number of steps in phase 7
1						= phase duration for phase 7
0	0	0	0	0	0	= strain increments for phase 7
0	0.5	0	0	0	0	= stress increments for phase 7
1	1	1	1	0	0	= boundary conditions
100						= number of steps in phase 8
1						= phase duration for phase 8
0	0	0	0	0	0	= strain increments for phase 8
0	30	0	0	0	0	= stress increments for phase 8
1	1	1	1	0	0	= boundary conditions
100						= number of steps in phase 9
1						= phase duration for phase 9
0	0	0	0	0	0	= strain increments for phase 9
0	-10	0	0	0	0	= stress increments for phase 9
1	1	1	1	0	0	= boundary conditions
100						= number of steps in phase 10
1						= phase duration for phase 10
0	0	0	0	0	0	= strain increments for phase 10
0	0.5	0	0	0	0	= stress increments for phase 10
1	1	1	1	0	0	= boundary conditions
100						= number of steps in phase 11
1						= phase duration for phase 11
0	0	0	0	0	0	= strain increments for phase 11
0	-0.5	0	0	0	0	= stress increments for phase 11
1	1	1	1	0	0	= boundary conditions
100						= number of steps in phase 12
1						= phase duration for phase 12
0	0	0	0	0	0	= strain increments for phase 12
0	-30	0	0	0	0	= stress increments for phase 12
1	1	1	1	0	0	= boundary conditions

B

Results of the single stress point simulations under stress-dependent, elasto-plastic conditions

Consolidated drained triaxial compression test simulation – Memory-Surface-Based formulation

Unexpected behaviour is observed in this test. An unloading–reloading (UL–RL) cycle occurs from loading steps 1 to 3 (see Figure B.1c). From figure B.1e, it becomes evident that the Memory-Surface-Based (MSB) formulation failed to recover the elastic shear modulus at the onset of the UL–RL cycle upon its closure. This is inferred from the fact that the stiffness at loading steps 1 and 3 is not identical. The MSB formulation failed to detect the strain reversal (SR) triggering unloading at loading step 1. As a result, the formulation did not store the corresponding deviatoric strain history tensor and the elastic shear modulus upon closure of the cycle at loading step 3 could not be restored. It should be noted that the small-strain component of the HSsmall model did detect a SR at loading step 1, therefore the elastic shear modulus does increase to its maximum value. A different tolerance was adopted for the small-strain component of the HSsmall model and the MSB formulation. The tolerance of the MSB formulation was changed in order to detect the SR triggering unloading. Figure B.2b demonstrates that the issue is resolved as the elastic shear modulus at loading steps 1 and 3 is identical.

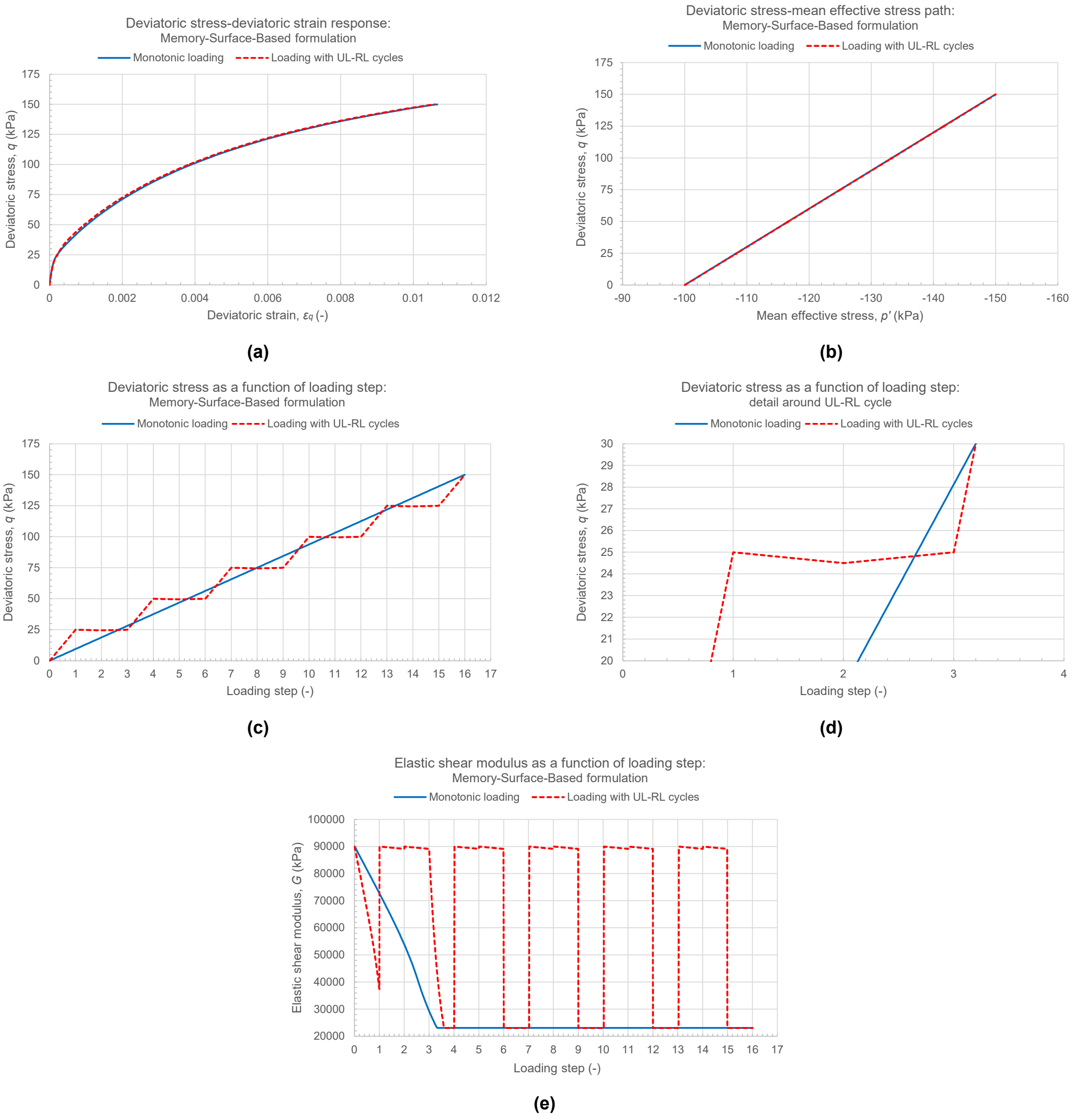

Figure B.1: Results of the CD triaxial compression test simulation under stress-dependent, elasto-plastic conditions obtained with the MSB formulation.

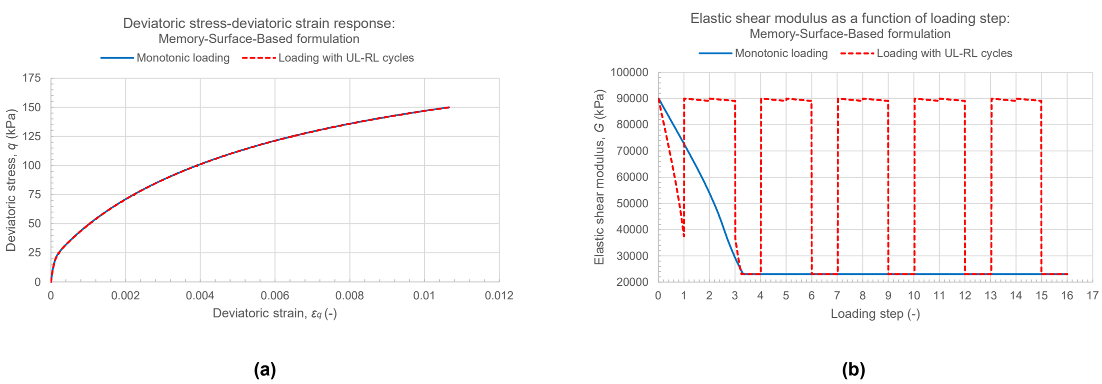

Figure B.2: Results of the CD triaxial compression test simulation under stress-dependent, elasto-plastic conditions obtained with the MSB formulation after implementing the discussed improvement.

Consolidated drained triaxial compression test simulation – Continuous Brick formulation

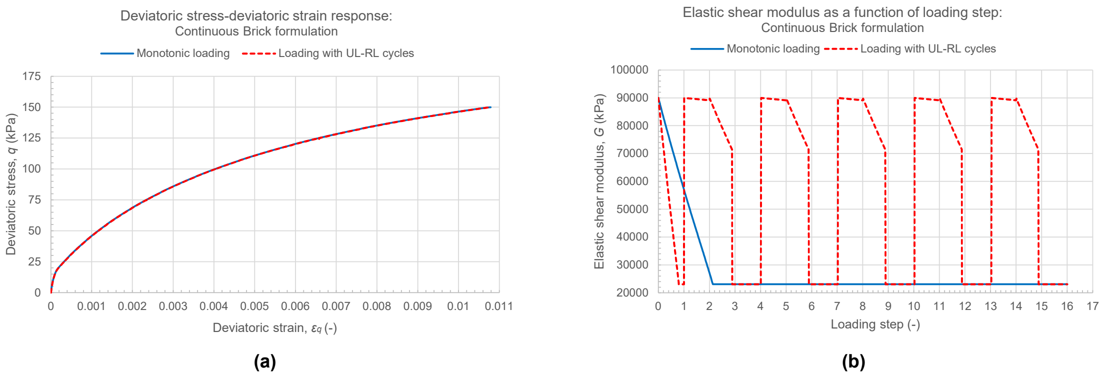

Figure B.3: Results of the CD triaxial compression test simulation under stress-dependent, elasto-plastic conditions obtained with the CB formulation.

Undrained direct simple shear test simulation – Memory-Surface-Based formulation

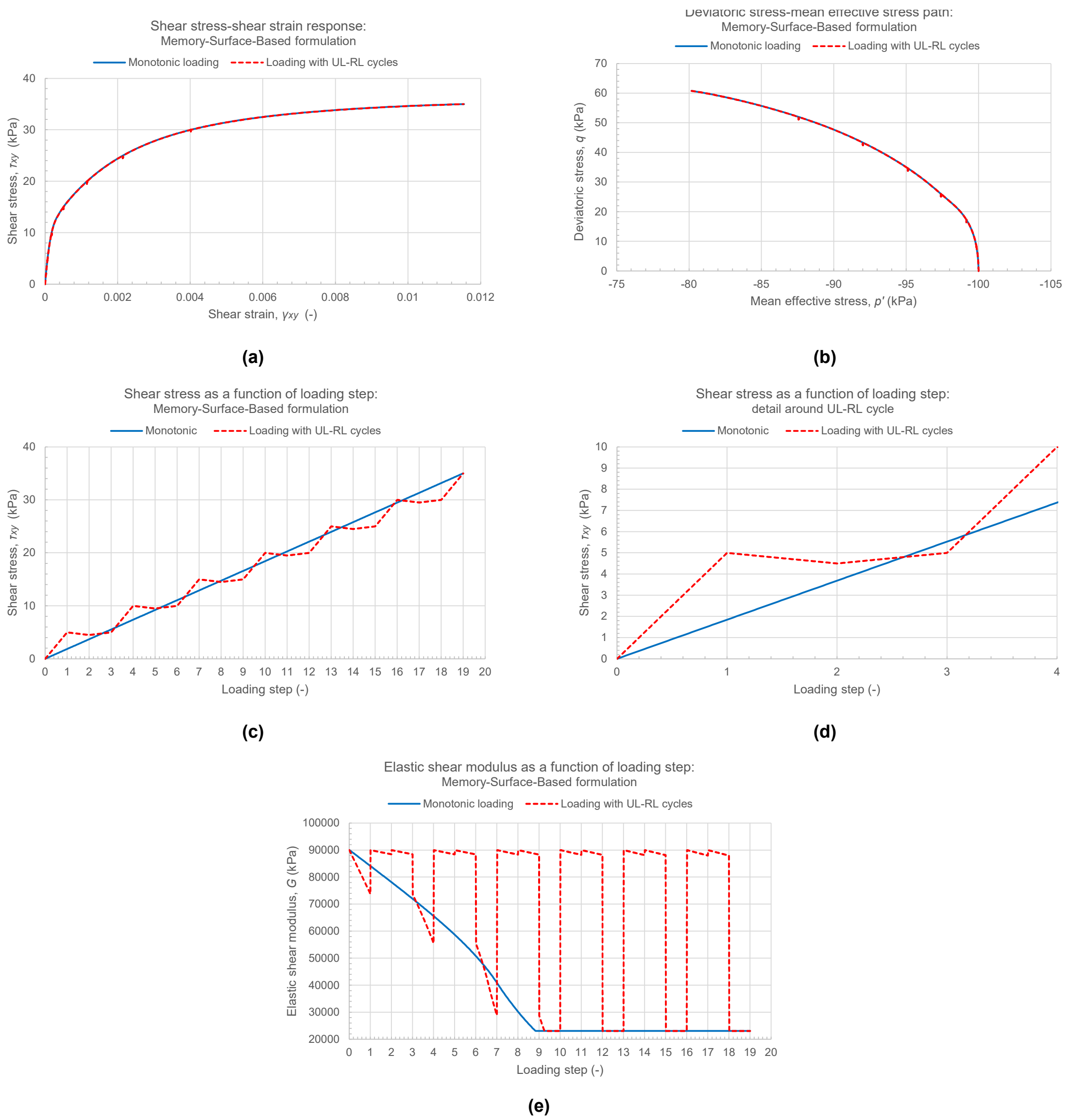

Figure B.4: Results of the undrained DSS test simulation under stress-dependent, elasto-plastic conditions obtained with the MSB formulation.

Undrained direct simple shear test simulation – Continuous Brick formulation

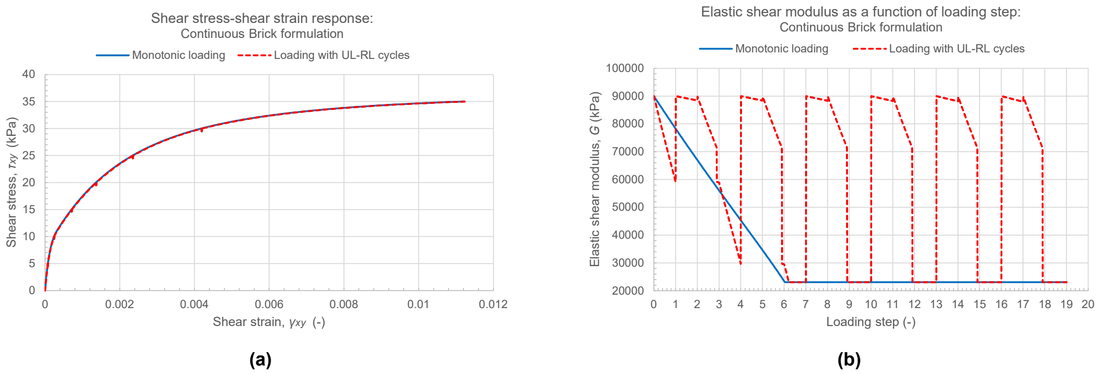

Figure B.5: Results of the undrained DSS compression test simulation under stress-dependent, elasto-plastic conditions obtained with the CB formulation.

Drained oedometer test simulation – Memory-Surface-Based formulation

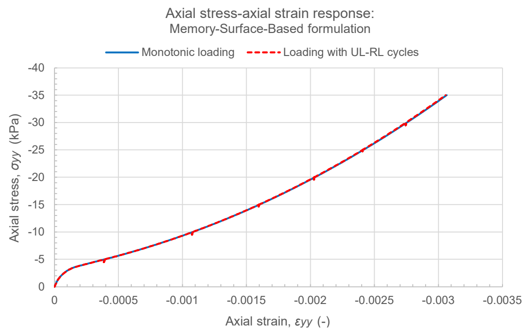

(a)

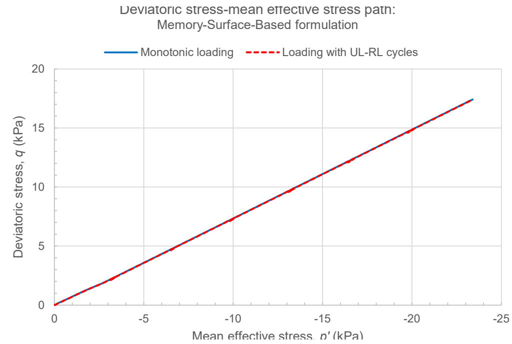

(b)

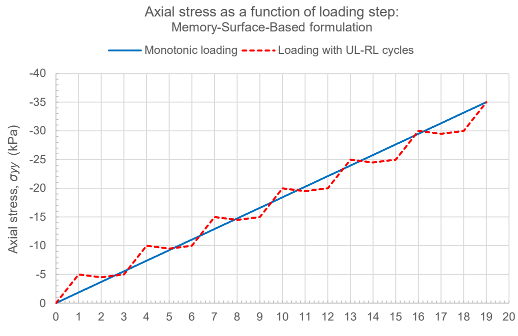

(c)

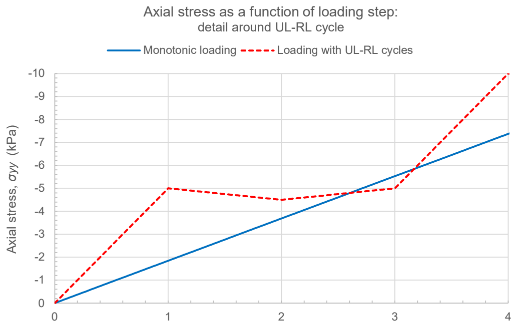

(d)

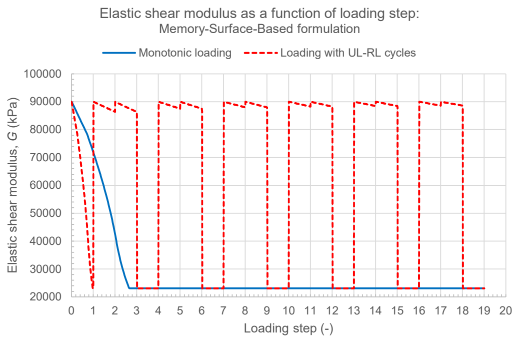

(e)

Figure B.6: Results of the drained OED test simulation under stress-dependent, elasto-plastic conditions obtained with the MSB formulation.

Drained oedometer test simulation – Continuous Brick formulation

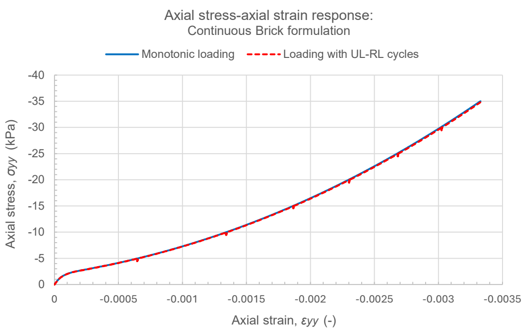

(a)

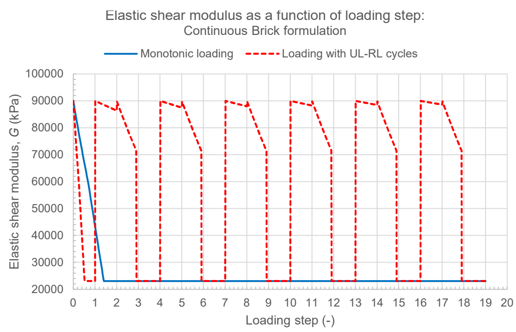

(b)

Figure B.7: Results of the drained OED test simulation under stress-dependent, elasto-plastic conditions obtained with the CB formulation.

C

Tailored consolidated drained triaxial test simulation to investigate the detection of strain reversals in triaxial extension and compression

This appendix discusses the results of the tailored consolidated drained (CD) triaxial test simulation designed to investigate whether strain reversals are correctly detected and classified as triggering either unloading or reloading in triaxial extension and compression.

Figure C.1a shows the applied deviatoric loading throughout the entire simulation, whereas Figure C.1b presents a detailed view of the shearing phase following the pre-loading phases.

The deviatoric stress is a stress invariant that, in principle, can only take positive values. However, in Figures C.1a and C.1b, its absolute value is not taken. As a results, negative values are also shown, which is necessary to visualise triaxial extension and compression in the figures. A negative deviatoric stress represents triaxial compression, while a positive value represents triaxial extension.

Under triaxial compression conditions (from loading step 1 to approximately loading step 7.5), a decreasing deviatoric stress indicates loading/reloading, whereas an increasing value indicates unloading. Under triaxial extension conditions (from approximately loading step 7.5 to loading step 12), these interpretations are reversed.

Thus, strain reversals triggering unloading should be detected at loading steps 2, 4, 6, 8, and 10, whereas strain reversals triggering reloading at loading steps 3, 5, and 9. Note that, although difficult to distinguish in the figures, strain reversals occur at loading steps 5, 6, 9, and 10.

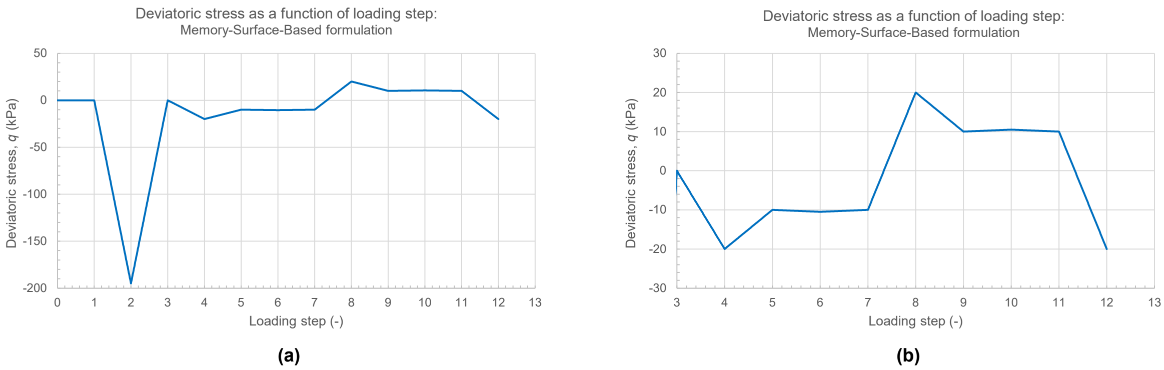

Figure C.1: Applied deviatoric loading throughout the simulation.

Figure C.2 presents the results obtained with the Memory-Surface-Based formulation. Four figures are shown: (i) the elastic shear modulus as a function of loading step (see Figure C.2a), (ii) the radius of the Memory Surface as a function of loading step (see Figure C.2b), (iii) the deviatoric strain history tensor $\mathbf{H_{SR,UL}}$ as a function of loading step (see Figure C.2c) and, (iv) a detailed view of the shearing phase of $\mathbf{H_{SR,UL}}$ as a function of loading step (see Figure C.2d).

Recall from Section 2.2.1 that, upon a strain reversal triggering unloading, the elastic state variable $\mathbf{H_{SR,UL}}$ is updated. Figures C.2c and C.2d confirm that this indeed occurs at the expected loading steps. When a strain reversal triggering reloading occurs, the size of the Memory Surface adjusts to the amplitude of the corresponding unloading–reloading cycle, resulting in sudden decrease of its radius. Figure C.2b shows that this is indeed the case at loading steps 5 and 9. Note that at loading step 3, although a strain reversal triggering reloading occurs, no significant change in radius is observed, as the unloading is of the same magnitude as the initial loading.

Figure C.2a demonstrates that, at each strain reversal, the elastic shear modulus resets to its high initial value, as expected.

Figure C.3 presents the results obtained with the Continuous Brick formulation. Three figures are shown: (i) the shear strain measure accumulation since the activation of the last brick until a strain reversal triggering unloading occurs, $\Delta\gamma_{SR,UL}$ as a function of loading step, (ii) the number of strain reversals, N_{SR}, as a function of loading step and, (iii) the elastic shear modulus as a function of loading step.

Recall from Section 2.2.2 that, upon a strain reversal triggering unloading, the elastic state variable $\Delta\gamma_{SR,UL}$ is updated. Figure C.3a confirms that this indeed occurs at the expected loading steps. The loading steps at which strain reversals triggering reloading are expected correspond to the strain reversals shown in Figure C.3b (at loading steps 3, 5, and 9) that were not classified as triggering unloading. Hence, it can be inferred that they are correctly identified as triggering reloading.

Figure C.3c demonstrates that, at each strain reversal, the elastic shear modulus resets to its high initial value, as expected.

It should be noted that, for both formulations, the elastic shear modulus is never reset to a value different from its high initial value, as no unloading–reloading cycles is ever closed.

In conclusion, both formulations are capable of correctly detecting and classifying strain reversals as triggering either unloading or reloading in triaxial compression and extension.

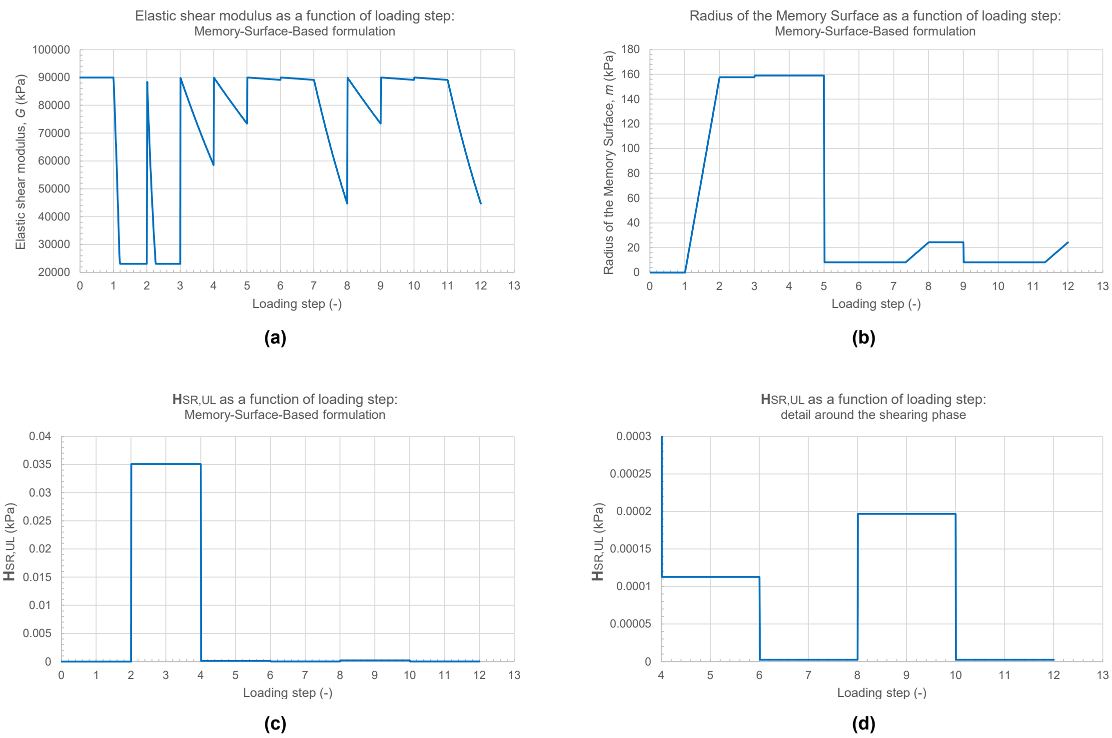

Figure C.2: Results obtained with the Memory-Surface-Based formulation: (a) Elastic shear modulus as a function of loading step, (b) Radius of the Memory Surface as a function of loading step, (c) Deviatoric strain history tensor $\mathbf{H}$ as a function of loading step and, (d) Detail around the shearing phase of $\mathbf{H}$ as a function of loading step.

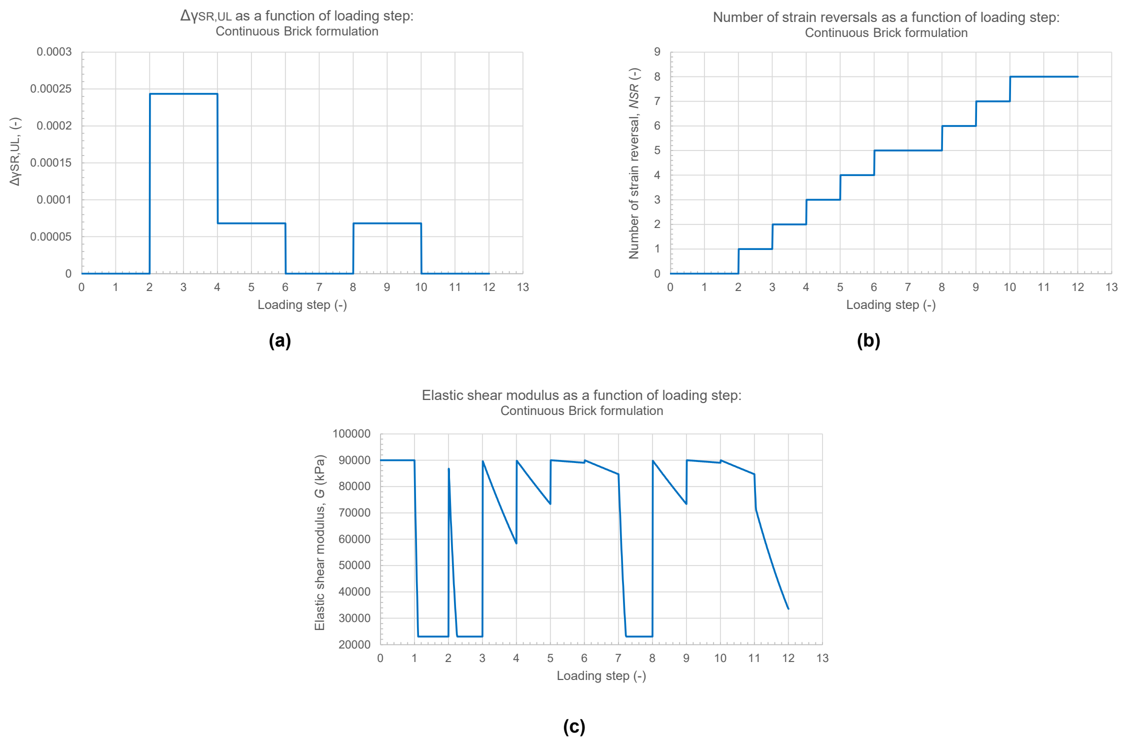

Figure C.3: Results obtained with the Continuous Brick formulation: (a) The shear strain measure accumulation since the activation of the last brick until a strain reversal triggering unloading occurs, $\Delta\gamma_{SR,UL}$ as a function of loading step, (b) Number of strain reversals, N_{SR}, as a function of loading step and, (c) Elastic shear modulus as a function of loading step.

D

Summary of the encountered issues and their solutions

This appendix provides a summary of the issues encountered in the single stress point simulations and the boundary value problem. The column *Type of issue* distinguishes between implementation issues, indicating that the numerical implementation did not correctly reproduce its underlying analytical formulation, or formulation issues, indicating that the formulation was correctly implemented but that the underlying formulation itself required improvement. Table D.1 provides a summary for the MSB formulation and Table D.2 for the CB formulation.

Table D.1: Summary of the encountered issues and their solutions in the single stress point simulations and the boundary value problem for the MSB formulation

	Type of issue	**Issue**	**Solution**
Single stress point simulations	Implementation	The formulation failed to store the memory at the onset of an UL–RL cycle	The tolerance for storing the memory is changed
	Formulation	-	-
Boundary value problem	Implementation	The formulation defined in the stress space uses the stress state from the previous calculation step, because the final stress state of the current step is not yet available. Therefore, it notices the closure of an UL–RL cycle one step too late, and the stiffness is recovered one step later than it should be.	The formulation is defined in the strain space because the final strain state of the current step is available
	Formulation	The Memory Surface was also updated when the formulation detected strain reversals that were not part of UL–RL cycles.	The strain reversal detection algorithm is therefore modified so that it only detects reversals that are part of an UL–RL cycle.
		The formulation failed to detect strain reversals when they were followed by strain increments that were too large for the detection algorithm to flag the reversal.	The strain reversal detection algorithm is updated to also evaluate fractions of the current strain increment.

Table D.2: Summary of the encountered issues and their solutions in the single stress point simulations and the boundary value problem for the CB formulation

	Type of issue	Issue	Solution
Single stress point simulations	Implementation	An elastic state variable was incorrectly initialised, which caused sudden drops in elastic stiffness under specific conditions.	This elastic state variable is now initialised correctly.
	Formulation	In a corner case, the loading conditions were identified opposite to what they actually were.	The criterion used to classify a strain reversal as corresponding to either unloading or reloading is therefore refined.
		The elastic stiffness stored in memory could be reset too early, i.e., before the corresponding UL–RL cycle had actually been closed.	Two new elastic state variables are introduced to check whether a cycle is actually closed at the moment the formulation would normally restore the stiffness. If this is not the case, the stiffness is not restored.
		The elastic stiffness was updated when the strain direction changed, even in cases where the stiffness should have remained equal to its lower bound, namely, when all bricks remained active after the change in direction.	It is now ensured that the elastic stiffness only updates upon a change in strain direction when not all bricks are active.
		The formulation retained the memory of a larger cycle when smaller UL–RL cycles occurred inside it during which no bricks were active. Because the formulation cannot determine whether the larger cycle has closed, this led to restoring its memory at an incorrect moment.	The formulation now reset the memory to zero whenever UL–RL cycles occur when no brick is active.
Boundary value problem	Implementation	-	-
	Formulation	-	-